University of Liège - Faculty of Applied Sciences

Graduation studies conducted for obtaining a Master's Degree in Civil Engineering in Constructions

Kinematics- Based Modelling of Deep Beams Retrofitted with FRP Wraps

Author
David ROMERO MOROCHO

Jury Members
Boyan MIHAYLOV (supervisor)
Frédéric COLLIN
Luc COURARD
Tom MOLKENS

Academic Year 2018-2019

Kinematics-Based modelling of deep beams retrofitted with FRP wraps

- ***Master's Degree in Civil Engineering***
- ***Faculty of Applied Sciences (ArGenCo)***
- ***Author***: David ROMERO MOROCHO
- ***Supervisor***: Boyan MIHAYLOV
- ***Academic Year***: 2018-2019

Abstract

Reinforced concrete deep beams are one of the most important elements used in civil engineering structures, not only because they are able to resist high compressive forces, but also because they can be used to increase the resistance of a structure under a dynamic loading. However, given that they are not exempt from degradation provoked by aging or unexpected loading, they tend to decrease in quality and resistance. To avoid this, Fiber Reinforced Polymers (FRP) appeared as one of the methods used for the strengthening of the deep beams.

The main goal of this thesis is to introduce and define the fundamental theory of the Five-Spring model, developed by Mihaylov et al. (2015), and extend it to deep beams strengthened with FRP wraps. The extended Five-spring model will account the effect of the FRP wraps depending on the following parameters: (1) the bond-slip relationship of the FRP strip to the concrete interface; (2) the process of debonding of the FRP strip; (3) the angle of the critical shear crack ; (4) the ratio between the depth of the FRP strip and the depth of the beam; (5) the wrapping scheme ; (6) the position of the strip with respect to the critical shear crack and (7) the shape of the critical shear crack. To account for the bond-slip model and the process of debonding, models developed by Lu et al. (2005) and Chen et al. (2012) were selected, yet in a simple manner. The shape of the critical shear crack on the other side was accounted by analyzing what is the shape that produce the most accurate response of the process of debonding. Once the influence of the seven parameters was considered, they were implemented one by one in the Matlab code to validate this extended Five-spring model with experimental data.

The extended Five-spring model was validated against test results from the literature and concluded that FRP has a positive effect in the pre-and-post peak behavior of deep beams. However, it was also observed that the accuracy of the predicted results would increase when more parameters, such as the concrete crushing around the loading plate, supports settlement or debonding of the FRP, were considered.

Acknowledgments

First of all, I would like to thank every member of the jury who consecrated his/her precious time in reading this thesis.

Above all, I would like to thank my supervisor, Professor Boyan Mihaylov, who helped me to clear my mind about what topic is the most stimulating to carry out for my Master's thesis according to our common benefit. He also provided me with invaluable recommendations and suggestions that finally helped me to achieve the objective of this work. Working with him helped me not only to develop a critical mindset to not jump to conclusions that quickly, but also was an unforgettable and enriching experience that I will never forget.

I would like also to give especial thanks to the University of Liège for giving me the opportunity of undertake my studies in Belgium, and also to the professors for sharing their expertise, knowledge and motivation with us, the future engineers.

Finally, I would like to thank my family and my friends for their support during all the development of this work.

Table of Contents

List of Figures

List of Tables

List of Alphabetical Notations

2PKT Two-Parameter Kinematic Theory
5SM Five-Spring Model
$A_{c, eff}$ Area of concrete providing tension stiffening for bottom reinforcement
A_{s1} Area of longitudinal bars on flexural tension side
A_{s2} Area of longitudinal bars on flexural compression side
A_{sv} Area of vertical shear reinforcement
A_{FRP} Total cross section of the FRP contributing to shear strength
a Shear-span
a' Length of the softening part of the FRP-to-concrete interface
a/d Shear-span effective depth ratio
a_{FRP} Mobilized bond length beyond which the interfacial shear stress is zero
$a_{FRP,1}$ Distance between the first FRP strip and the closest edge of the supporting plate
$a_{FRP,2}$ Full length strengthened by FRP
$a_{FRP,3}$ Width of one FRP single strip
$a_{FRP,4}$ Distance between two FRP strips
a_g Maximum size of coarse aggregate
a_u Effective bond length beyond which an increase of L does not increase P_u
b Width of cross section
b_f Width of concrete prism
b_c Width of FRP plate
C Compression force in section with maximum moment
CFRP Carbon Fiber Reinforced Polymers
CLZ Critical Loading Zone
DOF Degree of Freedom
d Effective depth
$d_{1, u}$ Maximum debonded length of the FRP strip/sheet
E_{ad} Young Modulus of the adhesive used between concrete and FRP
E_c Elastic modulus of concrete
E_{FRP} Young Modulus of an FRP strip/sheet
E_s Elastic modulus of longitudinal reinforcement
E_v Elastic modulus of vertical shear reinforcement
FEM Finite Element Model
FRP Fiber-Reinforced Polymers
f_c' Concrete cylinder strength
$f_{FRP, u}$ Ultimate stress of an FRP strip/sheet
f_{ct} Concrete tension strength
f_u Ultimate strength of longitudinal bars
f_y Yielding strength of longitudinal bars
f_{yv} Yielding strength of vertical shear reinforcement
f_{uv} Ultimate stress of vertical shear reinforcement

G_f Interfacial fracture energy
h Depth of cross section
h_{FRP} Depth of the beam strengthened by the FRP
I_{cr} Moment of inertia of cracked section
I_g Inertia of un-cracked zone
Ka Shear stiffness of adhesive layer
k Crack-shape factor
k_{bond} Bonding Factor
$k_{FRP, rupture}$ Value that accounts for strains concentrations in the edges of the section
L Bond length
L_e Effective bond length
l Length of deep beam
$l_{left-zone-x}$ Horizontal distance between the center of the support loading plate and the finish of the crack
l_0 Length of heavily cracked zone at bottom of critical diagonal crack
l_{b1} Width of loading plate parallel to longitudinal axis of member
l_{b1e} Effective width of loading plate parallel to longitudinal axis of member
l_{b2} Width of supporting plate parallel to longitudinal axis of member
l_k Length of dowels provided by bottom longitudinal reinforcement
m Length covered with FRP in which the stress increases linearly
N_{cr} Cracking force of zone influenced by bottom reinforcement
n_{bl} Number of bottom longitudinal bars
n_{bt} Number of top longitudinal bars
n Length covered with FRP in which the stress remains constant
P Applied concentrated load
P_u Measured ultimate applied load
$P_{u, FRP}$ Maximum Force carried by the FRP strip with a bond length L
P_{ur} Measured ultimate load for retrofitted beam
$r_{ight-zone-x}$ Horizontal distance between the center of the support loading plate and the starting of the crack
s Slip displacement in critical diagonal crack
s_0 Local slip at τ_{max}
s_f Local slip when bond stress τ reduces to zero
$s_{1, 1}$ Full length of the diagonal crack
$s_{1, 1}$ Horizontal projection of the diagonal crack covered with the FRP strip/sheet
s_{cr} Slip corresponding at critical diagonal crack
s_h Distance between horizontal shear reinforcement
s_{max} Local slip when stress in the FRP reduces to zero
s_{vh} Distance between horizontal shear reinforcement
s_{vv} Distance between vertical shear reinforcement
T Tensile force in bottom reinforcement

t_l Length halfway of the diagonal crack
t_{ad} Adhesive thickness
t_{FRP} Thickness of FRP strip/sheet
t_{sp} Thickness of steel plate
V Shear strength
V/P Ratio of shear force to Applied point load
V_{CI} Shear resisted by aggregate interlock
V_{CLZ} Shear resisted by the critical loading zone
$V_{cr, fl}$ Shear corresponding to flexural cracking
$V_{cr, sh}$ Shear corresponding to the propagation of critical diagonal crack
V_{exp} Measured shear strength
V_D Shear resisted by dowel action
V_{FRP} Shear resisted by the FRP strips/sheets
V_{pred} Predicted shear strength
V_S Shear resisted by stirrups
V_{sect} Sectional shear strength
w Crack width in the diagonal crack
w_v Vertical displacement in diagonal crack
w_{v0} Initial vertical displacement in the diagonal crack accounting for retrofitted beams
w_{v1} Vertical displacement in the diagonal crack so as to have the beginning of debonding between FRP and the concrete
w_{v2} Vertical displacement in the diagonal crack that indicates us that the debonding between the FRP and concrete has reached the edge of the section
w_{v3} Vertical displacement in the diagonal crack that indicates us that beyond this value the FRP strip ruptures
$w_{v, max}$ Maximal crack width developed by an FRP strip under a certain loading for a specific wrapping configuration
$w_{v, FRP, ideal}$ Maximal crack width in the FRP strip/sheet corresponding to an ideal configuration
$w_{v, FRP, real}$ Maximal crack width in the FRP strip/sheet corresponding to a real configuration
x_1 Maximal debonded length to develop in the vertical distance between the top edge of the FRP strip and the diagonal crack
x_2 Maximal debonded length to develop in the vertical distance between the bottom edge of the FRP strip and the diagonal crack
x_{total} Total debonded length of the FRP strip
z Lever arm between the tension in the flexural reinforcement and the compression side

List of Greek Notations

α Angle of line extending from inner edge of supporting plate to far edge of tributary area of loading plate responsible for shear force V

α_0 Angle α of short beam used for Vmax calculations

α_1 Angle of critical diagonal crack

β FRP orientation with respect to longitudinal axis of the beam

β_w Width ratio factor

ϕ Curvature in pure flexion region

ϕ_{l1} Diameter of longitudinal bars on flexural tension side

ϕ_{l2} Diameter of longitudinal bars on flexural compression side

ϕ_{sv} Diameter of vertical shear reinforcement

ϕ_{sh} Diameter of horizontal shear reinforcement

ρ_{l1} Ratio of longitudinal bars on flexural tension side

ρ_{l2} Ratio of longitudinal bars on flexural compression side

ρ_{FRP} FRP shear reinforcement ratio

ρ_{sv} Ratio of vertical shear reinforcement

ρ_{sh} Ratio of horizontal shear reinforcement

$\varepsilon_{t,\,avg}$ Average strain along bottom longitudinal reinforcement

ε_u Ultimate strain of longitudinal bars

ε_{uv} Ultimate strain of vertical shear reinforcement

ε_{FRPu} Ultimate strain of an FRP strip/sheet

Δ_{5sm} Deflection of shear span given by five-spring model

Δ Mid-span deflection of beam

Δ_c Shear distortion of critical diagonal zone

Δ_{exp} Measured midspan deflection at shear failure

Δ_{pred} Predicted midspan deflection at shear failure

Δ_t Deflection due to elongation of bottom longitudinal reinforcement

Δ_u Displacement at the loaded end corresponding to $P_{u,\,FRP}$

δ_x Displacement along x-axis

δ_z Displacement along z-axis

θ Angle of diagonal cracks in uniform stress field

τ Local bond stress

τ_0 Bond stress when the slip between one strip of FRP and concrete reaches its maximum value

τ_{max} Maximum bond stress between one strip of FRP and concrete

Ω_0 Area under stress-strain curve of concrete in uniaxial compression up to strain of -0.0035

σ Diagonal compressive stress in CLZ

σ_{avg} Average diagonal compressive stress in CLZ

σ_v Stress in transverse reinforcement

$\sigma_{FRP,\,max\,ideal}$ Maximal stress reached by an FRP strip in an ideal configuration

$\sigma_{FRP, avg, ideal}$ Average stress contributed by the FRP for an ideal configuration

$\sigma_{FRP, avg, real}$ Average stress contributed by the FRP for a real configuration

$\sigma_{crack, FRP(i)}$ Stress supported by each FRP's strip

$\sigma_{crack, FRP}$ Average stress supported by the total number of FRP's strip

υ_{ci} Aggregate interlock shear stress

1 Introduction

1.1 General information

Over the last decades, the use of reinforced concrete deep beams in civil engineering structures has increased considerably. They are found in several structural elements such as pile caps, tanks, folded plates, foundation walls or transfer girders, as shown in Figure 1 – 2. This last is commonly used in high-rise buildings or bridges to transfer heavy loads from the upper element to the surrounding elements. Owe to this, their depth must be high enough to not only not to deflect under a heavy loading configuration, but also to resist and redistribute vertical forces provoked by earthquakes in zones with high seismicity. If this was not the case, a deflection in this member of 10 cm for example, will provoke at least the same deflection on the lower floors. Eventually, this phenomenon translates into unsightly effects and an increasing of second order effects, which turns to be very harmful for structures that high.

Figure 2 Transfer girders in Brunswick Building (Fazlur Khan website 2011)

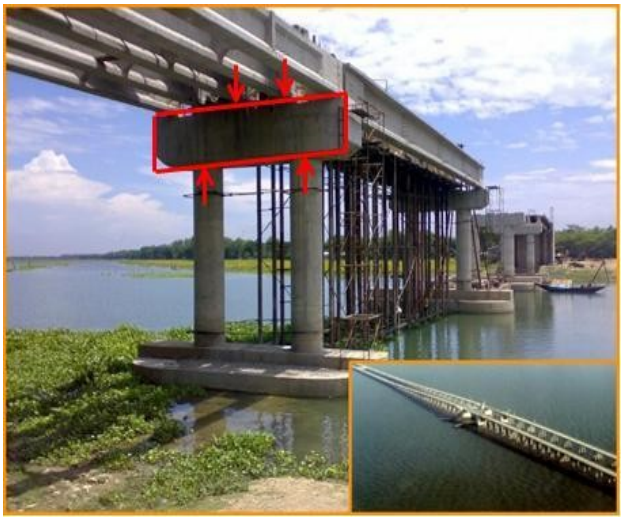

Figure 1 Transfer girders in bridges (Matt Ball blog 2015)

A deep beam is a member loaded at one face and supported on the other one (ACI 318M-14) whose shear-span-to-depth ratio (a/d) is smaller than slender beams. However, the transition from slender to deep beams is imprecise at somewhat a/d equal to 2. That is why for practical purposes, the a/d ratio is taken equal to 2.5. Besides, due to their large depth, their strength is mainly governed by shear rather than flexure, thereby strut-and-tie models are commonly used to design them. These models indicate that compressive stresses coming from the loading points are transferred directly to the supporting ones by means of concrete struts. Even though these methods are quite powerful for design purposes, it does not catch very well the influence in shear when changing some

parameters such as shear reinforcement, longitudinal reinforcement or beam's size (Mihaylov, Bentz and Collins 2010). One of the reasons is that many of the tests that were carried out assumed that deep beams behave in the elastic range. This assumption has the big disadvantage of considering an isotropic material obeying Hooke's law "*plane sections remain plane* ", which is not always the case, and therefore is not very useful for practical purposes. These kinds of tests were not changed until early sixties, wherein ultimate loading tests were carried out by De Pavia and Sies (1965) and Leonhardt and Walther (1966). These new tests were helpful to get a better understanding of the post-peak behavior so much so that, more than 490 tests have been carried out in order to investigate such non-linear behavior (F.K. Kong 2003).

One of the methods that determine the complete pre-and-post peak shear behavior of a deep beam is the one proposed by Mihaylov et al. (2015). This method, namely hereafter Five-Spring Model (5SM), is based on the Two-parameter kinematic Theory (2PKT) model developed also by Mihaylov et al. (2013). The 2PKT model considered that the complete deformed shape can be obtained in terms of two degrees of freedom: the average strain in the bottom flexural reinforcement ($\varepsilon_{t,\,avg}$) and the vertical displacement developed in the critical loading zone (CLZ). Once obtained the complete shear behavior is obtained by means of using the 5SM as the contribution of five different springs. Four of the springs represented the shear resistance mechanism of the beam, while the fifth spring modeled the flexural behavior (Mihaylov et al. 2015).

Eventually, deep beams are not exempted from suffering damages provoked by the passage of time, vandalism or accidental loads. Therefore, the use of strengthening and retrofitting methods becomes crucial in order to keep using such important elements. In the actual market, external or internal strengthening methods can be found. Among all of these, the use of external Fiber-Reinforced Polymers (FRP) was remarked. These polymers, usually made of carbon, glass or aramids, are glued to concrete. When using such method, it has been demonstrated that the failure mode is altered changing from brittle behavior to more ductile. Besides, it was also demonstrated that the shear, flexural and axial strength of the retrofitted elements was improved when bonding those elements to the concrete. However, their efficiency is mainly governed by the location of the strips, their wrapping configuration and the well practice made by the workers when applying them to the piece to repair (Bukhari and Vollum 2012).

1.2 Objectives and scope of the thesis

The work developed in the following master's thesis is an extension of the 5SM model developed by Mihaylov et al (2015). As it was previously described, 5SM

model determines the pre-and-post peak behavior of reinforced concreted deep beams by considering the contribution of five different springs.

As it was demonstrated by Taerwe and Vasseur (2009), the use of Carbon Fiber Reinforced Polymers (CFRP) sheets in a certain zone restrict the rotation of a plastic hinge at that zone and also allow additional plastic hinge formation in non-retrofitting zones. Also, the efficiency and effectiveness of using CFRP in upgrading the shear strength and ductility in beam-to-column joints subjected of frames placed in high seismicity zones was demonstrated by Al-Salloum and Alsayed (2009). After, the impact in shear strength of different FRP configuration was studied by Bukhari et al. (2012) concluding that depending on the position and depth of FRP sheets the contribution to shear and deflection will be higher or lower. Then, the effectiveness in the enhancement in shear strength depending on the ratios of CFRP wrapping and horizontal/ vertical shear reinforcement was demonstrated by Rasheed et al. (2016).

The main objective of the present thesis is to model the pre-and-post peak shear behavior of deep beams retrofitted with FRP sheets. This will be done by adding a new spring in the 5SM which will represent the contribution to shear strength of the FRP sheets/strips. The wrapping scheme (Fully, U-jacketing or Side wrapping) and the strip/sheet's position would be considered in this new spring. Then, this model will be validated against different experimental data to finally come up with some conclusions.

1.3 Thesis outline

The present thesis consists of nine chapters including the Chapter 1.

Chapter 2 provides more information about the difference of using FRP against another repair/retrofitting methods. It is also included the mechanical properties, the common uses and the main factors that influence in the behavior of reinforced concrete beams retrofitted with FRP strips. It is also included the observed behavior of beams retrofitted with FRP strips such as their common applications in civil engineering or their common failure modes and relevant information about the experimental data used for the validation of the new kinematic model such as test set-up or geometrical and mechanical properties of each specimen.

Chapter 3 describes the three different approaches that are commonly used when determining the shear strength of deep beams. In addition, it is explained more in detail the theory behind the 5SM and the 2PKT by Mihaylov et al. (2015). Those models would settle the foundations of a new model that captures the contribution to shear of an FRP strip/sheet.

Chapter 4 defines the necessary changes to make or to implement in the 5SM in order to capture the positive effect of FRP wrapping. At the very beginning the fundamental theory was given in order to have a clear ideal about the process of debonding of the FRP strip from concrete. Then, the process of debonding was particularized for any strip having any configuration and any wrapping scheme, provided that the FRP strips accomplished certain assumptions. Finally, an study about the influence of the crack-shape was done so as to evaluate which shape is the most convenient when determining the shear force supported by the FRP strips.

Chapter 5 validated the extended Five-Spring model with real experimental data. Discussion is given based on load-deflection curves on the pre-peak behavior.

Chapter 7 gives a summary of the previous results, a final conclusion as well as prospective opportunities of improvement.

2 FRP material for strengthening of concrete structures

2.1 Introduction

As previously mentioned, the use of FRP in engineering applications has raised over the last 40 years.
First of all, they were used in aeronautical and spatial engineering to build their spacecrafts. Then, they started being used in the car industry. During the last years, both industries had contributed enormously in the development of new proceedings and techniques for the improvement of the quality and effectiveness of FRP.
In the case of construction industry, two main epochs can be identified. In the first one, identified as the "*development era*" engineers, mainly from Japan and Europe, started considering the use of FRP as a strengthening material. Then, the second one, identified as the "*implementation era*" in the early 90's engineers started using FRP as a strengthening material. One of the first structures to be reinforced using such method was the Ibach Bridge, in Lucerna (Switzerland) (M.G. Argento 2015). During its construction, engineers considered two possible solutions to provide enough resistance in those needed sections, either they could use steel plates bonded to concrete, or FRP sheets bonded as well to concrete. Finally, they decided to use FRP due to its resistance to corrosion and its lightness. As it can be noticed, those two properties constitute two of the reasons why engineers prefer using FRP instead of another repair/strengthening method. Despite these benefits and the increasing amount of investigations carried out to improve the knowledge about its behavior, its real behavior is still far to be well known. That's why engineers are cautious about using such material as a retrofitting or strengthening one.

Figure 3 External Reinforcement of Ibach Bridge (Google 2019)

Figure 4 Ibach Bridge (Structurae.net 2016)

2.2 FRP components properties

FRP is a composite material constituted with two different elements: the matrix and the support. The properties of the composite materials are dependent of several parameters. They are dependent not only of the amount of each element composing the composite, but also their geometry, their size, their orientation and even the kind of additives used to constitute the matrix. This last is due to the fact that is not the same using silica than using rubber or carbon micro crystals. (M.G. Argento 2015). Here below a full explanation of the influence of the nature and the composition on the FRP properties is given.

2.2.1 Matrix "resins"

The matrix is usually composed with synthetical resins binding together the fibers (M.G. Argento 2015). Apart from his bonding role, it has more roles to accomplish such as:

a) Providing mechanical resistance of the composite
b) Granting the toughness and rigidity of the composite
c) Protecting fibers against abrasion and environmental corrosion
d) Transmitting and support the loads between the matrix and the fibers
e) Shaping the composite according to the client needings

As noticed, this element has important roles to accomplish. On the other side, it is important to note that the effectiveness of each role is directly influenced by the nature of the matrix. In the actual market, two groups of matrixes can be found:

a) Thermoset Resins: they are the most common for structural purposes for two main reasons: firstly, they can be found in a liquid state at room temperature prior to curing and secondly, they are impregnated into fibers before heating. However, it has a disadvantage in comparison with the other group, they cannot be reformed again, i.e., they will not be able to be recycled or reshaped once the heating or curing stage has finished.

In the construction market, as explained by Gevin. M (2014), four different types of resins can be identified, each one having their corresponding advantages and disadvantages as summarized below.

(1) Polyester: on the positive side, this material is easy to use and its cheaper in comparison to other materials. On the negative side, it is sensitive to UV

degradation and does not enhance too much the mechanical properties of the composite

(2) Vinyl ester: on the positive side, it is resistant against corrosion, waterproof and improves the mechanical properties of the composite. However, it cannot be exposed to high temperatures, and in some cases is more expensive than polyesters.

(3) Polyurethane: in comparison to vinyl esters, it has a higher strength, flexibility and a higher chemical/mechanical resistance than those. On the flip side, its cost is almost 2 times the vinyl esters.

(4) Epoxy: on one side, it possesses a high resistance to humidity and high temperatures, besides blue-collar workers are able to work with it during long periods of time. On the other side, is the most expensive resin in the market and its consistency can be critical to work under unexpected conditions. Besides, it has to be manipulated with especial equipment due to its profound corrosivity.

Since epoxy resins are the most common in the construction industry, and given that many of the tests have used this kind of material, it is important to compare its properties against those corresponding to concrete and steel. This is mainly because bonding between concrete and steel to FRP will depend on the relationship between Young Modulus and Poisson coefficient of those three materials.

Properties	***Epoxy***	***Concrete***	***Steel***
Density [Kg/m^3]	1100 - 1700	2350	7800
Young Modulus [GPa]	0.5 - 2	20 – 50	200
Shear Modulus [GPa]	0.2 - 8	8 – 21	80
Poisson coefficient [υ]	0.3 – 0.4	0.2	0.3
Tensile strength [MPa]	9 – 30	1 – 4	200 – 600
Shear strength [MPa]	10 – 30	2 – 5	200 – 600
Compressive strength [MPa]	55 – 110	25 – 150	200 – 600
Rupture strain [%]	0.5 – 5	0.015	25
Fracture energy [J/m^2]	200 – 1000	100	105 - 106
Thermal expansion coefficient [ΔT]	25 – 100	11 – 13	10 - 15
Water absorption [ ]	0.1 - 3	5	0

Table 1 General properties of epoxy resins, concrete and steel, (Argento M. G., 2015)

Finally, in the table below some important mechanical properties are given according to the nature of the resin.

Resin	*Density*	*Tensile strength*	*Young Modulus*	*Rupture strain*	*Maximal Temperature*
	[Kg/m^3]	[MPa]	[MPa]	[%]	[°C]
Polyester	1.2	50-65	3.00	2-3	120
Vinyl ester	1.15	70-80	3.50	4-6	140
Epoxy	1.1-1.4	50-90	3.00	2-8	120

Table 2 Mechanical properties of thermoset resins, (Argento. M. G., 2015)

b) **Thermoplastic Resins:** due to its difficulty when applying it, they are not so common in structural industry. If they have to be obtained in a liquid state, they have to be heated first at huge temperatures since they are found in solid state (pellets) at room temperature. Then, in order to impregnate them to fibers, they will be subject them to high pressures. Despite this disadvantage, they can be used as many times as possible since they can be reheated and reshaped to obtain therefore the final configuration.

(a.) (b.)

Figure 5 (a) Thermoset resins, (b) Thermoplastic Resins, Google images (2019)

Finally, according to (M.G. Argento 2015), three more concepts directly linked to the nature of the matrix should be keep in mind:

1. The maximal time of application: it is defined as the time left after the mixing of the components to apply the resin is attained. After this time, the application of the resin will be impossible since this has hardened. Usually depends on the external temperature, the quantity and type of resin.
2. Open time: it is defined as the maximal time after the application of the adhesive between the elements to joint.
3. Vitreous transition temperature: from this temperature the material starts to lose its properties and changes its behavior from vitreous to plastic. It is also inversely linked to the elasticity of the polymer.

2.2.2 Supporting element "fibers"

According to Gevin. M (2014), when building the resistant structure of the composite material, fibers made of three different materials: aramid, glass and carbon are used. Usually, they can be used in four different forms: short, long, chopped and woven as shown in Figure (6)

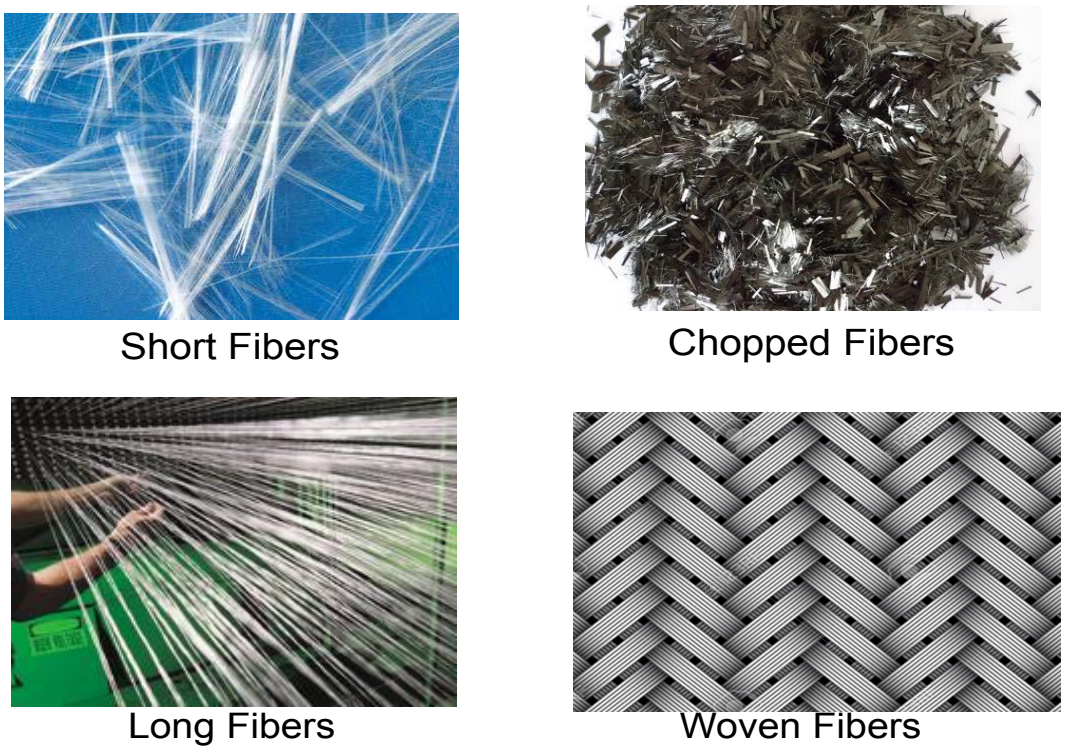

Figure 6 Common type of fibers, (Gevin M. 2014)

Glass fibers are the most common due to its low price. However, in the recent years an increase demand of carbon fibers has started. This is mainly because despite its higher price in comparison to other fibers, carbon fibers possess better mechanical properties McGuirk. G. N. (2012). Here below a comparison as well as an explanation of several mechanical properties of each fiber is given.

Compression strength

According to M.G. Argento (2015), it has been found that for each fiber's type, axial compressive stiffness is the same as axial tensile stiffness.

Tensile strength

As can be noticed in Figure 7, carbon fibers (PRFC) have a higher tensile strength than aramid (PRFA) or glass fibers (PRFV). However, these first ones have a more brittle behavior (low deformation) in comparison to aramid or glass fibers. On

the other side, aramid fibers possess a more ductile behavior (narrower cross section) and in some cases, higher tensile strength than carbon or glass fibers.

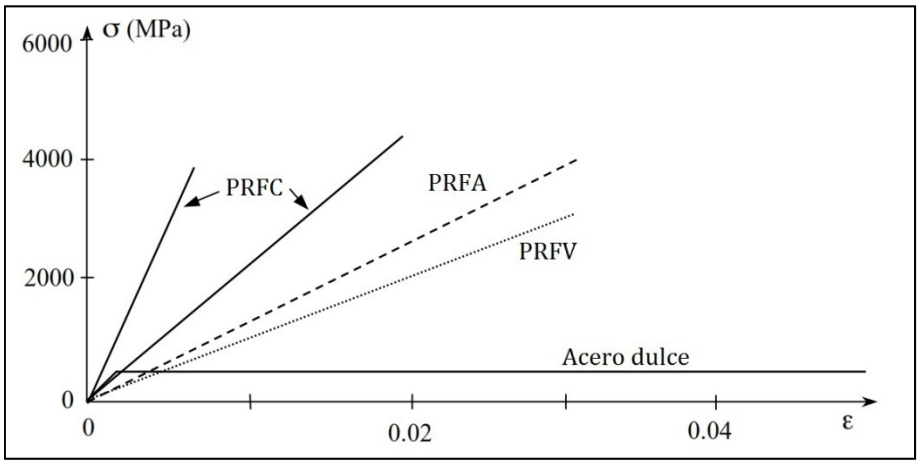

Figure 7 Stress-strain curve according to the nature of the fiber, (Argento. M. G 2015)

Thermal stability

Carbon fiber mechanical properties such as Young Modulus or tensile strength are not influenced by temperature. This is mainly because they are able to maintain their properties at about 2000°C . Nevertheless, once they are mixed with polymers matrixes, the new composite material will no be longer stable at such temperatures, but at a lower temperature (about 200°C). The principal reason is because polymers matrixes start to lose its properties at about 200°C.

Table 3 summarizes the tensile properties of each fiber type.

Fyper Type	*Young Modulus*	*Ultimate strength*	*Minimal rupture strain*
	[GPa]	[MPa]	[%]
Carbon			
General	220-240	2050-3790	1.2
High Strength	221-240	3790-4820	1.4
Ultra-high-strength	222-240	4820-6200	1.5
High-Modulus	340-520	1720-3100	0.5
Ultra-high-modulus	520-590	1380-2400	0.2
Glass			
E-glass	69-72	1860-2680	4.5
S-glass	86-90	3440-4140	5.4
Aramid			
General	69-83	3440-4140	2.5
High performance	110-124	3440-4140	1.6

Table 3 Tensile properties of common fibers used in FRP composites, (McGuirk G. N., 2012)

2.3 Advantages and disadvantages of using FRP against other strengthening methods

Before introducing the common application of FRP in civil engineering, it is important to keep in mind some important aspects that will govern their choice above another available options.

First, the fibers orientation has to be taken into consideration. Since fibers are able to resists higher tensile stresses but not compressive or flexural ones, FRP fibers should be placed following the most vertical orientation as possible (McGuirk. G. N. 2012). By doing so, FRP will be subjected just to tensile stresses. If this is not the case, FRP will be subjected to bending and tension that will decrease its contribution to the resistance of a member.

Second, it must be considered its poor fire resistance. This is not a problem for open spaces where structures such as bridges or harbors have an easy access to extinction means. However, it becomes a big deal for structures in close spaces, where the access to extinction means is not always possible. Despite this disadvantage, a good design procedure and an extra isolation can help us to have a good fire resistance (Cheng et al., 2008).

Third, its choice will be preferred in structures where steel plates bonded to concrete are not possible to use due to the following reasons: (1) the environmental conditions are too aggressive, such as structures close to the sea, where steel is easily corroded; (2) FRP sheets are usually thinner than steel plates, this allow us to maintain the same dead loads, and increase the bonding between FRP to adhesive this let us as well reduce interfacial shear stresses.

Despite all of these benefits, there are also some important disadvantages that hamper their use, namely: its placement must be done by skilled workers so as to avoid constant and expensive reparations, it is 6x more expensive than steel plates for instance, and it is highly sensitive to medium temperatures (40 °C) (Gergely. V. 2017)

2.4 Common applications of FRP reinforcement in Civil Engineering

According to Cheng et al., (2008), the use of FRP materials in civil engineering covers four different fields: (1) *strengthening material* for new or old structures where the resistance given by steel and concrete is not enough; (2) *repairing material* where the structural element has almost lost all his resistance due to aging or vandalism; (3) *alternative construction material* where for architectural

reasons, steel cannot be employed as concrete reinforcement; (4) as a material that allow the construction of a *hybrid structure*, such as concrete-filled FRP tubes. Here below a summary of different strengthening applications is given.

Columns: using FRP sheets around columns can increase their confinement and so, their flexural and axial capacity and ductility (Cheng G. M. 2008). Note also that this improvement will be much higher in circular columns not only because the concentration of stresses would not appear at the edges of the section, but also because circumferential pressure effect would be activated.

Slabs: according to Maadawy and Soudki, (2008) and Smith et al. (2010), FRP not only contributes to flexural resistance in positive and negative bending zones, but also in resisting against punching and shear.

Beams: depending on the position of the FRP this will enhance the flexural or shear capacity (Teng, 2002; Smith and Teng, 2002 & Aram et al. 2008). For example, if FRP is placed on the sides of the beam, shear capacity is increased as in the ends of dapped prestressed beams, but if they are placed on the tension side of the beam, flexural capacity is improved such as beam-to-column joints.

Walls: According to Antoniades et al. 2005, El Gawady et al., 2005 & Binice et al., 2006; when using FRP in walls, their in-plane shear capacity is increased, their in/out-of-plane flexural stability increases and unreinforced masonry walls are transformed into shear walls.

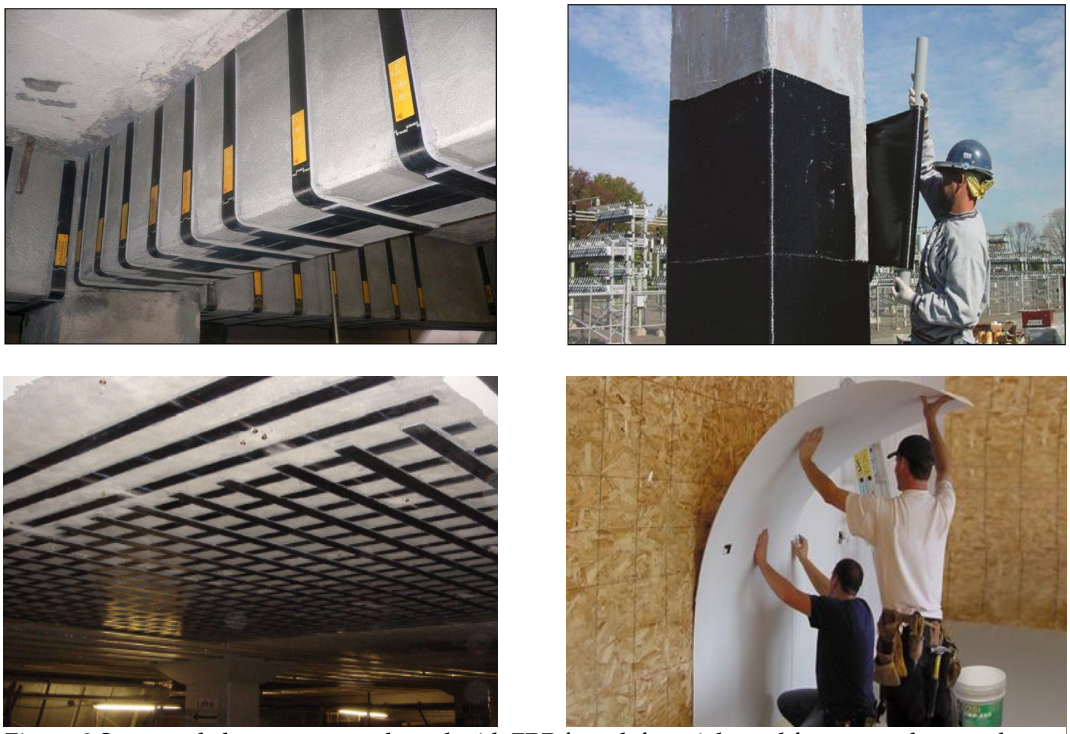

Figure 8 Structural elements strengthened with FRP from left to right and from up to bottom, beam, column, slab, wall, (Google 2019)

2.5 Strengthening of RC beams with FRP

According to Holloway and Teng 2008, reinforcement with FRP has become one of the top techniques either in the research field, or in the structural strengthening. In reinforced concrete beams, there are two common failures: shear and flexural. Shear failure is the most undesirable one since it is brittle, sudden and difficult to prevent, whilst flexural failure, is more ductile and therefore a redistribution of stresses between elements can be made. In beams, such failures can be prevented using the proper FRP configuration. Below, an explanation of the most common wrapping techniques used to decrease the risk of having a flexural or shear failure, as well as its ductility, is given.

2.5.1 Strengthening schemes

As mentioned above, depending on the FRP position the flexural or shear behavior is improved. In the Figure 9, Teng et al. (2002) summarized the most common wrapping schemes where several symbols for each configuration can be noticed. Below an introduction of each symbol is given.

Bonding configuration: there are three different possibilities: W, S, U. (*W*) represents fully bonded on the sides and on the upper and bottom faces of the beam; (S) represents side bonding of the beam with FRP sheets/strips; (U) represents U-jacketing, in this case bonding is applied on both sides of the beam, but also on the tension face of the beam.
Note also that for full bonding or U-jacketing schemes, is necessary to round the corners, of about 20 mm, in order to avoid having the rupture of the FRP. The principal reason is the stress concentration at these narrow zones.

Fiber distribution: (S) correspond to continuous and (P) to discrete strips.

Fiber orientation: there are two possibilities: vertical orientation ($\beta = 90°$) in cases where FRP is applied perpendicular to the beam's longitudinal axis, or diagonal (β/ϕ ><90°). As it was mentioned earlier, fiber's orientation has an enormous influence on the control of shear cracking. Regarding this point, there are three especial orientations: (1) according to Taljsten 2003; Zhang et al. 20004; Zhang and Hsu 2005, if fibers are parallel to beam's longitudinal axis, its contribution to shear resistance would be much lower than if they are perpendicular to the longitudinal axis of the beam (2); (3) if fibers are parallel to shear cracks no shear contribution is observed.

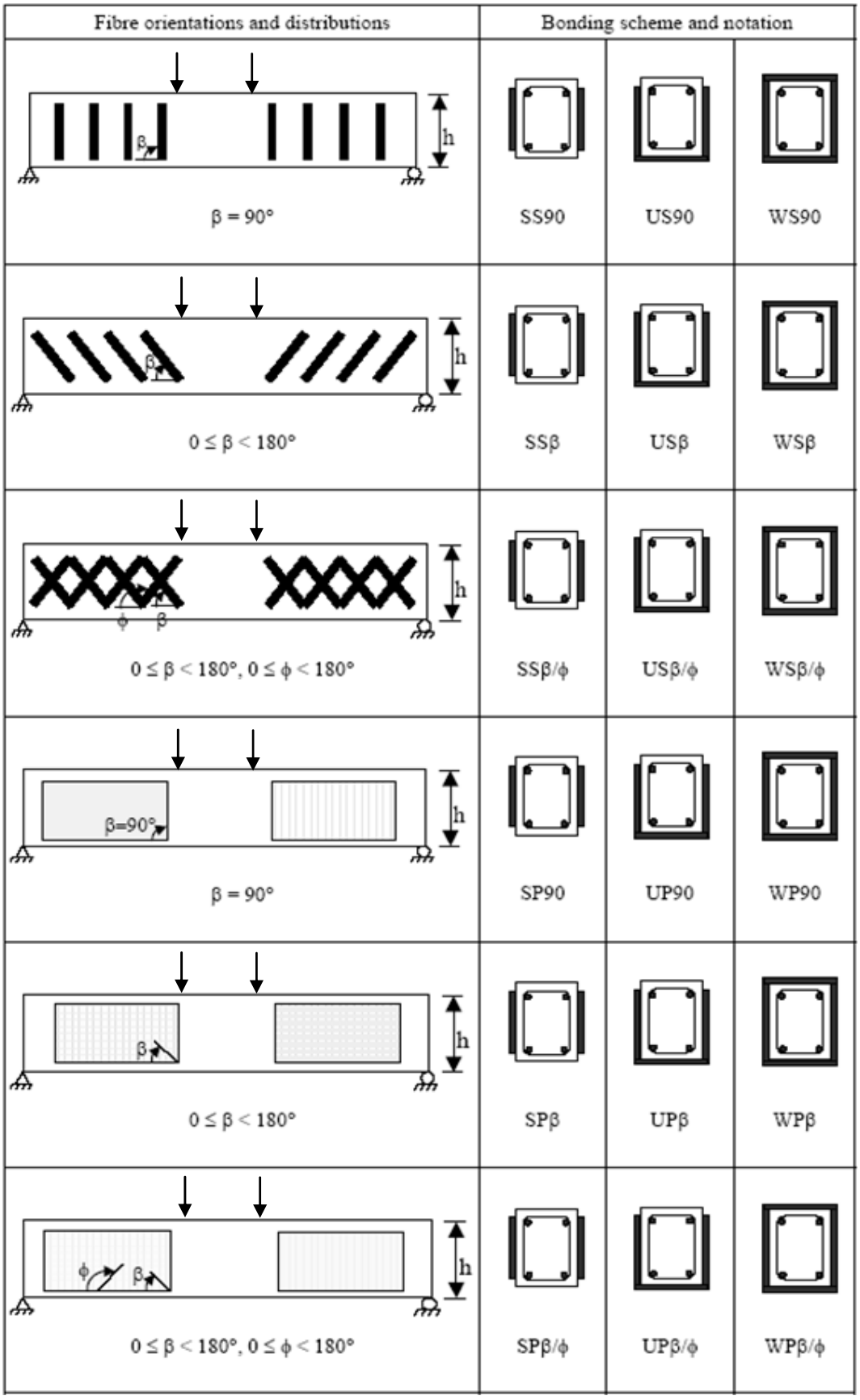

Figure 9 Common FRP strengthening schemes, (Teng et al. 2002)

2.5.2 Common failure modes

It is worth to mention that flexural failure is broadly studied in the scientific community and therefore enough information for an analysis is available. On the contrary, shear failure due to its brittle behavior it is extremely difficult to measure, and therefore the available information is not as wide as for flexural tests.

In this section, a description of the common failure modes observed during the last twenty years is given. As it would be noticed later, the understanding of their failure modes would allow to understand what were the failure modes observed in the experimental data used for the validation of the extended 5SM.

2.5.2.1 Flexural failures

According to Smith and Teng 2001, six different flexural failure modes Fig. 10 exist:

1. **Debonding Failures:** in these cases, beam fails before the strength of the FRP has been fully developed. They are the most common ones when using FRP, and someway are the most tricky and troublesome due to her brittle behavior. They are also divided into two categories:

    a. Intermediate crack induced debonding where debonding usually begins at an intermediate flexural or flexural or shear crack, and then propagates away from the crack, towards beam's edges.
    Depending on the propagation of the failure, concrete cover separation (Fig. 10.e) would exist, in which failure travels up to the tensile reinforcement and so concrete cover debonds, or plate end interfacial debonding (Fig. 10.f) where failure propagates between the FRP-concrete interface. McGuirk. G. N. (2012).

    b. Plate end interfacial debonding, where failure usually initiates at the end of the beam and then propagates towards the middle of the beam (Fig. 10.d)

    One aspect to keep in mind about these failure modes is that they usually initiate at zones with high stresses concentration, such as anchorage zones or sharped edges (Fig. 10 e-f). Also note that once failure initiates, there will be no more increment in the load capacity of the loaded member. (Smith S.T and Teng J.G. 2001)

2. **Non-debonding failure** in this group two main possibilities exist :

a. The beam fails because the FRP strip has reached its maximal strain (Fig. 10.a) and can no longer be stretched, identified as FRP rupture.
b. Beam fails either by concrete crushing (Figure 10.b) or by shear crack (Fig. 10.c). In both cases, FRP strength is not fully developed, i.e., neither the FRP sheet is unbonded, nor the FRP sheet has ruptured.

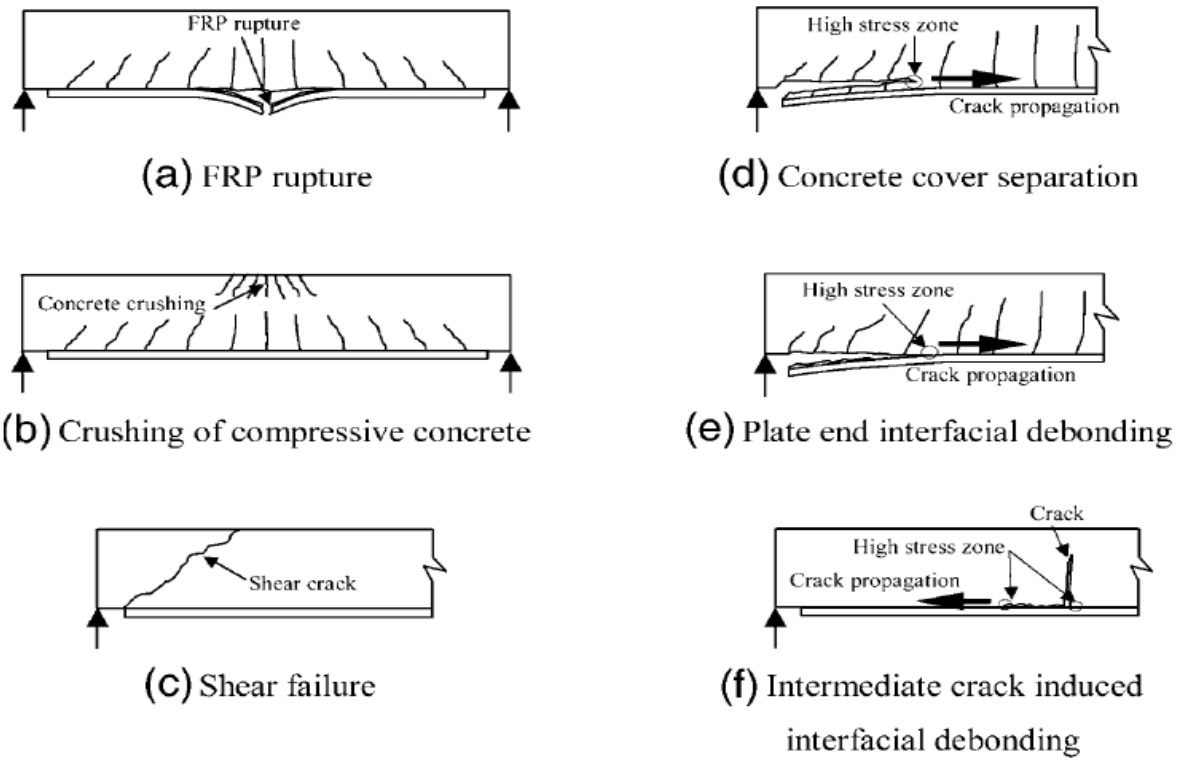

Figure 10 Flexural failure modes of RC beams strengthened with FRP sheets, (Smith. S.T & Teng. J.G, 2001)

2.5.2.2 Shear failures

Beams without FRP

According to Shirazi et al. (2011), beams without FRP reinforcement have the following failure modes:

1. **Shear tension failure** (Fig. 11.a), occurs when the diagonal crack propagates horizontally along the longitudinal reinforcement. One of the main causes is the poor anchorage of reinforcement. Besides, it is likely to happen for slender beams whose shear-span-to-depth ratio is between 2.5 and 6.0.
2. **Shear compression failure** (Fig. 11.b), this occurs at the end of the diagonal crack in the compression zone, which commonly is located around the loading plate that concentrates high stresses. Mostly happens when the concrete strength is not sufficient to support the applying load, showing it up as concrete crushing.

3. **Diagonal tension failure** (Fig. 11.c)**,** this failure is provoked by an inadequate shear reinforcement, forming a diagonal crack of 45°.
4. **Web crushing failure** (Fig. 11.d) commonly occurred in members with thin webs such as I or T profiles.
5. **Arch rib failure** (Fig. 11.e) usually happens in deep beams with inadequate shear reinforcement, provokeing the buckle of the web as well as the crushing and anchorage failure.

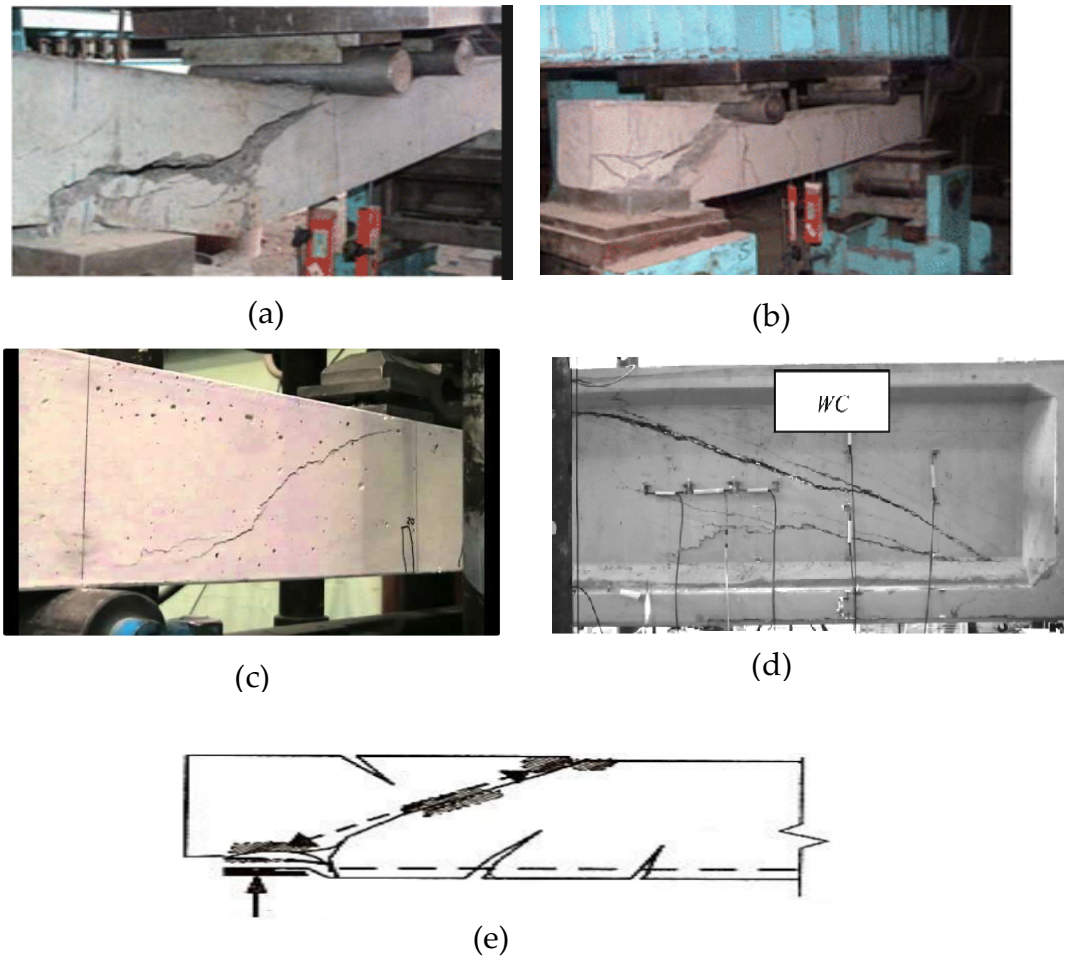

Figure 11 Shear failures of beams without FRP, (Google 2019)

Beams with FRP reinforcement

According to Cheng et al., (2010), there are seven failures modes but just two of them are the most common. Below an explanation of all of them is given according to its theoretical importance.

1. **FRP rupture** (Fig. 12.a)***:*** occurs when the maximal strain in the FRP reaches its ultimate strain. This failure mode is likely to happen to beams fully strengthened or in some cases, U-jacketing beams. This failure mode can co-exist with concrete crushing in the beam web where diagonal cracks co-exists.

Note that for many experiments, it has been observed that prior to FRP rupture there are some zones where the FRP has partially debonded. Such partial deboning however does not affect at all to shear capacity.

2. **Debonding of the FRP from the substrate concrete:** this failure mode is very common for beams side bonded and U-jacketing systems. In this case the failure initiates in the vicinity of a shear crack, and then propagates away from it. Then, when debonding has reached the free-end of an FRP strip, complete debonding of this strip occurs, followed by the shear failure of the beam. It is important to note that strips at some places may debonds first because of the non-uniform distribution of bond length and the shear crack-width. Nevertheless, own to the rapidity of the failure process, it is hard to determine the entire failure process Cheng et al., (2010).
3. **Fully peeling off of the concrete cover by the FRP*:*** usually happens when the FRP stiffness is larger than the concrete stiffness.
4. **Shear failure prior to FRP rupture*:*** common for FRP strengthening systems where the ultimate strain is very large. This failure mode was observed by Chajes et al. (2001) when an aramid strip with an ultimate strain of 2.5% was used.
5. **Local concrete crushing failure*:*** mostly observed with beams highly reinforced in shear.
6. **Local failure of FRP anchoring system*:*** usually observed in beams with U-jacketing system where the use of anchors implies high stress concentration.
7. **Combination of FRP rupture and FRP debonding*:*** as observed by Zhang et al. (2003) with a deep beam reinforced with a U system.

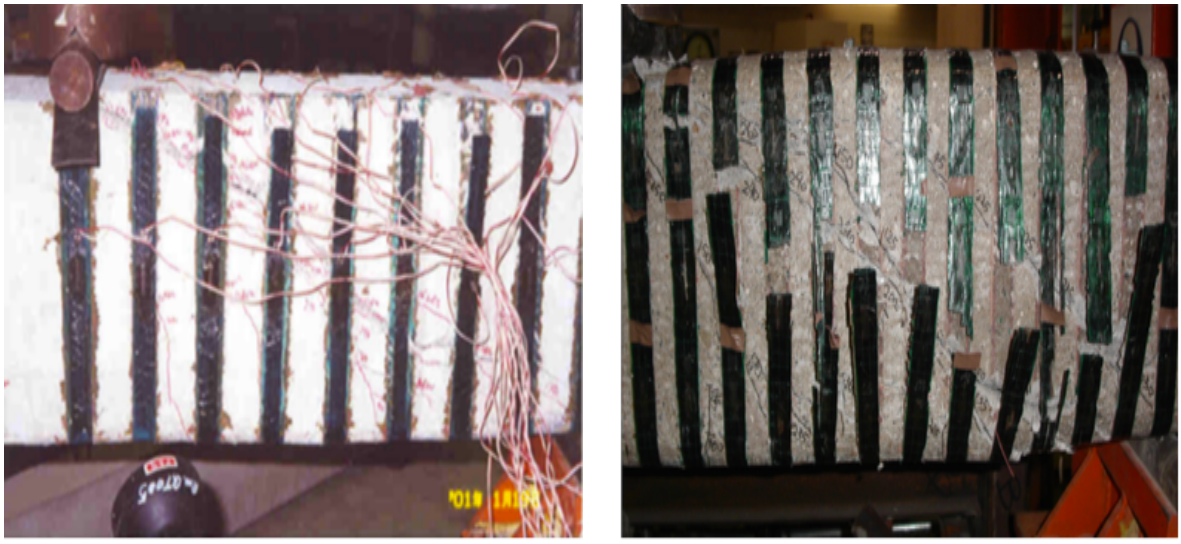

(a) (b)

Figure 12 Most common failure modes in beams retrofitted with FRP, (Cheng et al., 2010)

2.5.3 Failure prevention methods

As previously described, there are two common failure modes when using FRP as a strengthening material: (1) FRP rupture, which usually appear in fully bonded beams, is the most desirable one because the full strength of the FRP was used and therefore, its contribution to shear or flexure strength is maximal; (2) FRP debonding, commonly occurred in U-jacketing systems or side bonded beams, being the most undesirable due to its unpredictable and brittle behavior.

As it can be noticed, a special attention must be given to the later one in order to not only avoid its uncertain nature, but also to help the FRP sheet to use as much as possible its strength to shear or flexural strength of the beam. According to ACI 440.2R-08, FRP anchorage systems can be used to prevent or delay such failure mode. Nonetheless, it does not offer any practical information about its design and dimensioning. According to Cheng et al. (2010), a possible anchoring system would be as the one represented in Figure 13 where two important conclusions are obtained: (1) the zones where debonding starts depending on the shear crack can be identified and (2) depending on the crack pattern, the zones where the FRP anchors must be placed can be identified. For instance, if FRP sheet is expected to contribute to flexural strength, FRP sheets must be placed on the tensile sides of the beam, while anchors should be placed at the ends of the beam and along of the beam's length for two principal reasons: restraint plate end debonding and prevent intermediate crack induced debonding Cheng et al. (2010). On the other side, if FRP is expected to contribute to shear strength, FRP sheets must be placed on the side faces of the beam, while anchors should be placed at the free end of the FRP sheet.

A troublesome effect linked with the use of FRP anchors is the high stresses concentration around anchors. ACI 440.2R-08 proposes some recommendations to follow so as to reduce such effect, they are: (1) terminate the FRP sheet as close as possible to areas of zero stress; (2) increase the distance between the zones with maximum stress in the FRP sheet and the debonded length; (3) round the edges of FRP sheet to reduce stress concentration.

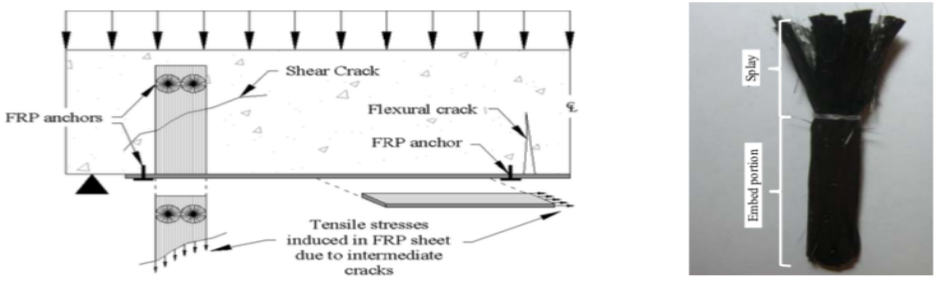

Figure 13 (Left) FRP anchoring system, (Right) FRP anchor, (Cheng et al., 2015)

2.6 Tests on Deep Beams retrofitted with FRP strips

2.6.1 Test setup

Since one major goal of this work is to validate the modified 5SM against experimental data, it is vital to choose the right tests to do so. As previously described, there exists more information about tests where the contribution of FRP to flexure is investigated rather than those where the contribution to shear is investigated. However, during the last decade it was noticed that the number of tests where the contribution to shear strength of FRP has raised considerably. Sarsam and Nabeel (2017) for instance, tested seven deep beams retrofitted with FRP strips, and analyzed their contribution to shear behavior depending on the FRP's orientation and the number of FRP layers. Bukhari et al. (2013) tested 12 short span reinforced concrete beams retrofitted with FRP. Their research focused on the effect to shear behavior depending on the FRP arrangement, the ratio between the depth of the FRP sheet and the depth of the beam and the area covered by FRP. Rasheed et al. (2016) tested 18 deep beams focusing on the influence of a/d ratio, vertical and horizontal shear reinforcement ratio and the amount of FRP.

Among of the available experimental test, only those matching the following requirements will be selected:

- The shear span-to-depth ratio (a/d) is lower than 2.5. Otherwise, 5SM cannot predict accurately its behavior given that a slender beam is considered instead a deep beam.
- FRP strips are perpendicular to the longitudinal axis of the beam. This is mainly due to the fact that the contribution of horizontal strips is not implemented in 5SM, and its contribution in shear is not as much as vertical strips as discussed in section 2.5.1.
- FRP strips do not have any anchorage systems. This was due to the fact that modified 5SM considers only two possible failure modes: FRP rupture or FRP debonding from the concrete surface, but not FRP anchorage failure.
- Its failure mode is other than concrete crushing around the loading or supporting plates. This is mainly because around these zones high stress concentration is localized in a narrow zone, and as occurs with FRP anchors, our modified 5SM does not consider such failure mode.
- They have only vertical shear reinforcement. Such restriction is due to our model capture just the effect of vertical shear reinforcement.

Given all the restrictions only the tests made by Bukhari and Rasheed were considered relevant for the validation of the modified 5SM. The geometrical and

mechanical properties for each test are summarized in the Figure 14 and in the Table 4-6. Nevertheless, it is important to highlight some important points:

- In Rasheed tests, there were some beams with horizontal shear reinforcement, and some other whose failure mode is concrete crushing. Those characteristics would discard those beams. However, they will be considered to predict the contribution to shear of horizontal shear reinforcement, and know what is the impact on the predicted and experimental result of such restriction.
- In all Bukhari tests, their shear-span to depth ratio is slightly closer to that of a slender beam, yet they are considered.
- Values highlighted in yellow are not directly given by the authors but could be obtained directly with the given geometrical or mechanical data. In the case of $\varepsilon_{FRP,u} = f_{FRP,u} / E_{FRP}$
- Values highlighted in blue are not given by the authors but guessed. An especial attention must be payed to l_{b2} of Bukhari tests since it was not given but assumed to be very little. However, such assumption implies having high stress concentration at those zones, and therefore shear compression failure that extended 5SM is not able to capture.
- For FRP properties in the configuration tab, WS means Wrapping scheme having three possibilities: S = side bonding; U= U-jacketing and W = complete wrapping. It can also be seen the words of FT meaning Fiber type, having 3 possible options, C= Carbon; G = Glass and 0 meaning no wrapping. And finally, PD meaning pre-damaged or not, if it is true the value assigned was 1 , if not the value assigned was 0.

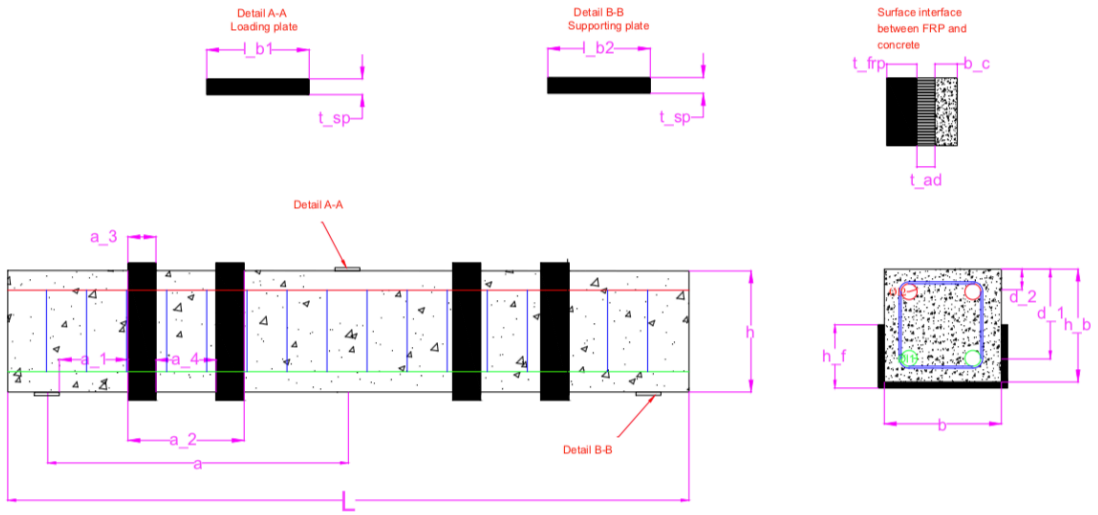

Figure 14 FRP and deep beam geometrical data

Author	Year	Name	a/d	Steel loading plate			Concrete properties						Longitudinal reinforcement								
							Geometric					Resistance	Resistance				Bottom configuration				
				t_{sp}	l_{b1}	l_{b2}	b	h	L	a	a_g	f_c'	f_y	f_u	ε_u	E_s	# bars	ϕ_{s1}	As_1	d_1	ρ_{t1}
			[-]	[mm]	[mm]	[mm]	[mm]	[mm]	[mm]	[mm]	[mm]	[MPa]	[MPa]	[MPa]	[-]	[GPa]	[-]	[mm]	[mm²]	[mm]	[%]
Bukhari	2010	CB	2.27	50	150	10	150	300	1675	600	19	49.13	494	543.4	0.1	200	2	19	567.06	264.36	1.43
		C-2	2.27	50	150	10	150	300	1675	600	19	49.1	494	543.4	0.1	200	2	19	567.06	264.36	1.43
		C-3	2.27	50	150	10	150	300	1675	600	19	48.28	494	543.4	0.1	200	2	19	567.06	264.36	1.43
		C-4	2.27	50	150	10	150	300	1675	600	19	49.1	494	543.4	0.1	200	2	19	567.06	264.36	1.43
		C-5	2.27	50	150	10	150	300	1675	600	19	48.62	494	543.4	0.1	200	2	19	567.06	264.36	1.43
		C-6	2.27	50	150	10	150	300	1675	600	19	49.79	494	543.4	0.1	200	2	19	567.06	264.36	1.43
		C-7	2.27	50	150	10	150	300	1675	600	19	48.97	494	543.4	0.1	200	2	19	567.06	264.36	1.43
		C-8	2.27	50	150	10	150	300	1675	600	19	47.93	494	543.4	0.1	200	2	19	567.06	264.36	1.43
		C-9	2.27	50	150	10	150	300	1675	600	19	50.35	494	543.4	0.1	200	2	19	567.06	264.36	1.43
		C-10	2.27	50	150	10	150	300	1675	600	19	51.38	494	543.4	0.1	200	2	19	567.06	264.36	1.43
		C-11	2.27	50	150	10	150	300	1675	600	19	49.38	494	543.4	0.1	200	2	19	567.06	264.36	1.43
		C-12	2.27	50	150	10	150	300	1675	600	19	48.41	494	543.4	0.1	200	2	19	567.06	264.36	1.43
Rasheed	2016	DB-1	1.10	20	150	75	115	400	1200	400	10	34	500	550	0.1	200	2	20	628.32	365	1.5
		DB-2	1.10	20	150	75	115	400	1200	400	10	34	500	550	0.1	200	2	20	628.32	365	1.5
		DB-3	1.10	20	150	75	115	400	1200	400	10	34	500	550	0.1	200	2	20	628.32	365	1.5
		DB-4	1.10	20	150	75	115	400	1200	400	10	34	500	550	0.1	200	2	20	628.32	365	1.5
		DB-5	1.10	20	150	75	115	400	1200	400	10	34	500	550	0.1	200	2	20	628.32	365	1.5
		DB-6	1.10	20	150	75	115	400	1200	400	10	34	500	550	0.1	200	2	20	628.32	365	1.5
		DB-7	1.10	20	150	75	115	400	1200	400	10	34	500	550	0.1	200	2	20	628.32	365	1.5
		DB-8	0.86	20	150	75	115	500	1200	400	10	34	500	550	0.1	200	2	20	628.32	465	1.17
		DB-9	1.34	20	150	75	115	333	1200	400	10	34	500	550	0.1	200	2	20	628.32	298	1.83
		RDB-1	1.10	20	150	75	115	400	1200	400	10	34	500	550	0.1	200	2	20	628.32	365	1.5
		RDB-2	1.10	20	150	75	115	400	1200	400	10	34	500	550	0.1	200	2	20	628.32	365	1.5
		RDB-3	1.10	20	150	75	115	400	1200	400	10	34	500	550	0.1	200	2	20	628.32	365	1.5
		RDB-4	1.10	20	150	75	115	400	1200	400	10	34	500	550	0.1	200	2	20	628.32	365	1.5
		RDB-5	1.10	20	150	75	115	400	1200	400	10	34	500	550	0.1	200	2	20	628.32	365	1.5
		RDB-6	1.10	20	150	75	115	400	1200	400	10	34	500	550	0.1	200	2	20	628.32	365	1.5
		RDB-7	1.10	20	150	75	115	400	1200	400	10	34	500	550	0.1	200	2	20	628.32	365	1.5
		RDB-8	0.86	20	150	75	115	500	1200	400	10	34	500	550	0.1	200	2	20	628.32	465	1.17
		RDB-9	1.34	20	150	75	115	333	1200	400	10	34	500	550	0.1	200	2	20	628.32	298	1.83

Table 4 Rasheed and Bukhari tests data

Name	Longitudinal reinforcement					Shear reinforcement									FRP properties								
	Top configuration					Resistance			Vertical config.			Horizontal config.			Configuration			Geometry						
	# bars	ϕ_{s2}	A_{S2}	d_2	ρ_{t2}	f_{yv}	E_v	ε_{uv}	ϕ_{sv}	s_{vv}	ρ_{sv}	ϕ_{sh}	s_{vh}	ρ_{sh}	WS	FT	PD	$a_{FRP,1}$	$a_{FRP,2}$	$a_{FRP,3}$	$a_{FRP,4}$	t_{FRP}	h_{FRP}
	[-]	[mm]	[mm²]	[mm]	[%]	[MPa]	[GPa]	[%]	[mm]	[mm]	[%]	[mm]	[mm]	[%]	[-]	[-]	[-]	[mm]	[mm]	[mm]	[mm]	[mm]	[mm]
CB	2	10	157.1	273.86	0.38	0	0	0	0	0	0	0	0	0	0	0	0	0	0	0	0	0	0
C-2	2	10	157.1	273.86	0.38	0	0	0	0	0	0	0	0	0	S	C	0	0	600	75	0	0.34	150
C-3	2	10	157.1	273.86	0.38	0	0	0	0	0	0	0	0	0	S	C	0	145	300	75	0	0.34	300
C-4	2	10	157.1	273.86	0.38	0	0	0	0	0	0	0	0	0	S	C	0	145	300	75	0	0.34	150
C-5	2	10	157.1	273.86	0.38	0	0	0	0	0	0	0	0	0	S	C	0	0	600	75	0	0.34	300
C-6	2	10	157.1	273.86	0.38	0	0	0	0	0	0	0	0	0	S	C	0	220	150	75	0	0.34	300
C-7	2	10	157.1	273.86	0.38	0	0	0	0	0	0	0	0	0	S	C	0	0	300	75	0	0.34	150
C-8	2	10	157.1	273.86	0.38	0	0	0	0	0	0	0	0	0	S	C	0	70	150	75	0	0.34	300
C-9	2	10	157.1	273.86	0.38	0	0	0	0	0	0	0	0	0	S	C	0	0	300	75	0	0.34	300
C-10	2	10	157.1	273.86	0.38	0	0	0	0	0	0	0	0	0	S	C	0	220	150	75	0	0.34	150
C-11	2	10	157.1	273.86	0.38	0	0	0	0	0	0	0	0	0	S	C	0	110	75	75	0	0.34	300
C-12	2	10	157.1	273.86	0.38	0	0	0	0	0	0	0	0	0	S	C	0	70	150	75	0	0.34	150
DB-1	2	4	25.13	378	0.06	0	0	0	0	0	0	0	0	0	0	0	0	0	0	0	0	0	0
DB-2	2	4	25.13	378	0.06	400	200	0.1	4	200	0.25	4	85	0.25	0	0	0	0	0	0	0	0	0
DB-3	2	4	25.13	378	0.06	400	200	0.1	6	160	0.52	6	110	0.52	0	0	0	0	0	0	0	0	0
DB-4	2	4	25.13	378	0.06	400	200	0.1	4	60	0.3	0	0	0	0	0	0	0	0	0	0	0	0
DB-5	2	4	25.13	378	0.06	400	200	0.1	6	80	0.5	0	0	0	0	0	0	0	0	0	0	0	0
DB-6	2	4	25.13	378	0.06	400	200	0.1	0	0	0	4	45	0.3	0	0	0	0	0	0	0	0	0
DB-7	2	4	25.13	378	0.06	400	200	0.1	0	0	0	6	65	0.5	0	0	0	0	0	0	0	0	0
DB-8	2	4	25.13	478	0.045	400	200	0.1	4	130	0.25	4	110	0.25	0	0	0	0	0	0	0	0	0
DB-9	2	4	25.13	311	0.07	400	200	0.1	4	265	0.25	4	65	0.25	0	0	0	0	0	0	0	0	0
RDB-1	2	4	25.13	378	0.06	0	0	0	0	0	0	0	0	0	U	C	1	62.5	200	50	100	0.13	400
RDB-2	2	4	25.13	378	0.06	400	200	0.1	4	200	0.25	4	85	0.25	U	C	1	62.5	200	50	100	0.13	400
RDB-3	2	4	25.13	378	0.06	400	200	0.1	6	160	0.52	6	110	0.52	U	C	1	62.5	200	50	100	0.13	400
RDB-4	2	4	25.13	378	0.06	400	200	0.1	4	60	0.3	0	0	0	U	C	1	62.5	200	50	100	0.13	400
RDB-5	2	4	25.13	378	0.06	400	200	0.1	6	80	0.5	0	0	0	U	C	1	62.5	200	50	100	0.13	400
RDB-6	2	4	25.13	378	0.06	400	200	0.1	0	0	0	4	45	0.3	U	C	1	62.5	200	50	100	0.13	400
RDB-7	2	4	25.13	378	0.06	400	200	0.1	0	0	0	6	65	0.5	U	C	1	62.5	200	50	100	0.13	400
RDB-8	2	4	25.13	478	0.045	400	200	0.1	4	130	0.25	4	110	0.25	U	C	1	62.5	200	50	100	0.13	500
RDB-9	2	4	25.13	311	0.07	400	200	0.1	4	265	0.25	4	65	0.25	U	C	1	62.5	200	50	100	0.13	333

Table 5 Rasheed and Bukhari tests data. cont.

Name	FRP properties					Experimental Results	
	Resistance			Adhesive			
	$f_{FRP,u}$	$\varepsilon_{FRP,u}$	E_{FRP}	t_{ad}	E_{ad}	V/P	V_{EXP}
	[MPa]	[-]	[MPa]	[mm]	[MPa]	[-]	[kN]
CB	0	0	0	0	0	0.5	121.15
C-2	3450	0.0147	234500	-	-	0.5	153.85
C-3	3450	0.0147	234500	-	-	0.5	153.85
C-4	3450	0.0147	234500	-	-	0.5	134.65
C-5	3450	0.0147	234500	-	-	0.5	187.55
C-6	3450	0.0147	234500	-	-	0.5	134.65
C-7	3450	0.0147	234500	-	-	0.5	139.5
C-8	3450	0.0147	234500	-	-	0.5	139.45
C-9	3450	0.0147	234500	-	-	0.5	168.25
C-10	3450	0.0147	234500	-	-	0.5	129.85
C-11	3450	0.0147	234500	-	-	0.5	129.85
C-12	3450	0.0147	234500	-	-	0.5	125
DB-1	0	0	0	0	0	0.5	94.5
DB-2	0	0	0	0	0	0.5	199
DB-3	0	0	0	0	0	0.5	217.5
DB-4	0	0	0	0	0	0.5	207.5
DB-5	0	0	0	0	0	0.5	209
DB-6	0	0	0	0	0	0.5	99
DB-7	0	0	0	0	0	0.5	134.5
DB-8	0	0	0	0	0	0.5	208.5
DB-9	0	0	0	0	0	0.5	178.5
RDB-1	3500	0.0152	230000	1	3800	0.5	209
RDB-2	3500	0.0152	230000	1	3800	0.5	267.5
RDB-3	3500	0.0152	230000	1	3800	0.5	234.5
RDB-4	3500	0.0152	230000	1	3800	0.5	277.5
RDB-5	3500	0.0152	230000	1	3800	0.5	302
RDB-6	3500	0.0152	230000	1	3800	0.5	259
RDB-7	3500	0.0152	230000	1	3800	0.5	236
RDB-8	3500	0.0152	230000	1	3800	0.5	267
RDB-9	3500	0.0152	230000	1	3800	0.5	251.5

Table 6 Rasheed and Bukhari tests data cont.

2.6.2 Tests by Bukhari

Bukhari and Vallum (2013) conducted a study with 12 short span reinforced concrete beams strengthened with externally bonded carbon fiber reinforced polymers (CFP). The main parameter observed in this research was the influence on shear behavior when changing the area and location of the CFRP sheet within the shear span.

All of the individual specimens had depth of 300 mm, width of 150 mm, length of 1675 mm, maximum aggregate size of 19 mm and yield strength of longitudinal reinforcement of 494 MPa. Shear-span-to-depth ratio was equal to 2.27 indicating that the beam is likely to have flexural-shear failure in some specimens, and therefore extended 5SM would not able predict very well. Tensile flexural reinforcement consists of 2 reinforcement bars with 19 mm diameter, while compressive reinforcement consists of 2 reinforcement bars with 10 mm diameter. Since the resistance parameters of the longitudinal reinforcement are not given, they are assumed. The ultimate strength is 10% more than f_y and the ultimate strain ε_u is assumed to be equal to 10%. Regarding vertical or horizontal shear reinforcement, none of them was used. With respect to the CFRP configuration, beams were divided into two groups. Group A comprises beams where the depth of the CFRP sheet is equal to beam's depth, whilst Group B comprises beams where the depth of the CFRP sheet is half to beam's depth as shown in Figure 15. Each CFRP sheet has thickness of 0.34 mm, Young Modulus of 234.5 GPa and ultimate tensile stress of 3450 MPa. Compressive cylinder strength of the concrete ranges from 49.1 to 51.38 MPa.

The test setup was as follows. Once the beams were casted and cured in steel molds, their surface were cleaned to avoid having any material that impedes the good bonding between the adhesive and the concrete surface. Then, a two part-epoxy adhesive was applied according to the manufacturer's recommendation, and then again, the beam's surfaces were grounded and cleaned to remove any loose dust particles. Next, the CFRP sheet was cut to its final length and infused with epoxy resin before being applied on the concrete surface. Finally, the sheets were applied but paying attention to two things: (1) the fiber's orientation, which was due to be vertical; (2) the presence of air bubbles between the epoxy adhesive and the sheet, and the excess of resin. Both of them eliminated by using a plastic roller. Each beam was tested under three-point loading, where at each increment in load, deflection and crack pattern were recorded at mid-span and supports. The layout of the longitudinal reinforcement, the CFRP sheet configuration and the test setup are given in the Figure 16.

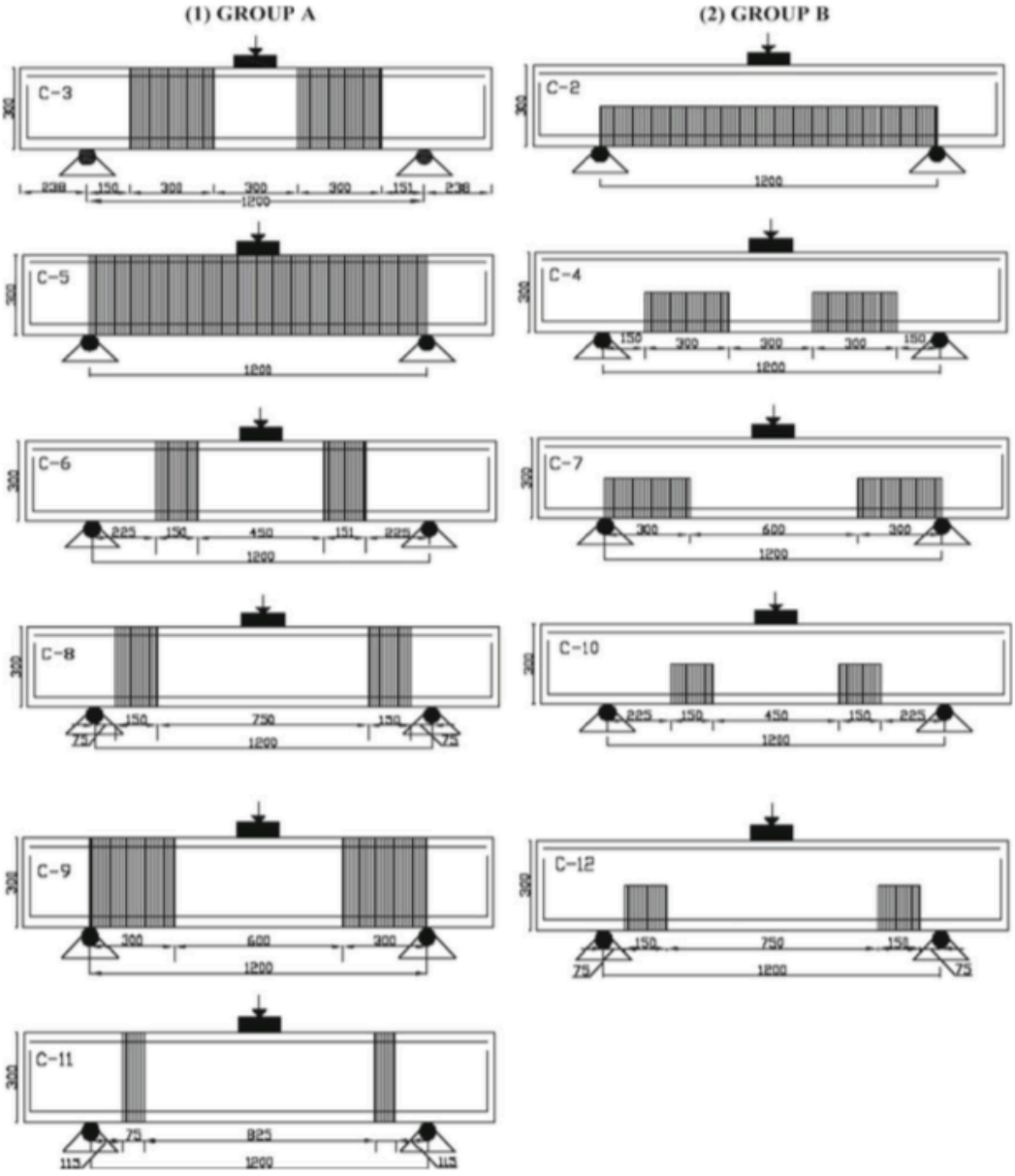

Figure 15 Beam's geometrical data and CFRP configuration, (Bukhari and Vollum, 2013)

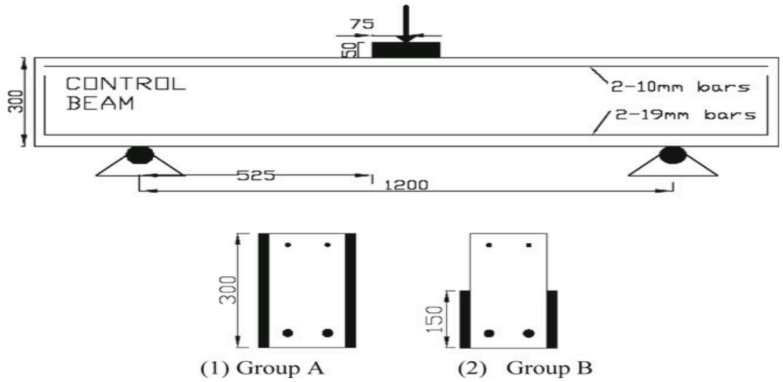

Figure 16 Beam's cross-section and setup, (Bukhari and Vollum, 2013)

2.6.3 Tests by Rasheed

Rasheed et al. (2016) also conducted a study with 18 reinforced concrete deep beams. Its main purpose was to determine the influence of vertical and horizontal shear reinforcement, shear-span-to-depth ratio and the presence of CFRP strips to the shear strength. In this case, deep beams were first tested under static loading failure. Then, they were retrofitted with external CFRP strips and reloaded again until failure.

All tested specimens, as shown in Figure 17, have depth of 400 mm, width of 115 mm, length of 1200 mm, maximum aggregate size of 10 mm and an average cylindrical compressive strength of 34 MPa. Tension flexural reinforcement was composed with 2 longitudinal steel bars of 20 mm diameter, whilst the longitudinal reinforcement on the compression side is formed with 2 steel bars of 4 mm diameter. They both are composed with steel of yielding stress of 500 MPa. Shear-span-to-depth ratio varies from 0.86 to 1.34. Ratio of horizontal and vertical transverse reinforcement varies from 0 to 0.05, with yielding strength of 400 MPa. With respect to external reinforcement, strips of 0.13 mm thickness were wrapped around each tested deep beam, Young Modulus of 230 GPa and ultimate tensile stress of 3500 MPa. Tested deep beams were supported with two steel rollers located 200 mm far from each end of the beam.

The test setup is shown in the Figure 18. First of all, 9 simply supported deep beams were loaded to failure under three-point bending measuring at each load step deflections at mid-span, and the corresponding applied load. This was done with the help of a universal hydraulic machine that applies a certain load to the beam, and also with the help of dial gauges that measures deflections. Once deflections and applied loads for the non-retrofitted beams (DB) are obtained, the retrofitting of those beams with 4 CFRP strips was applied, and then beams were again reload to failure.

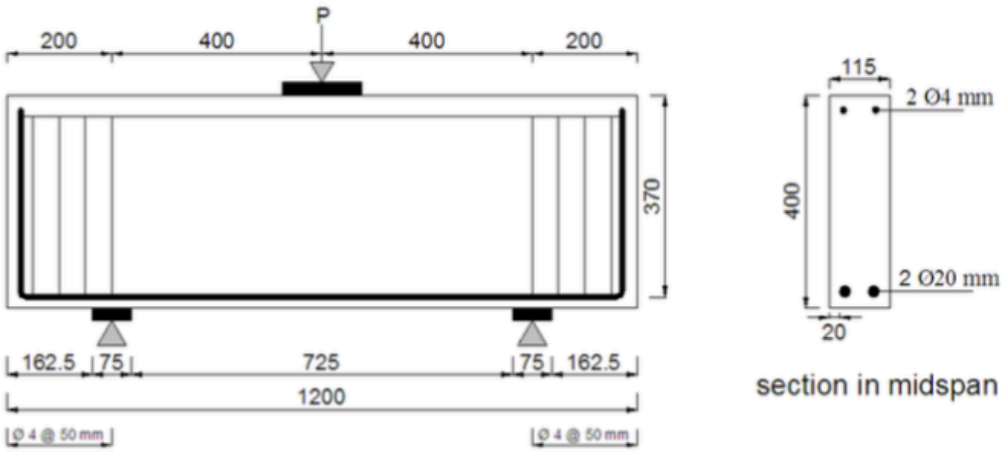

Figure 17 Rasheed deep beam's cross-section, (Bukhari and Vollum, 2013)

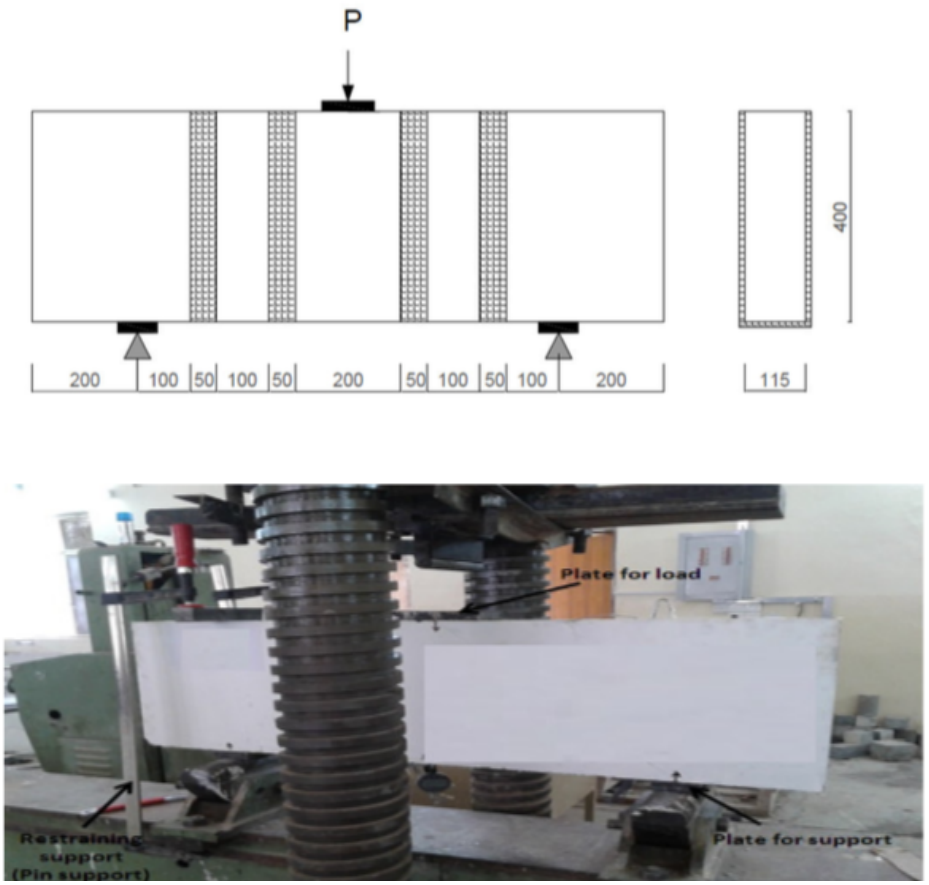

Figure 18 Rasheed deep beam setup, (Rasheed et al.,2016)

3 Modelling approaches for deep beams

When designing deep beams strengthened with FRP strips/sheets, there are three ways to do so. The first one is by using Strut-and-Tie models. The second one uses software that solve the problem with Finite Element analysis. And last but not least, 2PKT model developed by Mihaylov et al. (2013).

3.1 Strut and tie models

During the last years, several strut-and-tie models for the analysis of deep beams retrofitted with FRP have been proposed. However, despite their differences all of them use the same basic principle of strut-and-tie models.
The model proposed by Sagaseta and Vollum (2009) considers that the shear force is transferred directly to the supporting points via 2 ways: (1) a direct strut – dark grey in Figure 19 - and a truss system consisting of two indirect struts - Strut II and Strut III - equilibrated by stirrups. Even though this method is easy to apply, and is consistent with the design recommendations in EC2, it also imposes some restrictions that impedes its use for a general case. It considers that the depth of the FRP sheet must be equal to the depth of the beam. It also considers that the FRP sheet is placed in the center of the shear span and that the critical failure mode is the crushing of the direct strut (diagonal crack). As it can be noticed, not all the members will match these conditions, thereby it should be used carefully.

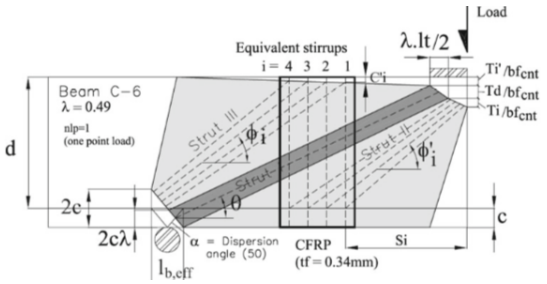

Figure 19 Strut-and-Tie model proposed by Sagaseta and Vollum, (Bukhari and Vollum, 2013)

3.2 Finite element modelling

Another way to analyze deep beams retrofitted with FRP is with Finite Elements models. Generally, they provide better results than strut-and-tie models since the variables involved during the analysis is higher. However, they also have some disadvantages that sometimes impedes their use: (1) they are time-consuming since a good definition of the boundary conditions must be done and also a full definition of the geometrical and mechanical properties of each finite element should be given; (2) they are not effective in capturing the post-peak behavior of reinforced concrete deep beams (Mihaylov et al. 2015).

3.3 Two-Parameter Kinematic Theory and Five-Spring Model

3.3.1 2PKT model

The Two-Parameter Kinematic Theory developed by Mihaylov et al. (2013), is a model capable of describing the deformed shape of deep beams, under single curvature, based on two degrees of freedom. This model is combined with equilibrium equations and stress-strain relationships to predict the shear strength and deformation patterns of deep beams at shear failure, Mihaylov et al. 2013). With this model, engineers are able not only to evaluate the safety of a building but also, they can assess crack deformations and crack widths. This can be very useful for structures that are about to collapse since engineers will be able to know for a given crack-width, what is the load acting on a deep beam and therefore, what is the maximum load that this beam can support. However, despite all of these advantages, this model is only capable of predicting pre-peak behavior, i.e., it cannot be used to know how much load the beam can still support or whether its behavior is ductile or brittle after reaching that peak point. Owing to this, Five Spring model was developed by Mihaylov et al. (2015). This new model, based on 2PKT theory, is capable of predicting the complete pre-and post-peak shear behavior of deep beams. With its help, a better analysis of complex structures comprising deep beams without wasting time or accuracy could be made.
In order to precisely define the 5SM and what are the main parameters involved, it is necessary to define under what assumptions this model relies on. As already mentioned, 5SM is based on 2PKT theory. This latter at the same time, relies under the conclusions drawn by Mihaylov et al. (2008). These indicated that cyclic loading failure does not have a detrimental effect on the shear behavior of deep beams, provided that the longitudinal reinforcement remains elastic.

Besides, members with transverse reinforcement showed an almost perfect envelope between cyclic and monotonic response. Once explained the main foundations used to formulate 2PKT theory, the assumptions of this one can be given.

2PKT assumes that the critical shear crack propagates from the loading point to the support along a straight line and then widens as the load increases. As it can be noticed in the Figure 20, this diagonal crack will divide the shear span into two big concrete blocks. The block located above the diagonal crack will be modelled as a single rigid block, while the block below the crack will be modelled as a series of rigid radial struts connected to the bottom flexural reinforcement.

Both blocks separated by the diagonal crack are thus connected to the bottom flexural reinforcement and the stirrups.

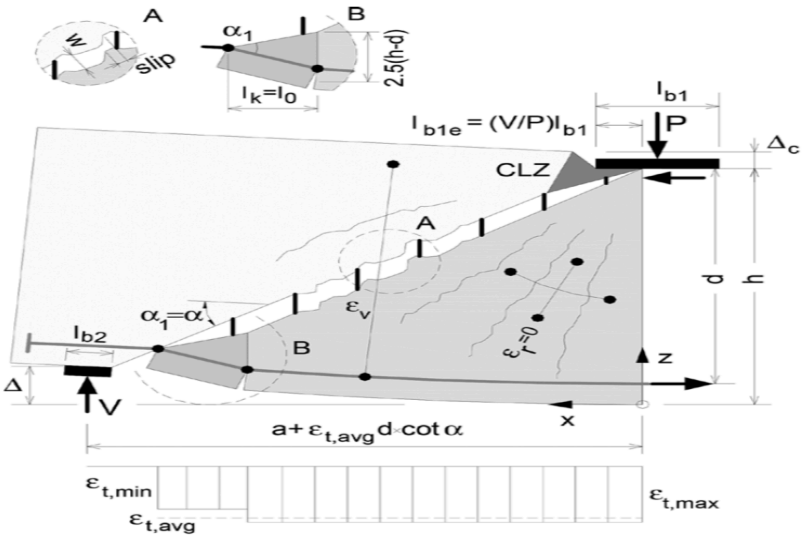

Figure 20 2PKT theory main assumption, (Mihaylov et al., 2013)

2PKT theory also assumes that the movement of each concrete block is different. The motion of the block above the diagonal crack, with respect to the loading plate, will be function of 2 parameters: a rotation about the top of the crack and a vertical translation of it. This rotation will be proportional to the average strain in the bottom reinforcement ($\varepsilon_{t,\,avg}$), and the translation will be function of the vertical displacement of the critical diagonal zone (Δ_c). These two parameters represented in the Figure 21, represent the two degrees of freedom on which this model relies on (Mihaylov et al. 2013). The transverse displacement in the critical loading zone (Δ_c) is normally associated with both widening and slip displacement of the critical shear crack, while the elongation of the bottom flexural reinforcement induces not only the rotation of the rigid radial struts but also the widening of the cracks. In addition to this, it can be observed that these 2 parameters provoke tensile strains in the transverse reinforcement.

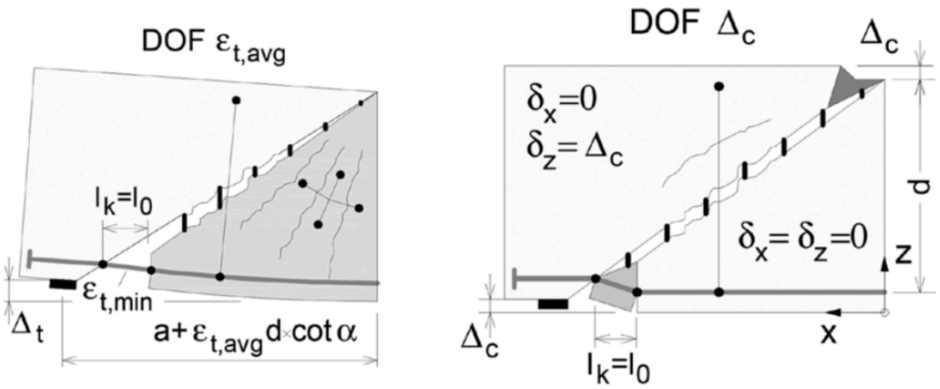

Figure 21 Degrees of Freedom of 2PKT, (Mihaylov et al., 2013)

As it is shown in Figure 22, one can observe that the angle (α_1) of the critical shear crack is dependent on the shear-span-to-depth ratio. The angle (α_1) must be taken as the maximum of two different angles: angle (θ) and angle (α).
On one hand, angle (θ) represents the angle of the cracks developed under the assumption of having a uniform stress field. This angle can be either be calculated with the help of the Modified Compression Field Theory (MFCT) proposed by Vecchio and Collins in 2006, or considering it equal to 35°. For the sake of simplicity, we will consider from now on equal to 35°.
On the other hand, angle (α) is the arctangent between the depth of the beam and the existing distance between the inner edge of the support to the tributary area of the loading plate.
As one can deduce, the higher is the value of (a/d), the more likely to have a slender beam is the chance, and therefore angle (α_1) should be always taken equal to (α). This means that the critical shear crack will always reach the support and the loading points. On the contrary, the smaller is (a/d), the more likely to have a deep beam is the chance, and therefore (α_1) should be taken equal to ($\theta = 35°$). This means that the critical shear crack will not reach the inner edge of the support and therefore the block above the critical crack will be much higher. This angle (α_1) as it will be seen later has a vital importance in the contribution to shear strength of the sheets of FRP.

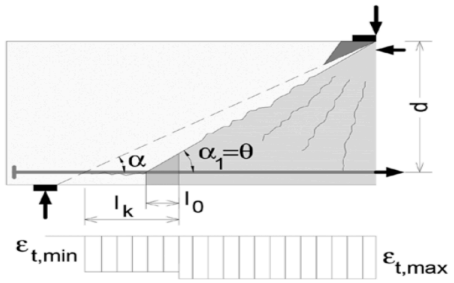

Figure 22 Definition of the angle of the critical shear crack, (Mihaylov et al., 2013)

Once defined the assumptions on which the 2PKT model relies on, horizontal (δ_x) and vertical (δ_z) displacements of all the points of the deep beam can be calculated based on the two degrees of freedom already mentioned.

Vertical and horizontal displacements of points located in the block above the critical crack, are obtained as follows:

$$\delta_x(x,z) = \varepsilon_{t,avg}(h-z)\cot\alpha \quad (1)$$

$$\delta_z(x,z) = \varepsilon_{t,avg}x\cot\alpha + \Delta_c \quad (2)$$

Vertical and horizontal displacements of points located in the block below the critical crack, are obtained as follows:

$$\delta_x(x,z) = \varepsilon_{t,avg}\, x \tag{3}$$

$$\delta_x(x,z) = \frac{\varepsilon_{t,avg}\, x^2}{h-z} \tag{4}$$

Another advantage that 2PKT model offers is the possibility of determining the width of the critical shear crack (Mihaylov et al., 2013). As shown in the equation (5), crack width depends not only on the two degrees of freedom of the Kinematic Model, but also on the length of the bottom reinforcement (l_k). The length (lk) is assumed to be equal to the length of the dowels provided by bottom longitudinal reinforcement and it is its elongation which contributes to the width of the critical crack. At the same time, the length (l_k) also depends on the value (l_0) being this equal to the length of the heavily cracked zone at the bottom of the critical shear crack, whose value must be higher than the spacing of the radial cracks at the bottom of the section (s_{max}).

$$w = \Delta_c \cos\alpha_1 + \frac{\varepsilon_{t,min}\, l_k}{2\sin\alpha_1} \tag{5}$$

$$l_k = l_0 + d(cot\,\alpha - \cot\alpha_1) \tag{6}$$

$$l_0 = 1.5(h-d)\cot\alpha_1 \geq s_{max} \tag{7}$$

$$s_{max} = \frac{0.28\, d_b}{\rho_{l1}}\,\frac{2.5\,(h-d)}{d} \tag{8}$$

3.3.2 Five-spring model or 2PKT model extended

Based on the assumptions developed to the 2PKT model, Mihaylov et al., 2015 extended such model and developed the 5SM model.

One of the fundamental contributions of 5SM, is the ability to predict the overall deflections (Δ) of deep beams based on the 2 degrees of freedom from the 2PKT model. Deflection (Δ) is defined as the relative vertical displacement between the zone with maximum bending moment and the loading plate. This value is obtained by replacing in equation (2) the x coordinate with the length of the shear span (a). Thus, the formula below is obtain:

$$\delta_z(x,z) = \varepsilon_{t,avg} x\cot\alpha + \Delta_c \rightarrow \Delta = \frac{\varepsilon_{t,avg}\, l_t}{d}\, a + \Delta_c = \Delta_t + \Delta_c \tag{9}$$

In equation (9), the value $\varepsilon_{t,avg}\, l_t$ corresponds to the elongation of the flexural reinforcement, whilst $\frac{\varepsilon_{t,avg}\, l_t}{d}$ corresponds to the angle of rotation of the rigid block about the loading point. As one can notice in equation (9) as well, the overall

deflection is composed of two different values. The deflection (Δ_t) linked to the strains in the flexural bottom reinforcement, and the deflection (Δ_c) linked to the shear deformations. In other words, deflection (Δ) is obtained taking into account the deflections from shear and flexure. Based on this, the shear span can be represented by a series of 5 springs connected in series and loaded by shear force V, as shown in Figure 23.

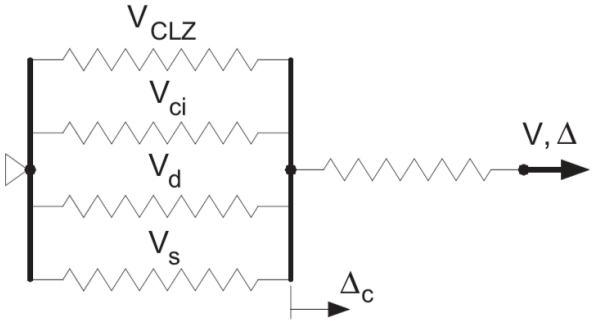

Figure 23 Springs of the Five-Spring model, (Mihaylov et al.,2015)

According to Figure 23, shear behavior is considered with the set of 4 parallel springs that elongates (Δ_c), whereas flexural behavior is considered with the remaining spring that elongates (Δ_t). In Figure 23, one can also observe that this set of 5 springs represents the different forces that contribute to shear behavior.
On one hand, we have the different forces that contribute to vertical equilibrium of the block, as shown in the free-body diagram of the Figure 24. Force V_{clz} represents the shear carried in the critical loading zone, V_{ci} represents the aggregate interlock shear along the critical shear crack, V_s represent the shear carried by the vertical transverse reinforcement and V_d represent the shear carried by the dowel action of the bottom flexural reinforcement (Mihaylov et al., 2015).
On the other hand, the force in the flexural spring is the shear derived from moment equilibrium in the shear span. This equilibrium is calculated with respect to the point of application of the compression force C in the section with maximum moment. The equilibrium results in a shear force (V) obtained according to the equation (10):

$$V = \frac{T(0.9d)}{a}; where \begin{cases} T = tension\ force\ in\ the\ flexural\ reinforcement \\ 0.9\ d = lever\ arm\ between\ forces\ C\ and\ T \end{cases} \quad (10)$$

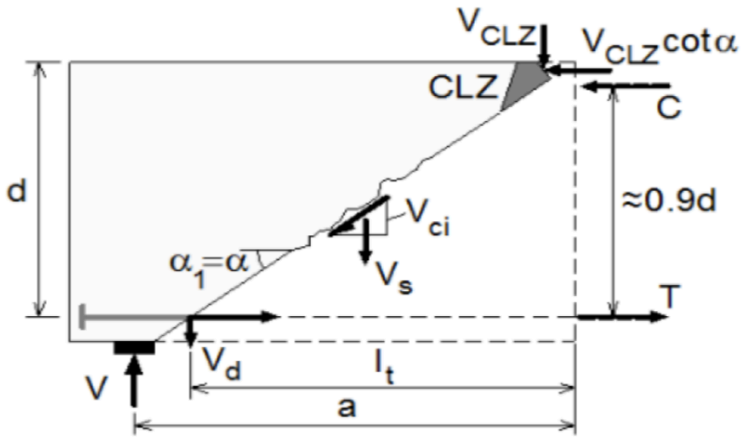

Figure 24 Free-body diagram of the rigid block

In conclusion, the equilibrium of the five different forces acting on a deep beam can be expressed as showed in the equation (11). Based on this equation, one can deduce that the beam will fail at shear, along a critical shear crack, if the right-hand side of the equation is lower than the left-side. On the other side, the beam will fail at flexure, if the right-hand side is lower than the left-side. This means that the flexural reinforcement at the section with maximum moment has yielded.

$$V = \frac{T(0.9d)}{a} = V_{clz} + V_{ci} + V_s + V_d \tag{11}$$

As one can notice, each of these forces is not yet expressed as a function of displacements (Δ_t) and (Δ_c), or as a function of the two degrees of freedom from the 2PKT model (Δ_c) and $\varepsilon_{t,avg}$. This is necessary to evaluate the equilibrium given by the equation 11.

Tension in the bottom flexural reinforcement **(T)** can be expressed as a function of $\varepsilon_{t,avg}$ according to the equation 12 as follows:

$$T = E_s A_s \varepsilon_{t,avg} + \frac{0.33\, f_c}{\sqrt{1 + 200\varepsilon_{t,avg}}} A_{c,eff} \leq A_s f_y \tag{12}$$

$$A_{c,eff} = b.min\left\{2.5(h-d); \frac{h}{2}\right\} \tag{13}$$

Left-hand side of equation 12 is comprised with two components that represent a different effect; (1) left component models the behavior of bare elastic reinforcement, (2) right component represents the concrete area $A_{c,eff}$ around the bottom reinforcement that provides the tension stiffening effect.

On the other side, right-hand side of the equation considers the yielding force of the bottom reinforcement.

As shown in the equation 14, shear carried by the critical loading zone ($\boldsymbol{V_{clz}}$) is dependent on the degree of freedom (Δ_c). As can be seen in the Figure 25, the critical loading zone depends upon the angle (α) of the critical crack in the vicinity of the load and the effective width of the loading plate (l_{b1e}). The concrete in the critical loading zone is subjected to compressive stresses (σ) and strains (ε). The strains are assumed to vary linearly from zero at the top face of the beam to a maximal value (ε_{max}) along the bottom inclined face of the zone. Considering the deformed configuration of the CLZ, strain ε_{max} can be expressed as a function of (Δ_c). Diagonal compressive stresses σ are calculated from strains ε by using an appropriate stress-strain relationship for the concrete under axial compression. In this case, the chosen relationship is Popovics's (1970) since it calculates the stresses in the CLZ as follows. Once the diagonal compressive force acting on the CLZ is obtained, the average stress in the concrete (σ_{avg}) was multiplied by the area of the section passing through the edge of the loading plate and perpendicular to the bottom face of the critical loading zone.

$$V_{clz} = k\,\sigma_{avg}[\varepsilon_{max}(\Delta_c)]bl_{b1e}sin_{\alpha}^{2} \tag{14}$$

$$k = \min\{\max[1 - 2\,(\cot\alpha - 2), 0\,], 1\} \tag{15}$$

The value (k) in the shear carried by the CLZ considers the crack-shape. This is mainly because for slender beams, the angle of the critical crack around the loading point is usually smaller than (α). Owing to this, the cracks developed in slender beams have a S-shape instead of a linear shape as proposed by 2PKT model. This is due to the s-shape of cracks developed in slender beams.

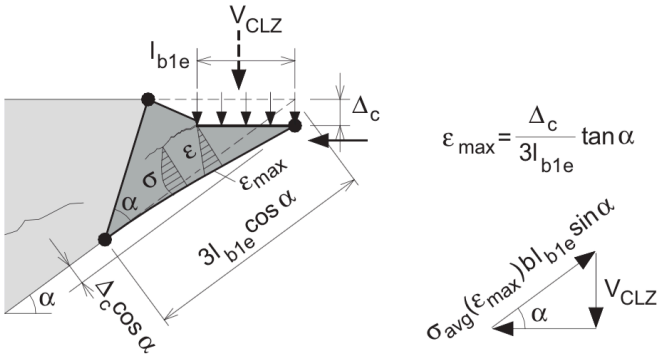

Figure 25 Critical Loading Zone (Mihaylov et al., 2015)

The next force to analyze is the shear carried by aggregate interlock **($\boldsymbol{V_{ci}}$).** This one is expressed as a function of the average stress transferred across the critical shear crack by means of interlocking of the rough crack surfaces (Mihaylov et al., 2015).

$$V_{ci} = 0.18\, v_{ci} bd \tag{16}$$

The stress v_{ci} is evaluated halfway along the critical crack as a function of the crack width (ω) and the slip (s), being this last defined in the equation 17.

$$s = \Delta_c \sin \alpha_1 \tag{17}$$

This close relationship between these three parameters is computed according to the Contact Density Model proposed by Li et al. 1989. Due to the fact that 5SM neglects the compressive stresses in the crack surfaces, the stress v_{ci} from the CDM is assumed equal to 0.18 adopted from Vecchio and Collins (1986).

The next force in the equilibrium equation (11) is the shear carried across the critical shear crack by the vertical transverse reinforcement (stirrups) **(V_s).** This force is expressed as the product of the stress in the stirrups (σ_v) times the area of the stirrups that are effective in providing shear resistance. This stress (σ_v), obtained from the strain in the stirrups (ε_v), is obtained on the basis of an elastic-perfectly plastic stress-strain relationship.

$$\varepsilon_v = 2\frac{\Delta_c + 0.25\varepsilon_{t,avg} d cot^2 \alpha_1}{0.9d} \tag{18}$$

$$\boldsymbol{V_s} = \sigma_v \rho_v b(d\cot\alpha_1 - l_0 - 1.5\, l_{b1e})\,;\ where \begin{cases} \sigma_v = \min(\varepsilon_v E_v;\ f_{yv}) \\ \rho_v \le 0.15\,\dfrac{f_c}{f_y} \\ (d\cot\alpha_1 - l_0 - 1.5\, l_{b1e}) \ge 0.5 d cot\alpha_1 \end{cases} \tag{19}$$

The last force carried across the critical shear crack is the shear resisted by dowel action ($\mathbf{V_d}$), which is defined as follows:

$$\boldsymbol{V_d} = \frac{E_s\ 12}{l_k^3} I_{cr}\Delta_c \le n_b f_y \frac{d_b^3}{3l_k}\left[1 - \left(\frac{T}{A_s f_y}\right)^2\right];\ where \begin{cases} I_{cr} = \dfrac{n_b \pi d_b^4}{64} \\ n_b = n^\circ\ of\ flexural\ bars \\ \left[1 - \left(\dfrac{T}{A_s f_y}\right)^2\right] \ge 0 \end{cases} \tag{20}$$

Left-hand side of Eq. (20) is derived by assuming that the dowels behave like elastic fixed-fixed beams subjected to a relative vertical displacement Δ_c.
On the other hand, right-hand side of the equation corresponds to the formation of plastic hinges at the ends of the dowels. The expression inside the square brackets accounts for the reduced moment capacity of the plastic hinges due to the tension in the bars T.

The Five-spring model is solved by increasing the mid-span deflection of the beam (Δ). Nonetheless, the value (Δ) cannot be directly input into the model but obtained with the help of the two degrees of freedom derived from the 2PKT model, $\varepsilon_{t,avg}$ and Δ_c. Due to this, the load-deflection curve envelope will be obtained with increasing values of Δ_c as this value is an input parameter.
For practical and theoretical purposes, this load-deflection curve was built for a sample beam whose properties are defined in the Table 7 and in the Figure 26.

a/d	b	d	h	L	ρ_{l1}	A_{s1}	ϕ_{l1}	n_{b1}	f_y	a_g	f_c'	f_{yv}	ρ_{sv}	ϕ_{sv}
[-]	[mm]	[mm]	[mm]	[mm]	[%]	[mm²]	[mm]	[-]	[MPa]	[mm]	[MPa]	[MPa]	[%]	[%]
1.55	400	1095	1200	3900	1.27	3040.2	25.4	6	652	20	33	490	0.1	10

Table 7 Sample beam properties (Mihaylov et al., 2010)

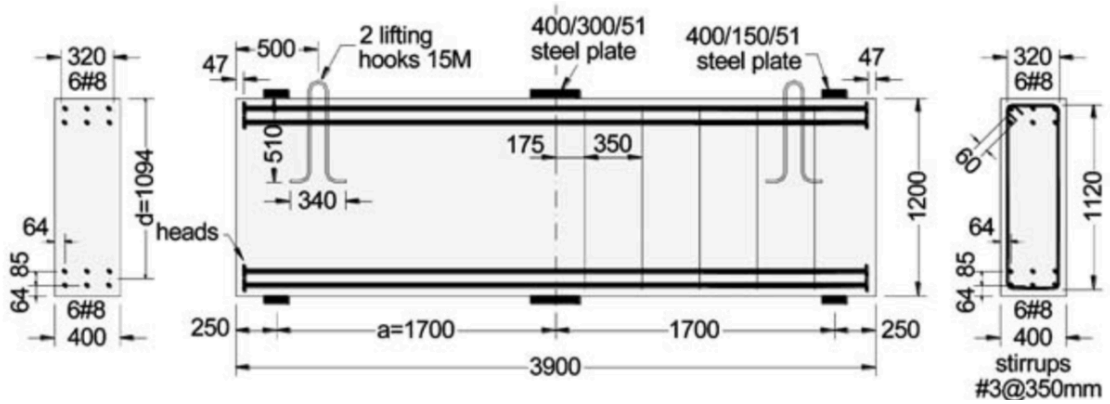

Figure 26 Sample beam geometrical properties, (Mihaylov et al., 2010)

In the Fig. 27, a deflection (Δ_c) of 7 mm with a step of 0.1 mm was imposed. Then, the strains in the bottom flexural reinforcement $\varepsilon_{t,avg}$,and the corresponding shear force developed by each spring of the 5SM are obtained. Both of these two values are represented in the vertical and horizontal axis of the same Figure.
Green discontinuous line represents the total contribution to shear of all shear forces. As it is shown in the Fig. 27, shear force carried by the CLZ **(V_{clz})** is only dependent on the transverse displacement of the CLZ (Δ_c), but not on the average tensile strain $\varepsilon_{t,avg}$. Thus, most of the time this force remains constant. The shear force resisted by the vertical stirrups **(V_s)** remains as well constant. This is because the stirrups for this (Δ_c) have already yielded. Thus, V_s will no longer be dependent on $\varepsilon_{t,avg}$, being therefore constant. The shear carried by aggregate interlock **(V_{ci})** changes in time. It is observed that this parameter decreases as $\varepsilon_{t,avg}$ increases. This is due to the widening of the critical shear crack that leads to a lower interaction between aggregates and eventually leads to a lower transmission of stresses between aggregates. The shear force carried by the dowel effect **(V_d)** is divided into two zones: an increasing and a decreasing stage. One can observe that during the increasing stage, **(V_d)** will increase as the strain increases. Then, as the strain continued to increase, its value decreases until

becoming and remaining equal to zero. In this last stage, dowels will no longer be able to transfer stresses and therefore resisting any shear force.

Magenta discontinuous line on the other side, represents the shear obtained from moment equilibrium equation. Its initial stiffness is dependent on the properties of the concrete matrix as well as the properties of the bottom flexural reinforcement.

The intersection of both discontinuous lines, represented as a black dot, is found iteratively using the bisection method. Its value gives us the corresponding strain and shear at equilibrium for a given value (Δ_c).

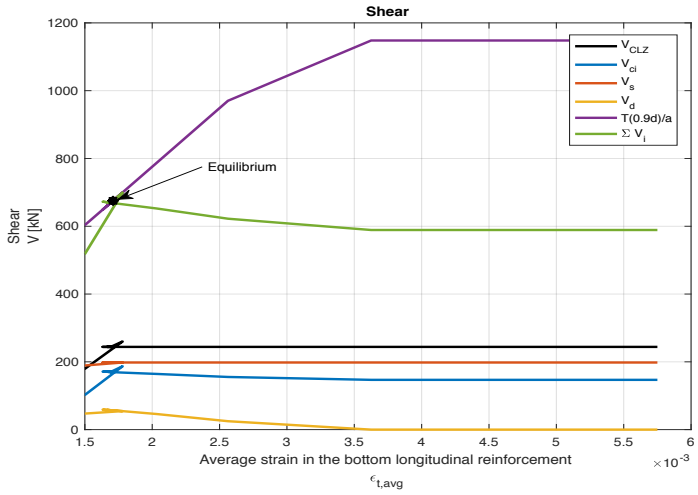

Figure 27 Shear forces in sample specimen under a given transverse displacement of the CLZ (Δ=7mm)

At the end, the final load-mid-span deflection curve is obtained by repeating the same procedure but giving a different value to (Δ_c). The range of values given to the transverse displacement of the CLZ goes from 0 to 20 mm, with a step of 0.1 mm. The horizontal axis in the Figure 28 represents the mid-span deflection (Δ), while the vertical axis represents the shear force resisted by the beam. The curve represents the sum of all shear forces, defined in the 5SM, that contributes to shear strength. The rest of the curves represent each one of the four parallel springs of the 5SM.

As it is shown in Fig. 28, the element that contributes the most to shear strength is the critical loading zone. It can be noticed that the shear force provided by CLZ increases parallel to the deflection, and then decreases. The deflection value that gives us this separation of V_{CLZ} into two zones is approximately equal to 7.5 mm. At the same time, one can observe that this deflection also separates the total shear strength into two zones. This indicates that the failure of the deep beam is governed by the failure of the CLZ. The shear force provided by the stirrups V_s is divided also into two zone, a linear and a constant zone. This indicates that

under a deflection of about 4.0 mm, the contribution to shear by the stirrups is dependent on the 2 degrees of freedom from the 2PKT. Beyond 4.0 mm, the stirrups will have yielded and therefore they are no longer dependent on both degrees of freedom. Shear force provided by the aggregate interlock V_{ci} not only has a similar behavior than V_{CLZ}, but also becomes the second element that contributes the most to shear strength. Its behavior however differs from V_{CLZ} in the decreasing branch, starting this one later. Finally, the shear force resisted by the dowel effect Vd is the one that contributes the least to shear strength.

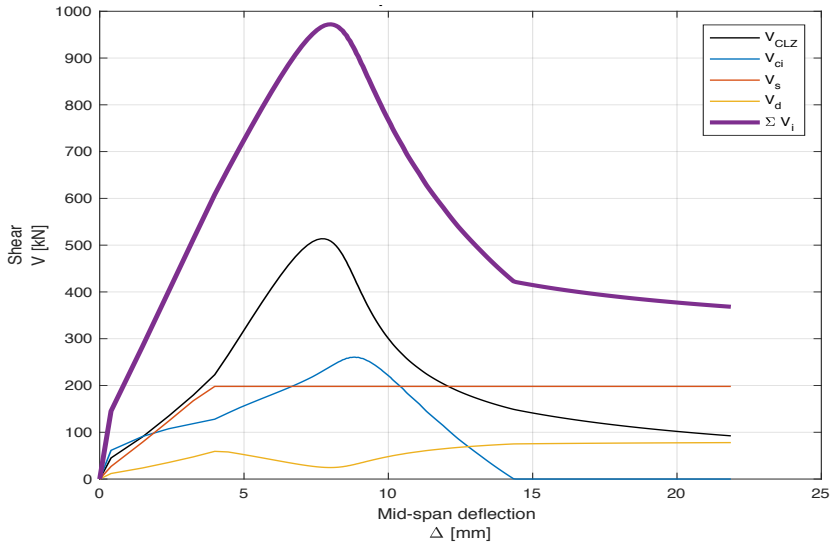

Figure 28 Predicted load-mid-span deflection curve

As it was previously introduced, the 5SM developed by Mihaylov et al. 2015 is capable of predicting pre and post-peak behavior of deep beams with or without vertical stirrups. This model does not consider neither the beneficial effect of FRP, nor its contribution according to the FRP strips position. The aim of this thesis is to modify the 5SM and implement the beneficial effect of FRP strips depending on its position, wrapping configuration or material properties.

4 Extended 2PKT for Deep Beams strengthened with FRP strips

4.1 Introduction

As already mentioned, despite the fact that 2PKT is capable of predicting very well the displacement capacity of deep beams reinforced or not with vertical stirrups, it is not capable of capturing the beneficial effect of FRP wraps on the pre and post-peak behavior of deep beams. In this section, 2PKT model will be modified in order to implement such beneficial effect and then the predicted results will be compared against experimental data from Bukhari and Rasheed tests. In order to do so, a new spring will be implemented in the 5SM having therefore 5 forces representing the shear resistance, and 1 force representing the flexural resistance. This new spring will account for the contribution of using FRP wraps to shear strength according to: (1) the ratio between the depth of the FRP strip and the beam's depth; (2) the position of the strip within the shear span, (3) the type of wrapping scheme and (4) the difference between using continuous or spaced strips. As these different effects could not be treated together, each one would be implemented following a strict order to eventually model the contribution of the FRP wraps. The procedure followed is given below.

First of all, the theory about the bond-slip model used is introduced. Since different models are available, a choice between all models needed to be made. In this case, the choice was governed by the accuracy and simplicity of the model where changes were introduced if necessary.

In second place, a choice between all models accounting for the process of debonding is explained. This choice accounts for the failure occurring between the bonded FRP wrap and the concrete interface. As for the previous section, modifications and simplifications were implemented if necessary.

As observed, during the two initial sub-sections the theory behind the bond-slip model and the process of debonding were explained. However, the theory of these models was developed only for a concrete prism bonded with an FRP wrap, it does not represent the real scheme of deep beams used in civil engineering structures. Thus, it is necessary to consider new geometrical and mechanical aspects that will transform these simplistic models into a general one representing a real deep beam strengthened with FRP wraps. This would be done in the third sub-section where step-by-step the procedure of implementation is explained. Besides, since a Matlab code was used during the realization of this work, a flow chart is also given.

Finally, the shear force representing the force resisted by the stirrups was replaced by another more accurate and realistic formula.

4.2 Local bond-slip models for FRP strips bonded to a concrete prism

4.2.1 Introduction

As already mentioned, debonding failure is one of the failure modes that need to be avoided since it is unpredictable, brittle and beams have shown a little contribution to shear or flexure strength after the failing of the FRP.

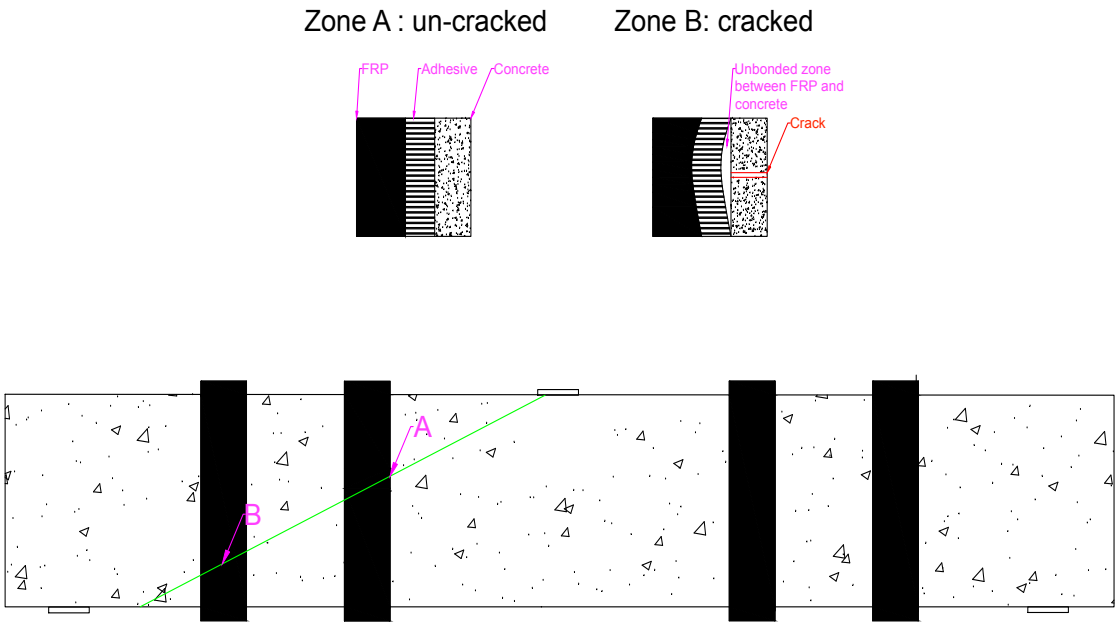

Figure 29 Difference in bonding between cracked and un-cracked zones

Figure 29 shows the different zones that exist when the process of debonding has started.

- In the zone A, a perfect adhesion between FRP and concrete is observed. This is because the crack has not reached any section covered with FRP, or in cases where the crack starts to propagates.
- In the zone B on the contrary, the adhesion between FRP and concrete is no longer the same as in the initial stage, and in the worst cases the adhesion is already lost. This is because there exist two voided areas (inside the concrete and in between the concrete and adhesive) where the adhesive has no effect at all, and therefore no bonding between the concrete and the FRP wrap exists.

Given that FRP wraps contribute to the enhancement of flexural and shear strength, and the behavior of cracked or un-cracked zones is rather different a necessity of focusing on only several parameters is made. Hereafter, these parameters are given:

1. Members strengthened to shear since the topic of the master thesis is to study the contribution to shear strength of FRP wraps, rather than flexure strength.
2. Zones where there is a perfect adhesion between the concrete and the FRP wrap, i.e., zones prior to crack developing.

4.2.2 Formulation of the local bond slip models

As already mentioned, one of the main problems linked to the use of FRP strips as a strengthening method is the possibility of debonding of the FRP strip from the concrete surface. During the last years, many researches have shown that the well understanding of the behavior between the FRP and the concrete interface[1] increases the possibility of controlling debonding failure (Lu and Teng 2005). However, since it is rather difficult to measure the stress state developed in this interface, it is also difficult to predict its behavior, and therefore control debonding failure. Despite this problem, it was also observed that the stress state developed in a simple pull test, where a plate is bonded to a concrete prism and then subjected to tension, it is quite similar to the stress-state generated in the FRP-to-concrete interface. Owe to this and the simplicity of the testing, the pull test was chosen as one of the experimental methods providing a better approximation of the behavior of the FRP-to-concrete interface.

Pull test not only delivers the ultimate load of the FRP-to-concrete interface, but also the local bond-slip behavior of the interface. This latter can be determined in two ways: (1) from axial strains measurements of the FRP plate or (2) from load displacement curves. Even though, the first method is the easiest one in terms of testing, it does not deliver good results since the measured strains vary dramatically because of the roughness of the underside of the debonded FRP plate and the heterogeneity as well as the discrete nature of concrete cracks. Given that, load-displacement curves are used instead of measure axial strains. Nonetheless, load-displacement curves are more time consuming due to the necessity of make an intermediate curve before obtaining them.

[1] Lu and Teng 2005 defined this interface as the interfacial part of the FRP-to-concrete bonded joint, including the adhesive and a thin layer of the adjacent concrete, responsible for the relative slip between the FRP plate and the concrete prism.

4.2.2.1 *FRP-to-concrete bond behavior*

As previously mentioned, the pull test is used to understand the local bond-slip behavior of the FRP-to-concrete interface. Here below in the Figure 30 a typical scheme of a pull test is given.

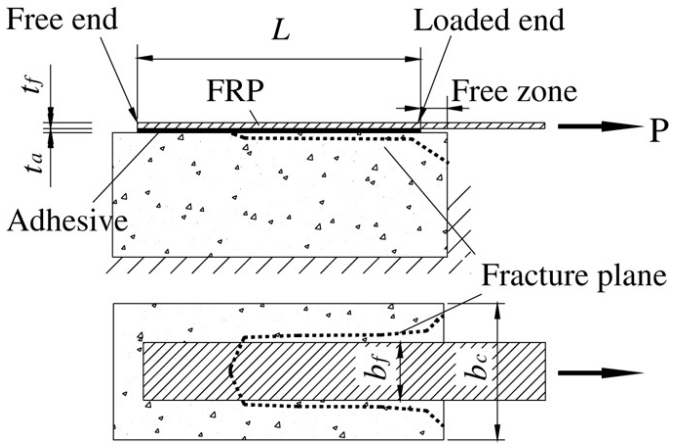

Figure 30 Typical scheme of a Pull test

Figure 30, corresponding to a pull test, shows an FRP plate (width equal to b_f) bonded to a concrete prism (width equal to b_c) being pulled with a force P at one of the ends, commonly named loaded end. Usually, the debonding starts at the loaded end and then propagates to the free end. It is clear that the pulled concrete area would be higher in the loaded end and lower in the free end since the stresses generated by the effect of pulling are higher in the loaded end rather than in the free end.

Once the pull test has finished either by the debonding of the FRP plate, or by the rupture of the FRP plate, a debonded area is observed. This area, commonly named Fracture plane, varies depending on the wrapping scheme. In this case, pull test simulates the FRP plate bonded to the sides of a beam, but in cases where the wrapping scheme is a U-jacketing the Fracture plane changes. In this case, the free end does not exist such, and therefore a lump of concrete near the loaded end will be pulled off the concrete prism. This change in the fracture plane shape may lead to the conclusion that the local bond-slip behavior is rather different in cases where the free end exists or not. However, this is not the case since as long as the bond length is long enough, the bond-slip behavior simulating the side bonding scheme could be also applied for U-jacketing schemes where there is no free end.

One important aspect of the behavior of bonded joints is the existence of an effective bonded length L_e, whose value marks the point where the maximal load is supported. Beyond this value any increase of it will not increase the ultimate load. This is a fundamental difference between an externally bonded plate and an internal reinforcing bar. In a reinforcing bar, a sufficient anchorage length is provided so that the full tensile strength is achieved, while for an external FRP plate the full tensile strength would be attained only when having a full wrapping, otherwise the attained tensile strength would be always lower such as the case of U-jacketing or side bonded schemes.

It is important to mention that during the realization of the pull test, the estimated adhesive thickness varies from one test to another, and so does the shear adhesive stiffness. Such variation would imply that tests having a higher adhesive thickness would have a higher shear stiffness, and therefore the bond-slip behavior would be better. Such variation would imply that the adhesive thickness has to respect a calculated value in order to assure a shear strength. Nevertheless, recent researchers investigated this effect and concluded that despite the fact that adhesive thickness is important for assuring the bonding between the FRP plate and the concrete, it has a little influence on the bond-slip behavior. Owing to that, and the fact that in real-life structures is quite difficult to control the thickness of the adhesive the bond-slip models proposed by Lu and Teng, 2005 assumed that all pull tests utilized the same adhesive thickness.

Finally mention that, in spite of local bond-slip behavior is not affected by the presence of free end zones, it is when changing some of the following properties: (a) the bond length L, (b) the FRP plate axial stiffness, (c) the concrete strength, (d) the FRP-to-concrete width ratio, (e) the adhesive stiffness and (f) the adhesive strength. During the validation of experimental data some of these values changed however, a study analyzing the influence of them is not carried out due to its vast range which goes beyond the topic of this master's thesis.

4.2.2.2 Bond-slip model

The bond-slip models that were utilized during this work are those corresponding to Lu and Teng 2005. In order to do so, different models with the same properties were compared between them, and furthermore compared with new proposed bond-slip model. These properties as well as the comparison between them are given in the Table 7 and Figure 31.

f_c' [*MPa*]	f_t [MPa]	b_f [mm]	b_c [mm]	$E_f t_f$ [*GPa*.mm]
32	3.0	50	100	16.2

Table 8 FRP-bonded joint properties for the elaboration of Lu and Teng Model

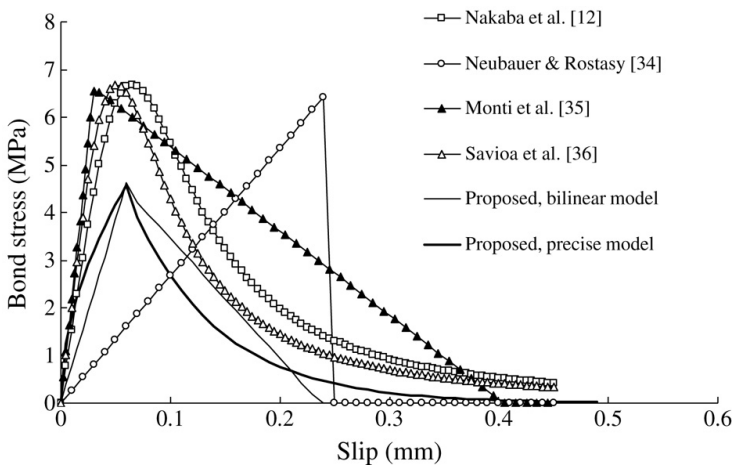

Figure 31 Bond-slip curves from existing bond-slip models, (Lu and Teng, 2005)

For a local bond-slip curve to be considered appropriate, this has to have an appropriate shape and a correct value of the interfacial fracture energy which is equal to the area under the bond-slip curve. To sum up, the bond-slip curve must have an ascending branch until reaching τ_{max} and then a descending branch until reaching s_f. These points are identified as: (1) the maximum bond stress τ_{max}; (2) the slip at maxim bond stress s_f; (3) the ultimate slip at zero bond stress s_f.
Despite these three points are identified in each curve, the shape of the curve is not the same, and in some cases this shape is completely different from what is expected to be. This is the case of Neubauer and Rostasy curve where a reduction of the bond stress at the ultimate slip is observed. This would imply the existence of an effective bond length beyond for which an increase in the bond length will not increase the ultimate load, which is impossible.

Due to the difficulty to obtain an accurate bond-slip curve from strain measurements in a pull test, and also owe to the huge range of possibilities between different bond-slip models a Finite Element approach was proposed by Lu and Teng (2005). With this approach a bond-slip curve, whose shape is equal to the obtained experimentally, is obtained. Even though this approach is really useful, it has to consider the modelling of the failure of the concrete layer, otherwise none benefits would be attributed to the curve. A comparison of the three different bond-slip models proposed by Lu and Teng (2005) is given in Figure 32. As shown, each curve has a different of accuracy and therefore of difficulty.

Despite the fact that these curves differ in accuracy between them, the same observations for each one of them can be made:

1. Each curve represents very well the shape of a bond-slip curve since it consists of an ascending and a descending branch, with the bond stress reducing to zero when the slip is considerably large.
2. The initial stiffness of the curve, representing the stiffness of the linear elastic state of the interface, is higher than the secant stiffness at the peak stress. This decrease in stiffness is due to the appearance of micro-cracks in the concrete layer.
3. The maximum bond stress τ_{max} and the corresponding slip s_0 increases almost linearly with f_t.

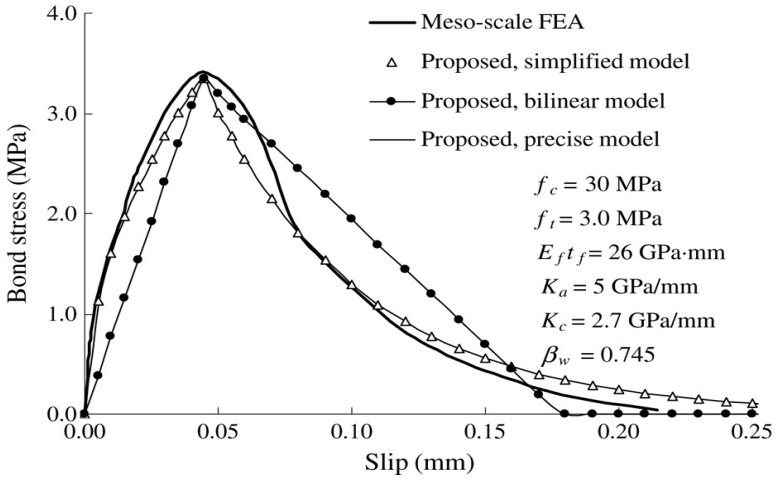

Figure 32 Comparison between bond-slip curves obtained with a FE approach, and the proposed bond-slip curves, (Lu and Teng, 2005)

Even though the precise model offers a better approximation to the Finite Element model, the increase in accuracy of this first is very little in comparison to the simplified model. Given that, the simplified model was chosen to make this work.

4.2.3 Simplified bond-slip model

Simplified bond-slip model was considered in this work due to its simplicity and accuracy in predicting bond-slip behavior. To elaborate this model, the initial stiffness was considered to be larger than the secant stiffness at the maximum bond stress, i.e., the initial stiffness could be considered as infinite. Given that, the formulas for the ascending and descending branch are given here below:

$$\tau = \tau_{max} \frac{s}{s_0} \qquad if\ s \leq s_0 \tag{21}$$

$$\tau = \tau_{max} \frac{s_f - s}{s_f - s_0} \qquad if\ s_0 < s \leq s_f \tag{22}$$

$$\tau = 0 \qquad if\ s > s_f \tag{23}$$

where

$$s_f = \frac{2\,G_f}{\tau_{max}} \tag{24}$$

$$s_0 = 0.0195\,\beta_\omega\,f_t \tag{25}$$

$$f_t = 0.33\sqrt{f_c} \tag{26}$$

$$G_f = 0.308\beta_\omega^2\sqrt{f_t} \tag{27}$$

$$\tau_{max} = 1.5\,f_t \tag{28}$$

$$\beta_\omega = \sqrt{\frac{2.25 - \frac{b_f}{b_c}}{1.25 + \frac{b_f}{b_c}}} \tag{29}$$

Below a bilinear curve with the characteristics of the FRP bonded joint are represented:

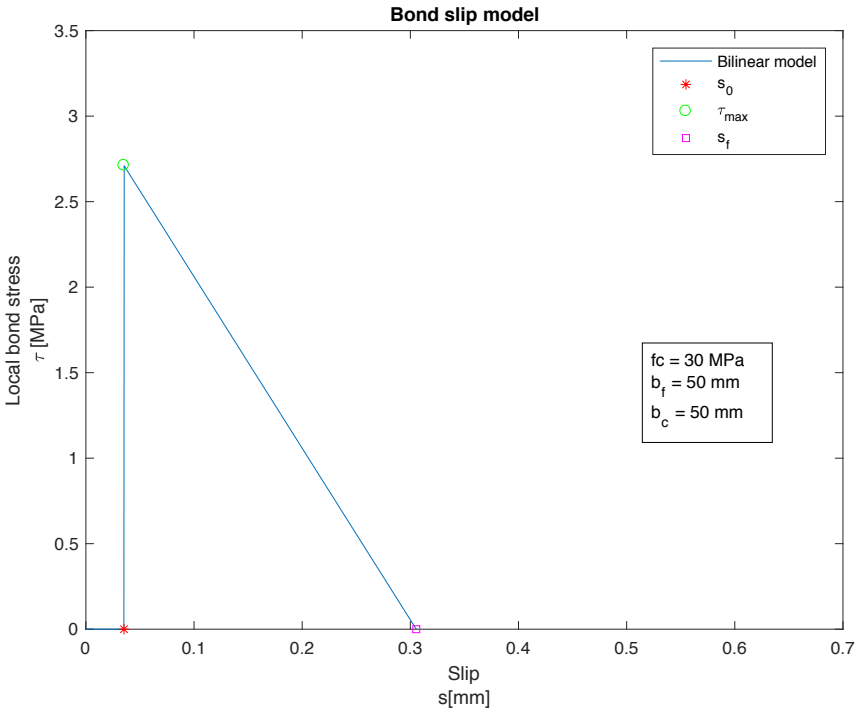

Figure 33 Bilinear bond-slip curve proposed by Lu and Teng

4.3 Process of debonding of an FRP strip bonded to a concrete prism

4.3.1 Introduction

As already mentioned, debonding process is one of the main problems associated with the use of FRP as a strengthening material, not only because has a brittle behavior, but also because limits the maximal crack width of the diagonal crack, and therefore the possibility to attain the ultimate load. Shear reinforcement is one of the elements affected by the use of FRP strips since this limitation of the maximal crack-width limits the possibility of the steel stirrups to yield, and so the possibility of contributing to shear strength.

One the other side, since the process of debonding is influenced by the wrapping scheme. It is therefore necessary to well understand the behavior for each one of the wrapping schemes used when strengthening beams.

Given that, an analytical load-displacement method was proposed by Chen and Teng in 2012. This method is not only capable of predicting the full debonding process of FRP plates bonded to concrete, but also considers the influence of the wrapping scheme to shear resistance, as well as the position of the FRP within the shear span.

Even though this method is capable of considering different aspects, its use is restrained to some fundamental assumptions. Those assumptions are given below:

1. Despite Chen and Teng model was formulated using discrete strips, an FRP sheet was not considered. However, an FRP sheet could be considered using discrete FRP strips with non-zero gaps.
2. The crack-width varies linearly from the crack-tip to the crack-end. Thus, a triangular shape is considered.
3. The slips at the two sides of the shear crack are not symmetrical, but must be determined.
4. Only the bond behavior in the fiber direction of the FRP is considered.
5. Side bonding, U-jacketing and full wrapping are considered as the only wrapping schemes to analyze.
6. A linear bond-slip model is used to capture the behavior of U and side wrapping schemes. Hereafter the bi-linear bond-slip model proposed by Lu and Teng (2005) is used.

4.3.2 Type of FRP-to-concrete bonded joints

An important aspect to be considered during the elaboration of Chen and Teng model is the type of FRP-to-concrete joints. Each joint is obtained according to the intersection of the FRP strip with the shear crack, and are used to model the type of wrapping scheme. Figure 34 shows the 2 types of joints obtained at the upper and bottom side after the intersection of the shear crack with the FRP strip.

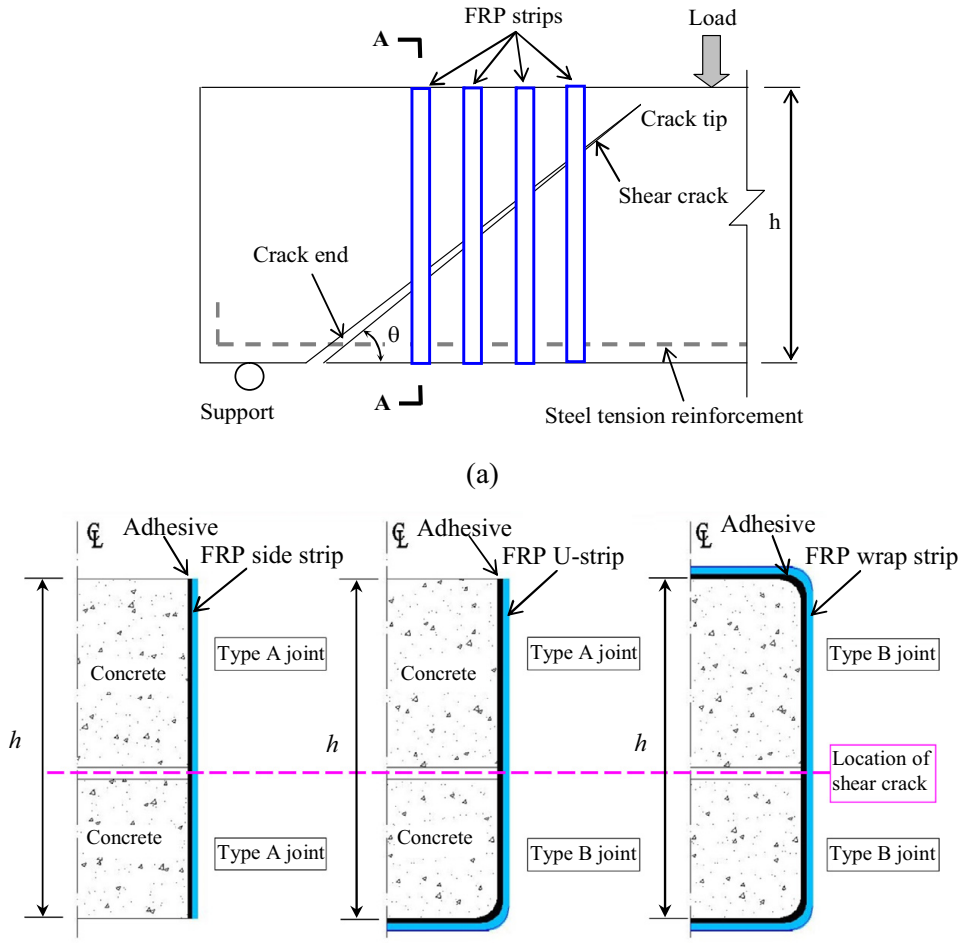

Figure 34 Type of joints, (Chen and Teng 2012)

In the last decades, the joint that has been studied the most is type A joint since as mentioned before, its behavior is analogous to a pull test. As shown in Fig. 34, this joint is obtained either at the bottom and upper side of the side strip after the intersection of the shear crack with the FRP strip, or at the upper side of a U-strip. This joint is characterized with the existence of a free far end zone, usually placed at the bottom or the top of the cross section of the beam, and a loaded end zone commonly placed at the location of the shear crack Fig. 35.

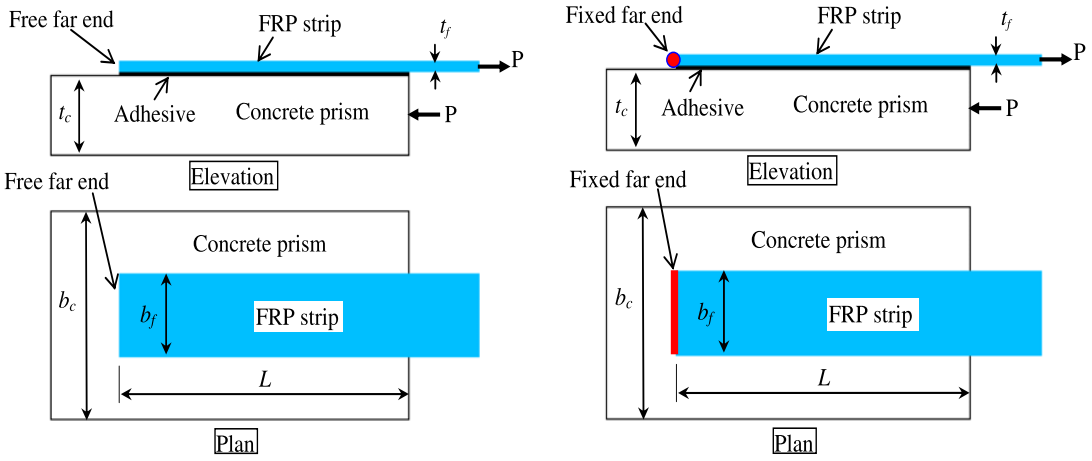

Figure 35 Type A joint & Type B joint, (Chen and Teng, 2012)

According to the literature, the debonding process of a side strip is the easiest one to obtain since it is composed with two type A joints Figure 36 (a). However, in the cases where the beam is fully wrapped Fig. 36 (b) or uses a U-jacketing scheme Fig. 36 (c), the anchorage condition at the free and the loaded end of both, the lower and upper side of the divided strip, changes. Hereafter the process of debonding of a type A joint is explained, and then an expansion of it is made in order to obtain the process of debonding of a type B joint, whose behavior would be used to model the process of debonding of a full wrapped or U-jacketing scheme.

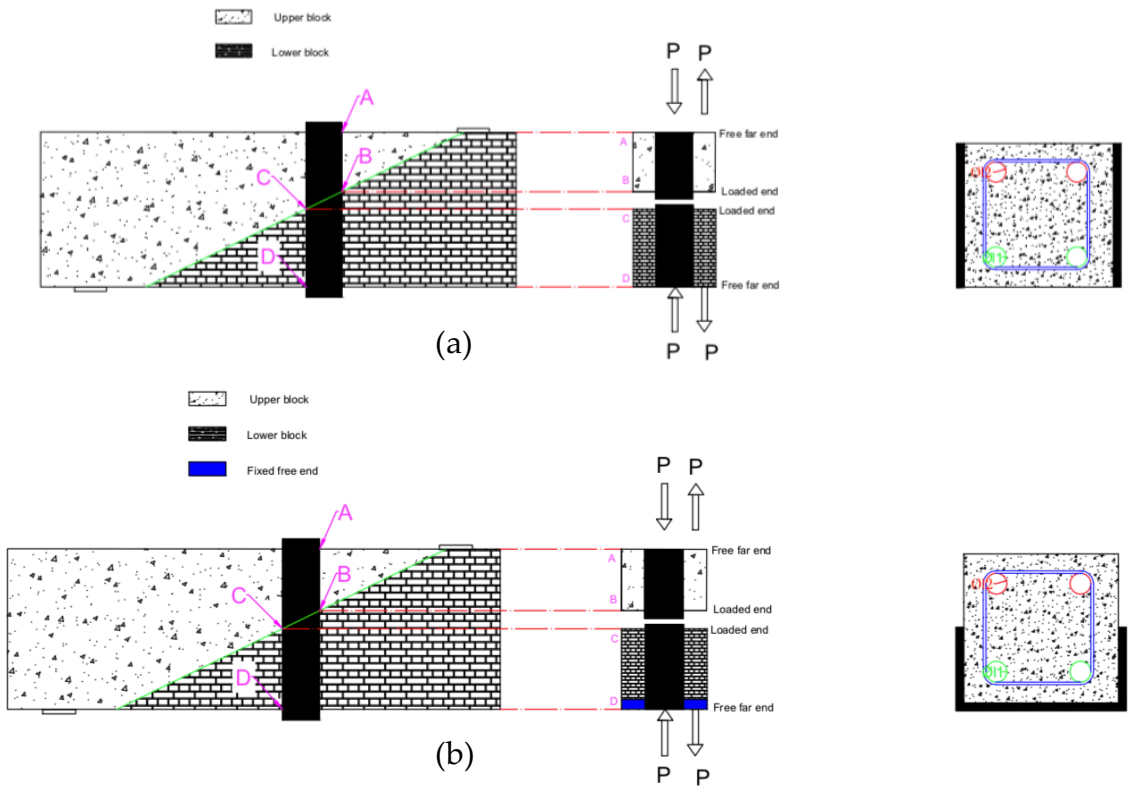

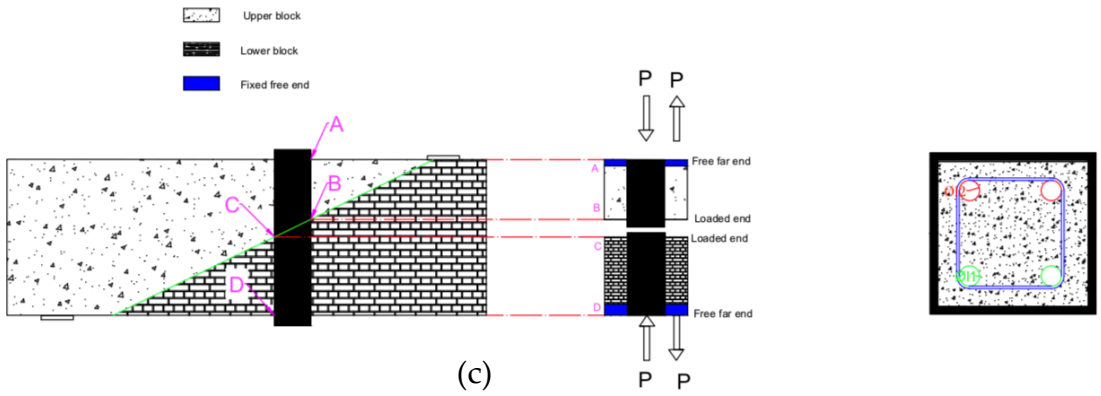

Figure 36 Wrapping schemes and their corresponding type joints

4.3.2.1 *Type A joint*

Below a representation of the load-displacement curve Fig.37 and the evolution of interfacial shear stresses Fig. 38 are given.

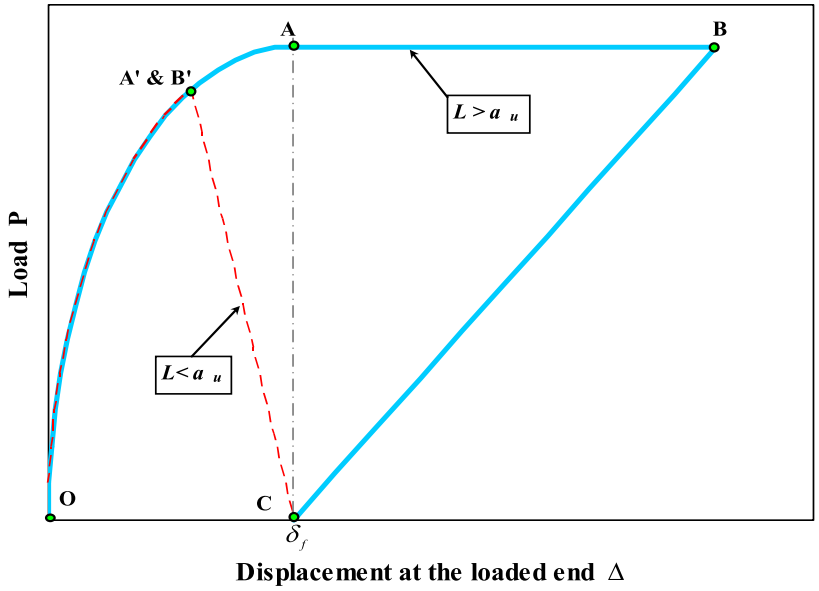

Figure 37 Full range load-displacement of a type A joint, (Chen and Teng, 2012)

Before the figures above are explained, it is necessary to define some values shown in those figures. Those values are: load P corresponding to the applied load at the loaded end, slip at the loaded end (Δ) which is equal to the width of the crack w_v used hereafter, the letters "S", "D" and "R" meaning softening, debonded and rigid part of the interface, the length (L) standing for the bond length of the FRP, the length (a_u) standing for the effective bonded length of the FRP, the length (a) corresponds to the mobilized bonded length of the FRP; the length (d) corresponding to the debonded part of the FRP-to-concrete interface and the letters "δ", "δ_f" and "τ_f" meaning the slip, the slip at maximum bond stress and the maximum bond stress.

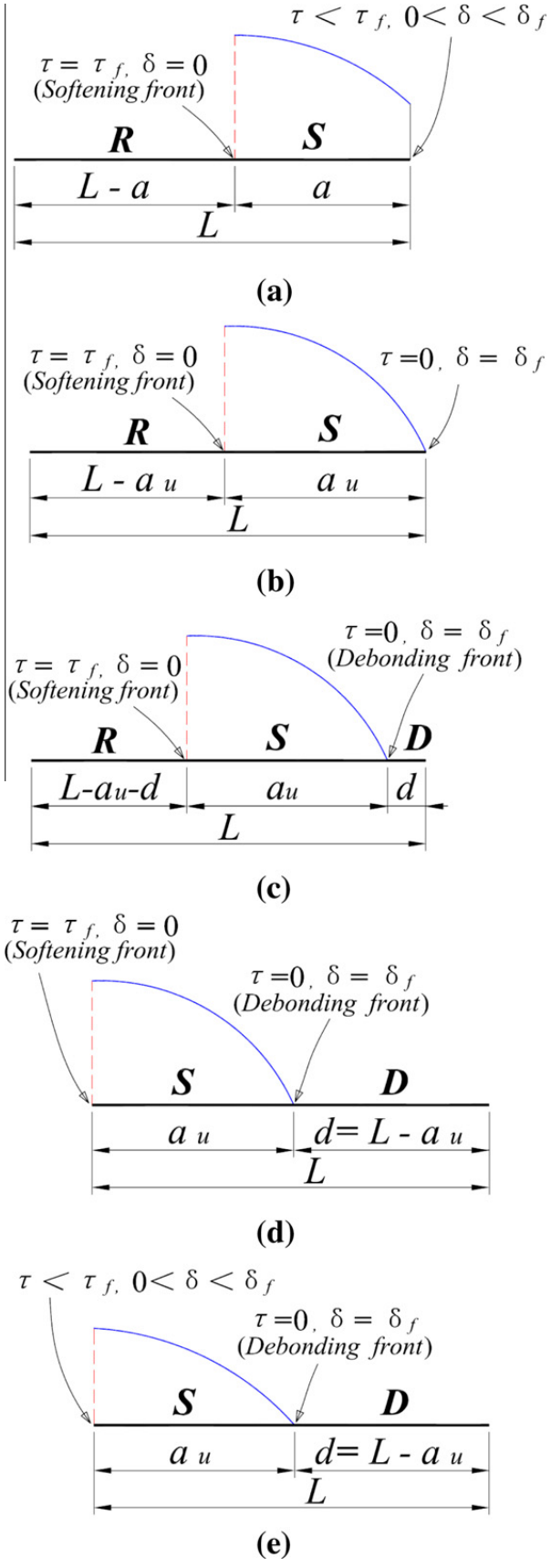

Figure 38 Interfacial shear stresses at different stages, (Chen and Teng, 2012)

Based on the figures given above, the following conclusions can be made:

1. First of all, an ascending branch between points 0 and A is observed at Fig. 37. This implies having a unique relationship between the load and the displacement. Thus, if a side FRP strip is intersected by a shear crack, the slips on the two sides of the shear crack are symmetrical.
   On the other side, along this ascending non-linear branch two main stages can be identified:
   a. The stage (a) between the point O and the point before A. In this stage, a softening front develops and starts to propagate towards the rigid zone (R), unbonded zone. Thus, the slips at the loaded end belonging to the softening front increases from zero to a maximal value $\delta_f = s_0$. This implies an evolution of the softening front and therefore a change in shape of the softening zone until reaching the stage (b).
   b. The stage (b) correspond to the initiation of debonding of the loaded end. In this stage, the slip at the loaded end is equal to δ_f, and the mobilized bonded length of the FRP (a) is equal to the effective bonded length of the FRP (a_u). Therefore, at this stage debonding starts to propagate from the shear crack towards the bottom and the top of the beam.
2. Second of all, on the plateau between points A and B, the unique relationship between load and displacement is no longer valid. Therefore, if an FRP strip is intersected by a shear crack, the slips on the two sides of the shear crack are no longer symmetrical, but different. In this plateau, two different stages are also observed:
   a. Stage (c), in between points A and B, corresponds to the propagation of debonding. In this stage, the rigid zone starts to decrease in value until its vanishing (stage d) due to the propagation of the softening zone towards the rigid zone, and the appearance of a new zone, named debonded zone.
   b. Stage (d) corresponds to an increase of the debonded zone and the completely vanishing of the rigid zone. This means that the debonding has propagated more and more into the anchored length, hence the effective bonded length has decreased each time until reaching a minimal value.
      In this stage, the softening front has reached the end of the rigid zone, i.e., the bottom and the top of the cross section of the beam, and the length of the debonding zone has increased in value, meaning that the debonded length is equal to the bonded length.
3. Stage (e), in between curve CB, corresponds to a linear unloading of the FRP strip.

4.3.2.2 Type B joint

So far, a type A joint has been explained. As already mentioned, this joint is really helpful when describing the process of debonding of side strips or one part of a U-strip. However, when there is a need of describing the total process of debonding of a U-strip or a full wrapping scheme, joint A has to be extended. Here below an expansion of the load-displacement of the type A joint is given.

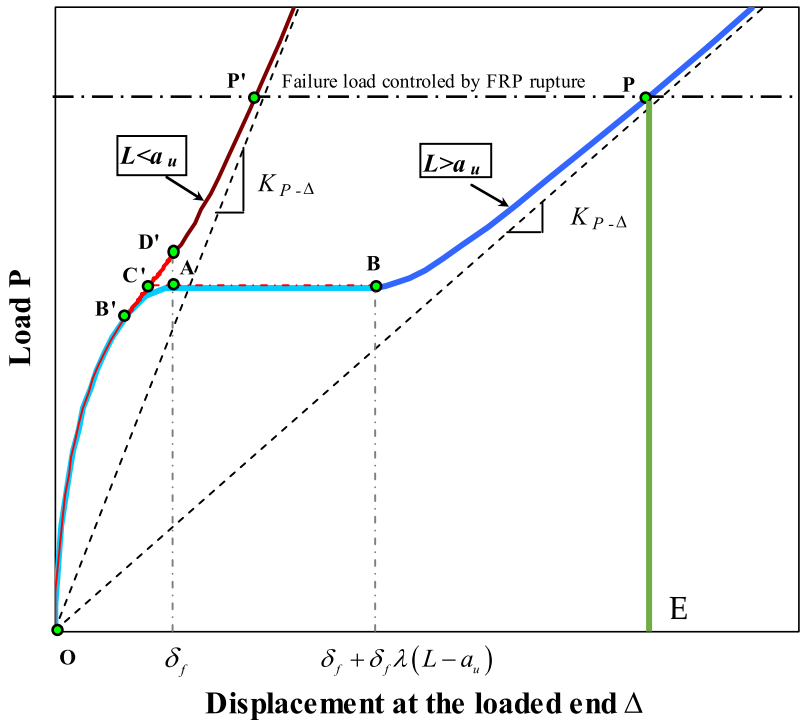

Figure 39 Full range behavior of a Type B joint, (Chen and Teng, 2012)

Based on the Figure 39, it is observed that the full range behavior of a type B joint is divided into three segments: OA, AB and BP if the bonded length is large enough, or in OA', B'D' and D'P' in case where the bonded length is insufficient. Hereafter, only the first case is considered since it is the most common. Thus, based on this curve some conclusions are made:

1. The solutions of segments OA and AB are the same as for a type A joint, since the load-slip response are not affected by the anchorage type at the free-far end.
2. The segment BP indicates that the presence of a fixed end allows the FRP strip to be stretched until reaching its ultimate strain at point P, where eventually the FRP strip is ruptured due to strain concentrations at the corners of the section fully bonded.
3. The segment PE indicates the drop-in resistance of the FRP strip.

Figure 40 shows the interfacial shear stress distribution at different stages. Stages A to D are equal to the stages A to D of a type A joint. The only difference is the stage (e) that indicates the final propagation of debonding since the FRP is ruptured.

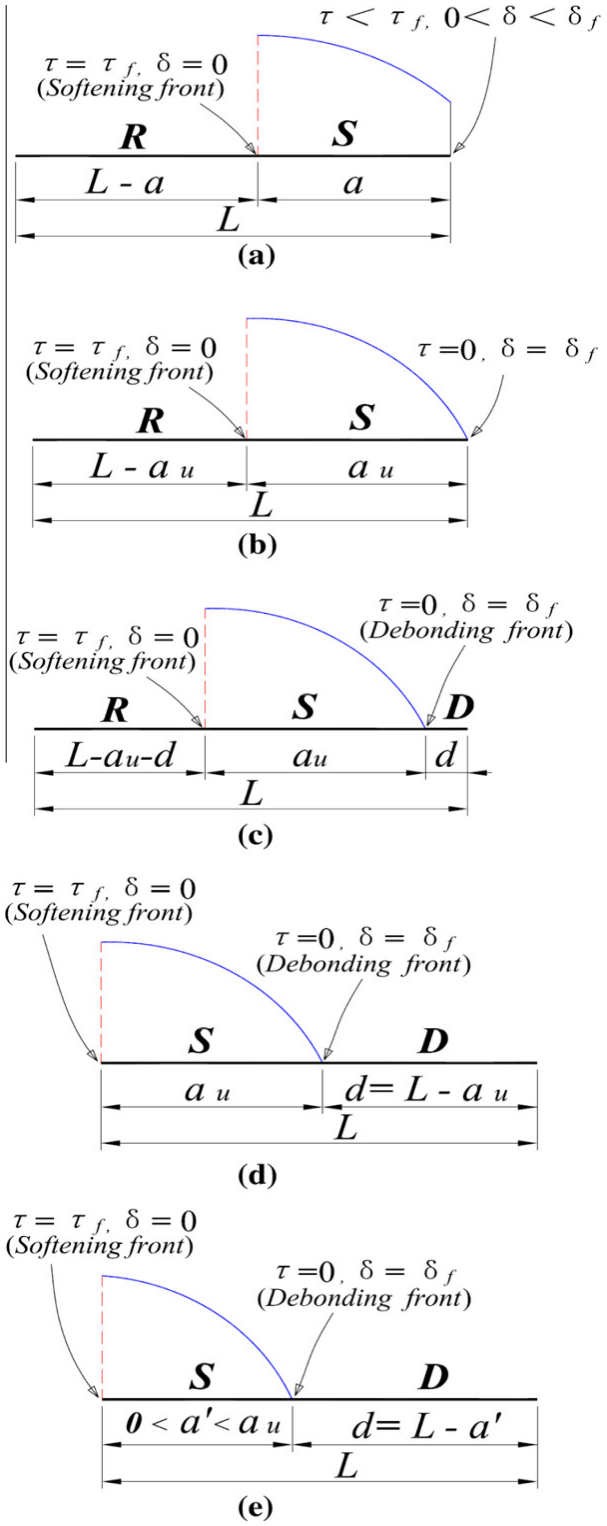

Figure 40 Interfacial shear stress distribution at different stages of debonding process, (Chen and Teng, 2012)

4.3.3 Simplified model for the process of debonding

Based on the behavior of the type B joint, the process of debonding for a deep beam strengthened with different wrapping schemes can be obtained. However, since the formulas given by Chen and Teng implies the knowledge of some values that are only obtained experimentally, Chen and Teng model was simplified in a simpler manner based on the simplifications given below:

1. The non-linear ascending branch is simplified by a linear ascending branch. Despite the fact that the load at the free end is now lower than with a non-linear ascending branch, the maximal load and the corresponding slip at the initiation of the process of debonding (point A at figure 39) remains the same.
2. The width of the crack, or slip, at the beginning of the process of debonding (point 0 at figure 39) is equal to zero. A positive value indicates that the beam is retrofitted, hence the slip at the loaded end is non-zero. This value is modified in cases where the beam is already damaged and a retrofitting is applied after.
3. The width ratio factor β_w of the formula 29 is equal to 1, hence $s_f = 1.5_{fct}$

With these assumptions, the full range behavior of the process of debonding for a type B joint in terms of stress in the FRP in the crack σ_{FRP} vs the width of the crack w_v is given below:

For segment OA

$$\sigma_{FRP} = \frac{\tau_f . s}{\lambda . t_{FRP} . 2\, s_f} \qquad if\ s \leq s_A \tag{30}$$

$$\omega_{v1} = s_A = 2. s_f \tag{31}$$

$$\lambda = \sqrt{\frac{\tau_f}{s_f} . \frac{1}{E_{FRP} . t_{FRP}}} \tag{32}$$

For segment AB

$$\sigma_{FRP} = \frac{\tau_f}{\lambda . t_{FRP}} \qquad if\ s_A < s \leq s_B \tag{33}$$

$$\omega_{v2} = s_B = \frac{\tau_f}{\lambda} . \frac{h_{FRP}}{E_{FRP} . t_{FRP}} \tag{34}$$

For segment BP

$$\sigma_{FRP} = \frac{E_{FRP}.s}{h_{FRP}} \qquad if\ s_B < s \leq s_P \tag{35}$$

$$\omega_{v3} = s_P = s_E = k_{FRP,rupture}.\varepsilon_{FRP}.h_{FRP} \tag{36}$$

If the segment is located beyond the point P, the stress is equal to 0.

As an example of this simplified model, Figure 41 was elaborating showing the full range behavior of a type B joint. The mechanical properties of the FRP-to-concrete bonded joint used during the construction of such curve are given in the Table 9.

f_c [*MPa*]	t_{FRP} [mm]	E_{FRP} [MPa]	$k_{FRP,\ rupture}$ [-]	ε_{FRP} [-]	h_{FRP} [mm]
48.62	0.34	234500	0.5	0.0147	300

Table 9 FRP-to-concrete joint properties

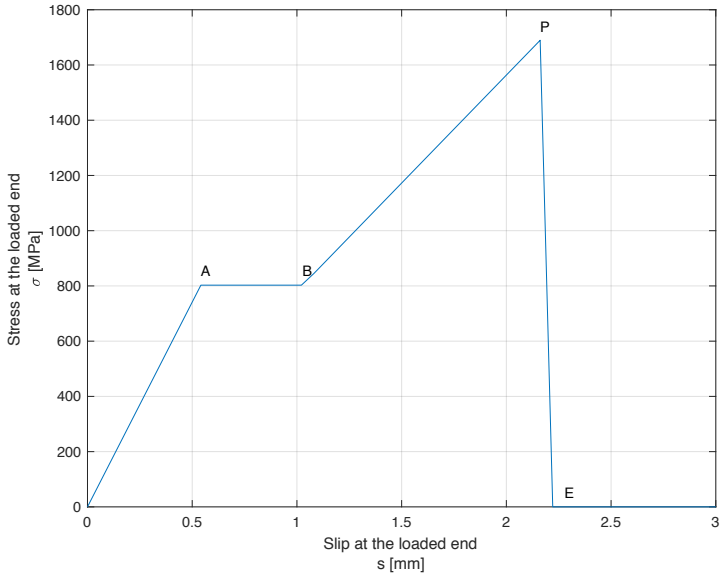

Figure 41 Full range behavior of a Type B joint with the SPD

4.4 Implementation of FRP wraps into the 2PKT

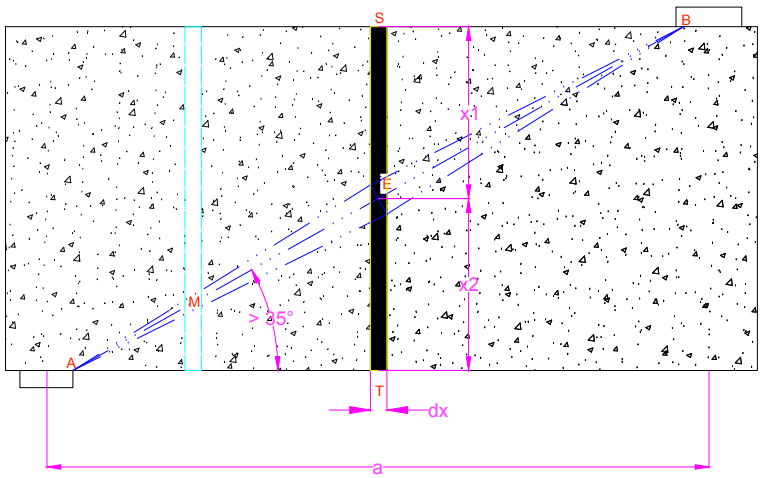

Figure 42 Ideal configuration of an FRP strip located within the shear span

So far, the process of debonding and the bond-slip model of a single FRP strip has been considered. Nonetheless, this FRP strip is not supposed to be located anywhere within the shear span, but in an assumed location respecting some crucial assumptions that are given below.

1. The beam is bonded along the entire depth, hence (h_{FRP}) = (h);
2. The strip is located at the center of the shear span;
3. The shear crack, intersecting the FRP strip at point E, separates the strip in two equal lengths (x_1 and x_2). Thus, the debonding of points S and T (Fig. 42) will be attaint at the same time;
4. Given that, the width of the critical crack varies linearly from point A/B to E. It is supposed that an FRP strip located at a position other than the point E, at point M for example, would have a lower crack-width and different lengths x_1 and x_2. Nevertheless, this effect is not considered at all;
5. The angle of the shear crack is higher than 35°. Thus, the shear crack starts at point B and finishes at point A, which is always located at the inner edge of the support. For slender beams, this is not always the case since $\alpha_1 = 35°$.

As deduced, these assumptions impede evidently the determination of the process of debonding, and therefore the contribution to shear strength of an FRP strip in a position other than the one represented at point E in the Figure 42. Thus, for a beam such as the shown in Fig. 43 the solution cannot be obtained directly without some important modifications on the theory previously described. In this section, a beam such as the shown in the Fig. 43 will be analyzed for eventually calculating the contribution to shear strength of a certain FRP configuration.

4.4.1 Overview of implementation

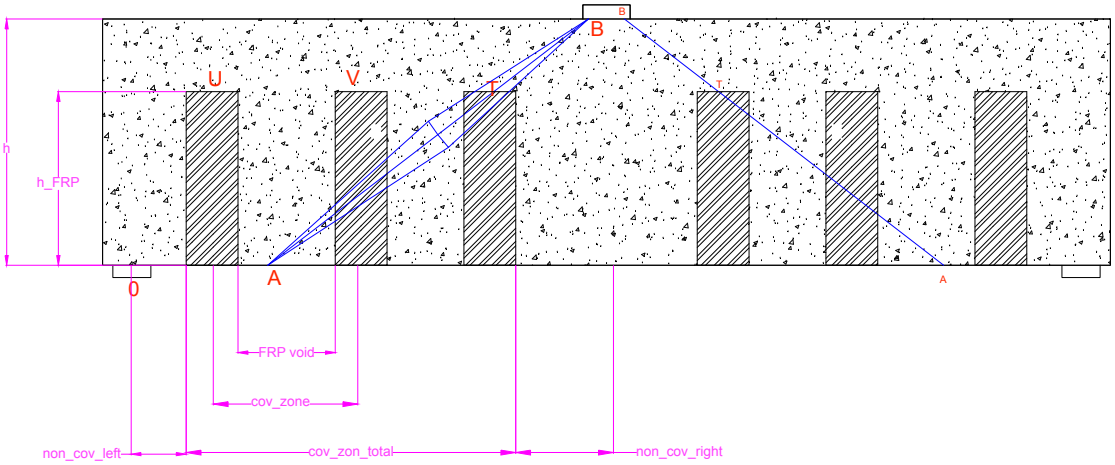

Figure 43 General deep beam strengthened with smeared FRP strips

As mentioned before and as represented in the Figure 43, different values can influence the contribution to shear of a deep beam strengthened with FRP strips. Those values are:

- The ratio between h and h_{FRP}
- The length of zone on the left of the shear span non-covered with the FRP strips, [$non_{cov,\ left}$] ;
- The length of the zone of the shear span where the FRP strips/sheets are placed, [$cov_{zone,\ total}$] ;
- The length of zone on the right of the shear span non-covered with the FRP strips, [$non_{cov,\ right}$] ;
- The void distance between two FRP strips, [FRP_{void}] ;
- The distance between the center of two consecutive strips [cov_{zone}] ;
- The angle of the shear crack, and therefore the position of the end of it (point A);
- The shape of the shear crack (bi-triangular, rectangular or triangular);
- The intersection of the shear crack with the top of the last strip [point T] since it marks the last point where the FRP contributes to shear;

Based on the values mentioned above, it is observed that multiple parameters must be considered to obtain the shear behavior of a deep beam strengthened with FRP strips. However, since it is not clear what is the procedure to follow to obtain such behavior, a routine must be created. Given that the stated problem was solved using a Matlab code, a flow chart indicating the steps to follow is given to final obtain the shear force resisted by the FRP strips.

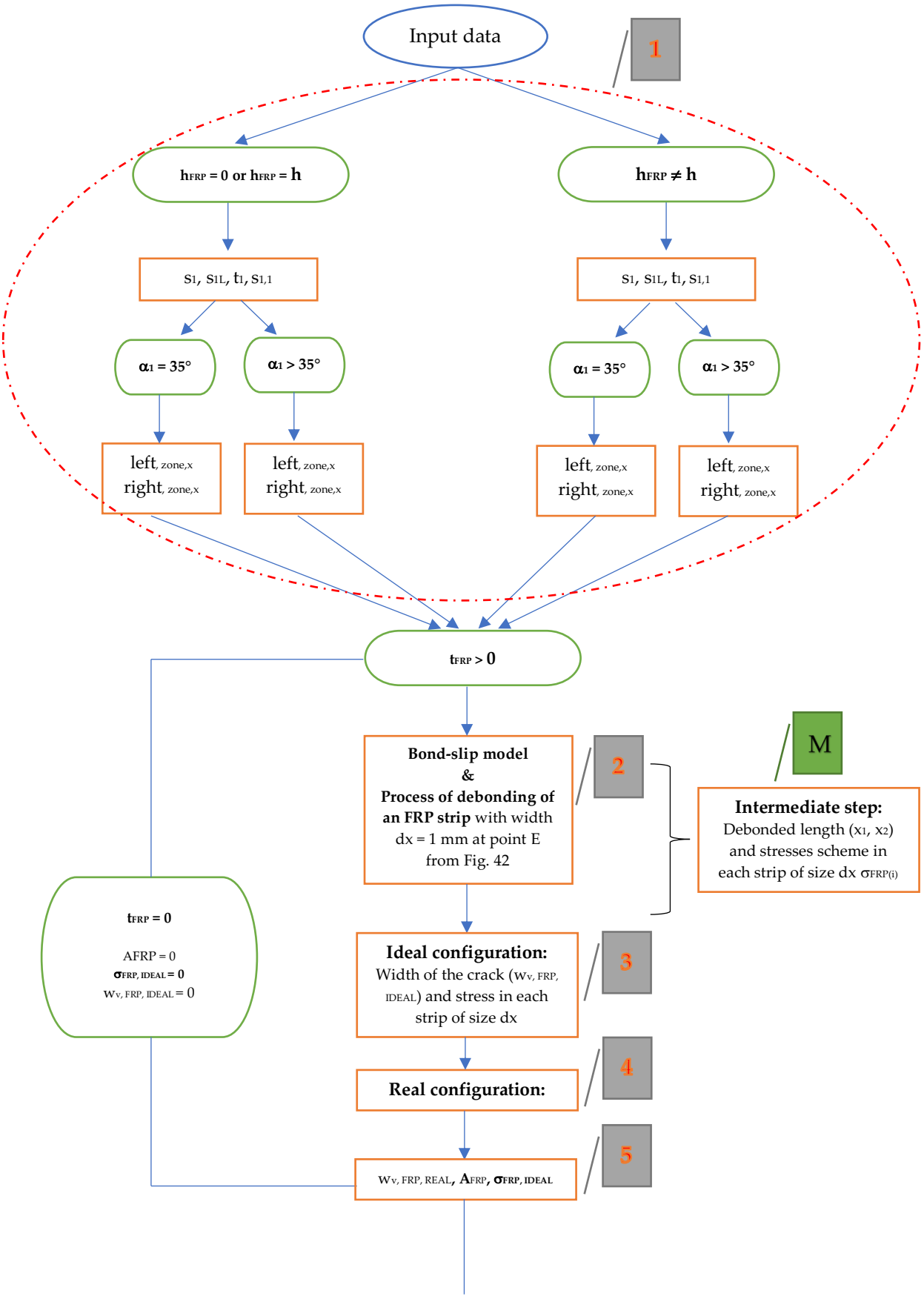
Input data
1
$h_{FRP} = 0$ or $h_{FRP} = h$
$h_{FRP} \neq h$
s_1, s_{1L}, t_1, $s_{1,1}$
s_1, s_{1L}, t_1, $s_{1,1}$
$\alpha_1 = 35°$
$\alpha_1 > 35°$
$\alpha_1 = 35°$
$\alpha_1 > 35°$
left, zone,x
right, zone,x
left, zone,x
right, zone,x
left, zone,x
right, zone,x
left, zone,x
right, zone,x
$t_{FRP} > 0$
Bond-slip model
&
Process of debonding of an FRP strip with width dx = 1 mm at point E from Fig. 42
2
M
Intermediate step:
Debonded length (x_1, x_2) and stresses scheme in each strip of size dx $\sigma_{FRP(i)}$
$t_{FRP} = 0$
AFRP = 0
$\sigma_{FRP, IDEAL} = 0$
$w_{v, FRP, IDEAL} = 0$
Ideal configuration:
Width of the crack ($w_{v, FRP, IDEAL}$) and stress in each strip of size dx
3
Real configuration:
4
$w_{v, FRP, REAL}$, A_{FRP}, $\sigma_{FRP, IDEAL}$
5

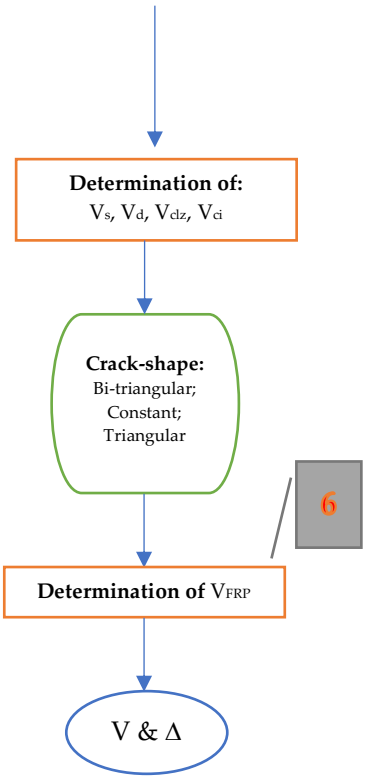

Figure 44 Flow chart followed in the Matlab code

As shown in the flow chart given at the Fig. 44, six main steps must be followed before obtaining the contribution to shear strength of an FRP configuration. In the following sub-sections each of these six steps are explained in detail, but before doing so, a modification in the force V_s was made in order to proportionate a more accurate response.

4.4.2 New shear force V_s

Even though the shear force obtained with the formula 19 gives a good approximation to model the load-displacement behavior, a more accurate formula is needed since the strain in the stirrups are not function of the average strain in the longitudinal reinforcement, but function of the crack displacement w_v.

This new approach, proposed by Sigrist et al. 1995, assumes that the bond-slip behavior between the concrete and the steel bars is rigid-plastic, with a maximum resistance twice the tensile strength of the concrete. Once the stirrup yields, this bond resistance drops to a value equal to $0.33\sqrt{f_c'}$.

The new shear force derived from this new approach can be calculated with the formulas given below:

$$V_S = \sigma_{v,avg}.\rho_v.b.(0.9d)$$

$$\sigma_{v,avg} = \begin{cases} \dfrac{E_s.\varepsilon_v}{2} & if \ \varepsilon_v \leq \varepsilon_{yv} \\ \dfrac{\dfrac{f_{yv}.\varepsilon_{yv}}{2} + f_{yv}(\varepsilon_v - \varepsilon_{yv})}{\varepsilon_v} & if \ \varepsilon_v > \varepsilon_{yv} \end{cases} \quad (37)$$

As illustrated in the Figure 53, the new force V_s attaint its maximal shear force at a deflection of almost three times higher than for the old formula of V_s. This is because of instead of considering the average yielding strain of the flexural reinforcement, it is considered that the stirrups yield one by one. Therefore, when a stirrup has yielded, the rest are still able to deform, hence the beam can still deform. It is also observed that the maximal shear force is the same as for the old law, with the difference that once the peak force is reached, the shear force decreases as the deflection increases. This approach is more accurate since after the peak force is attained, the force V_s decreases as the deflection increases, which is not the case for the old relationship that considers that once the peak point is reached, the force Vs remains the same even if the deflections increases.

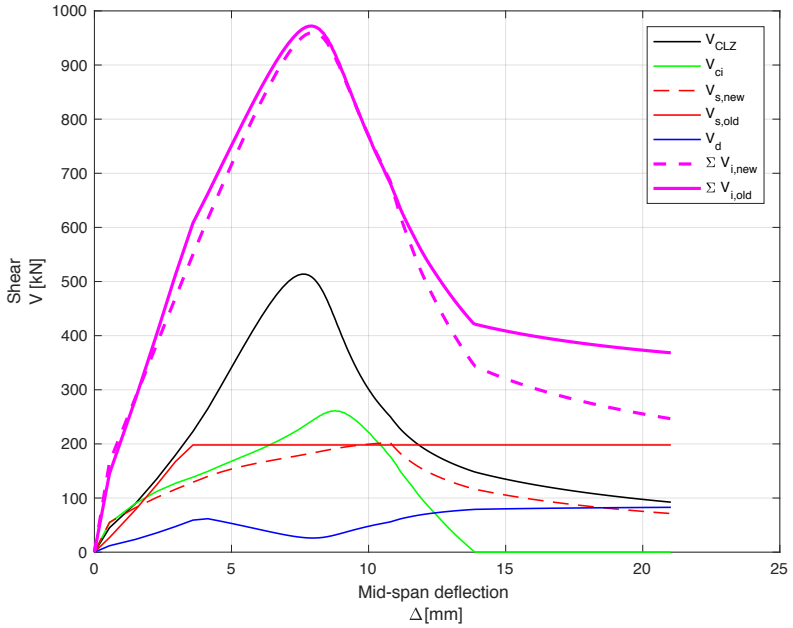

Figure 45 New force V_s and comparison between the old V_s

4.4.3 Influence of the angle α_1 (step 1)

As previously mentioned, beams can be classified in slender or deep beam according to the shear span-to-depth ratio. This value directly influences on the angle of the shear crack (α_1), and therefore the position of the tip and the end of it (points A-B). According to the Fig. 46, beams are divided in two big groups: group (a) with beams where $\alpha_1 > 35°$, group (b) with beams where $\alpha_1 = 35°$. It is observed that either the beam belongs to the group (a), or to the group (b), the beam is divided into three important regions:

- Region (OAPG) on the left of the shear span where the shear crack has no influence at all;
- Region (AGKB) where the shear crack is located;
- Region (KMNB) on the right of the shear span where the shear crack has no influence at all;

Besides, it is also observed that the shear crack divides the shear span into two big concrete blocks. The first block, hereafter called upper-block, comprises the entire region (OAPG) and the triangle (AGB) from the region (AGKB). The second block, hereafter called bottom block, comprises the entire region (KMNB) and the triangle (AKB) from the region (AGKB).

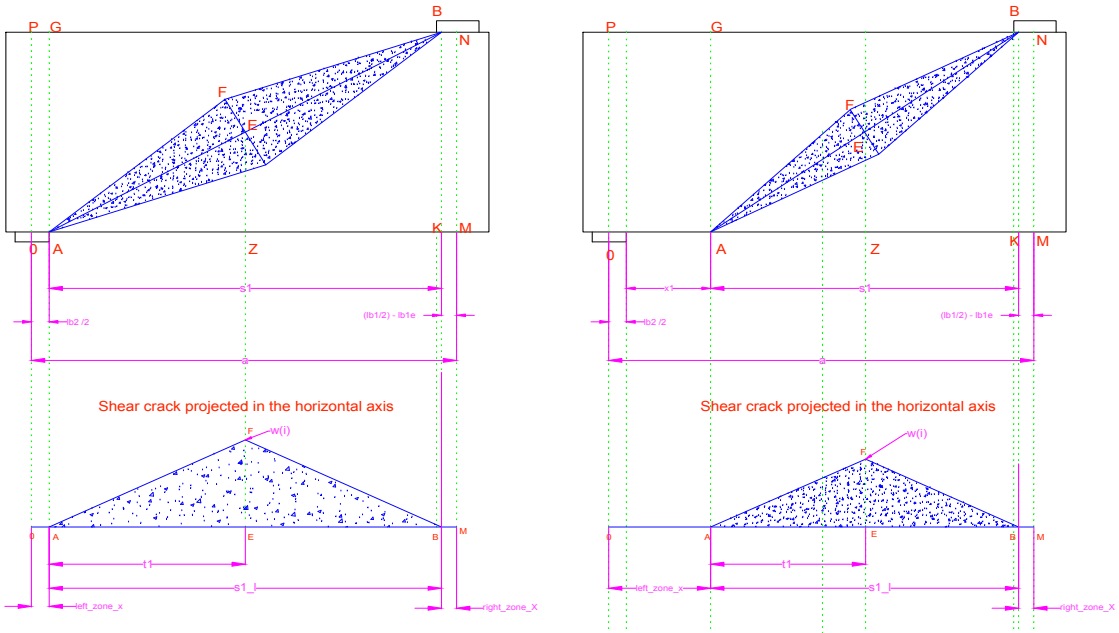

Figure 46 Division of beams according to the angle α_1, (a) $\alpha_1 > 35°$, (b) $\alpha_1 = 35°$

Based on these observations, beams belonging to the group (b) have a region (OPGA) higher than beams belonging to the group (a). This is an important aspect to keep in mind since this region as well as the region (KMNB) are those where the crack has no influence at all. Thus, an FRP strip located in any point

inside those regions will have no contribution to shear strength, since this is not subjected to any stress, and therefore an unnecessary cost.

Once the beam is divided into the three regions described above, the next step is to model the FRP configuration of the deep beam. Nevertheless, the modelling of the FRP configuration cannot be obtained directly since the parameters to consider are enormous. Thus, the solution to a specific FRP configuration is obtained dividing the problem into four steps that are described below:

1. Initially, it is supposed that the beam is strengthened with discrete FRP strips along the entire shear span.
2. Then, a function is implemented to obtain the real configuration of the FRP.
3. Next, the influence of the crack shape within the shear span is implemented.
4. Finally, the contribution of the real FRP configuration to the shear behavior is obtained when combining the three previous steps.

4.4.4 Influence of the (h_{FRP}/h) ratio in the process of debonding

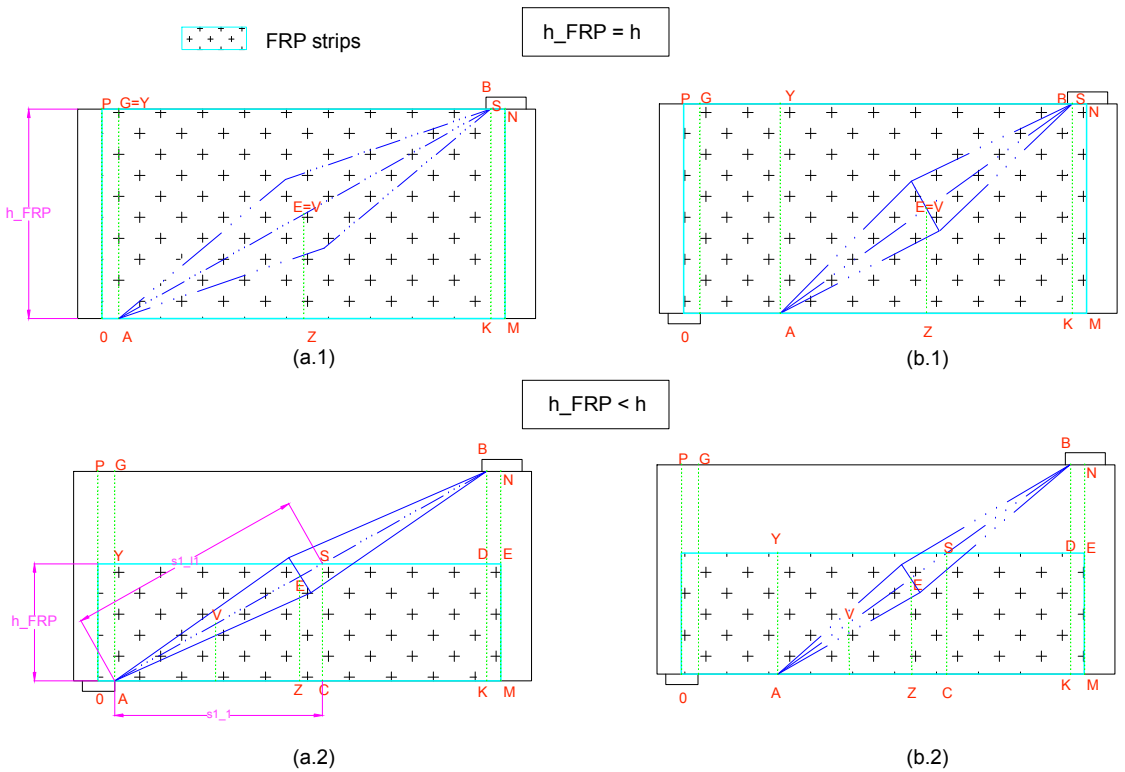

Figure 47 Beams divided according to h_{FRP}/h ratio and the angle of the shear crack

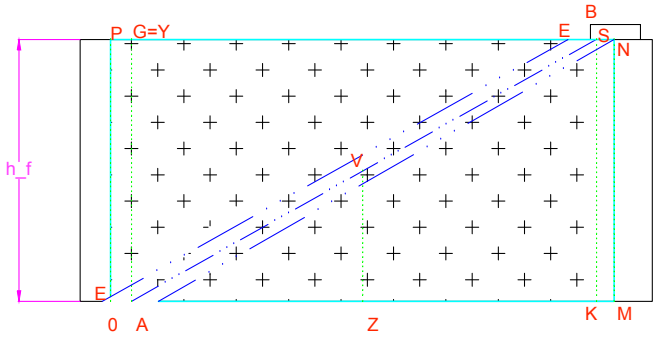

(Rectangular shape)

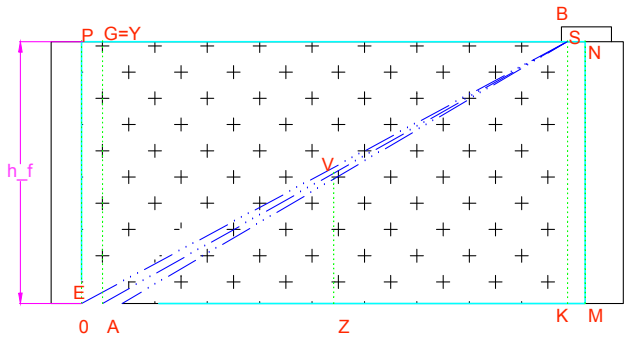

(Triangular shape)

Figure 48 Alternative crack shapes

As shown in Fig. 47, an ideal FRP configuration is considered. This configuration considers that the FRP is placed all along the shear span, hence the three regions described above are covered with it. It is observed that the beams can be classified into two big groups and two sub-groups. The first group (a) corresponds to the beams where $\alpha_1 > 35°$, while the second group (b) corresponds to the beams where $\alpha_1 = 35°$. On the other side, the first sub-group (a.1 & b.1) gathers the beams where the depth of the FRP is equal to the depth of the beam, while the second sub-group (a.2 & b.2) gathers the beams where the depth of the FRP is lower than the depth of the beam.

It is also noticed that three additional points appear in the Fig. 47: point T, point S and point V, whose description is given below:

- Given that the problem is based on the 2PKT model, the crack shape is assumed to be rhombical. Based on this assumption the maximal crack width is produced at **point E** coinciding with the point V at the center of the shear span and at the half of the beam's depth. In cases where the shape is other than the rhombical, the position of point E changes. If the shape is rectangular, the point E is located everywhere along the shear CRACK, while if the shape is triangular, the point E is located at the end of the shear crack, i.e., at point E.

As an example, the Figure 48 gives the position of point V according to the crack shape for a beam strengthened with FRP strips in its entire depth.

- The position of the **point V** on the contrary depends only on the (h_{FRP}/h) ratio, the crack shape has no influence at all. In cases where this ratio is equal to 1 (configuration a.1 & b.1), the position of point V is equal to that of point E. In cases where this ratio is lower than 1, meaning that the FRP does not covers the entire depth of the beam (configuration a.2 & b.2), point V moves towards the support along the shear crack, and therefore its position will be more on the left and lower than the point E.
- Regarding **point S** position**,** it is observed that this will be influenced by two parameters: (1) the intersection of the shear crack with the right side of the last FRP sheet, and (2) the (h_{FRP}/h) ratio. Thus, for beams belonging to group (a1 & b1), the point S and point B coincides, while beams belonging to group (a2 & b2) the point S and point B does not coincide.

In conclusion, the lower is the (h_{FRP}/h) ratio, the higher is the ineffective area (CMES), and therefore a lower contribution to shear strength is due to the use of FRP strips.

Here below the formulas used for obtaining each of these regions are given:

For the triangle **AKB**, if (h_{FRP}/h = 1) or (h_{FRP}/h < 1),

$$S_1 = \frac{h}{\tan \alpha_1} \tag{38}$$

$$S_{1,L} = \sqrt{h^2 + s_1^2} \tag{39}$$

$$t_1 = \frac{S_{1,L}}{2} \tag{40}$$

For the triangle **ASC,** only if (h_{FRP}/h < 1),

$$S_{1,1} = \frac{h_{FRP}}{\tan \alpha_1} \tag{41}$$

$$S_{1,L,1} = \sqrt{h_{FRP}^2 + s_{1,1}^2} \tag{42}$$

$$t_{1,1} = \frac{S_{1,L,1}}{2} \tag{43}$$

For the length **OA**,

$$left_{zone,x} = \frac{lb_2}{2} + \left[a - \frac{lb_1}{2} - \frac{lb_2}{2} + lb1_e - S_1\right] \quad if\ \alpha_1 = 35° \tag{44}$$

$$left_{zone,x} = \frac{lb_2}{2} \quad if \quad \alpha_1 = 35° \tag{45}$$

For the length **KM**,

$$right_{zone,x} = \left[\frac{lb_1}{2} - lb1_e\right] \quad if\ \alpha_1 \geq 35° \tag{46}$$

For the coordinate X and Y of the point **E**,

$$Coordinate\ X\ of\ point\ (E) = \frac{a}{2} \tag{47}$$

$$Coordinate\ Y\ of\ point\ (E) = \frac{h}{2} \tag{48}$$

For the coordinate X and Y of the point **V**

$$if\ \frac{h_{FRP}}{h} = 1;\ \begin{Bmatrix} Coordinate\ X\ of\ point\ (V) = left_{zone,x} + \frac{S_1}{2} \\ Coordinate\ Y\ of\ point\ (V) = \frac{h}{2} \end{Bmatrix} \tag{49}$$

$$if\ \frac{h_{FRP}}{h} < 1;\ \begin{Bmatrix} Coordinate\ X\ of\ point\ (V) = left_{zone,x} + \frac{S_{1,1}}{2} \\ Coordinate\ Y\ of\ point\ (V) = \frac{h_{FRP}}{2} \end{Bmatrix} \tag{50}$$

4.4.5 Effective and ineffective regions

As previously defined, beams were divided into two big groups depending on the angle of the shear crack. Then, beams of each group were divided into three different regions depending if they are influenced or not by the shear crack. Then, depending on the (h_{FRP}/h) ratio and the crack-shape, three main points were determined. In this new sub-section all these effects are considered are put

together to determine which zones really contribute to shear strength and which do not.

As shown in the Figures 49 three regions are localized, but their size is now modified due to the influence of the FRP. Those regions are:

- An ineffective region on the left (OAYQ) whose size is dependent on the angle of the shear crack and the (h_{FRP}/h) ratio. Furthermore, it is observed that the value that contributes the most to increase the size of this region, as described before, is α_1 since for beams where $\alpha_1 > 35°$ the width of this region decreases, while for beams where $\alpha_1 = 35°$ the width of this region increases, and therefore the size of this region.
- An ineffective region on the right (KMDE) of the beam whose size is dependent on the (h_{FRP}/h) ratio. Thus, the smaller is the (h_{FRP}/h) ratio, the higher is this region, and therefore much lower the contribution of FRP to shear resistance.
- An effective region (AYSC) where the FRP contributes the most in resisting shear.

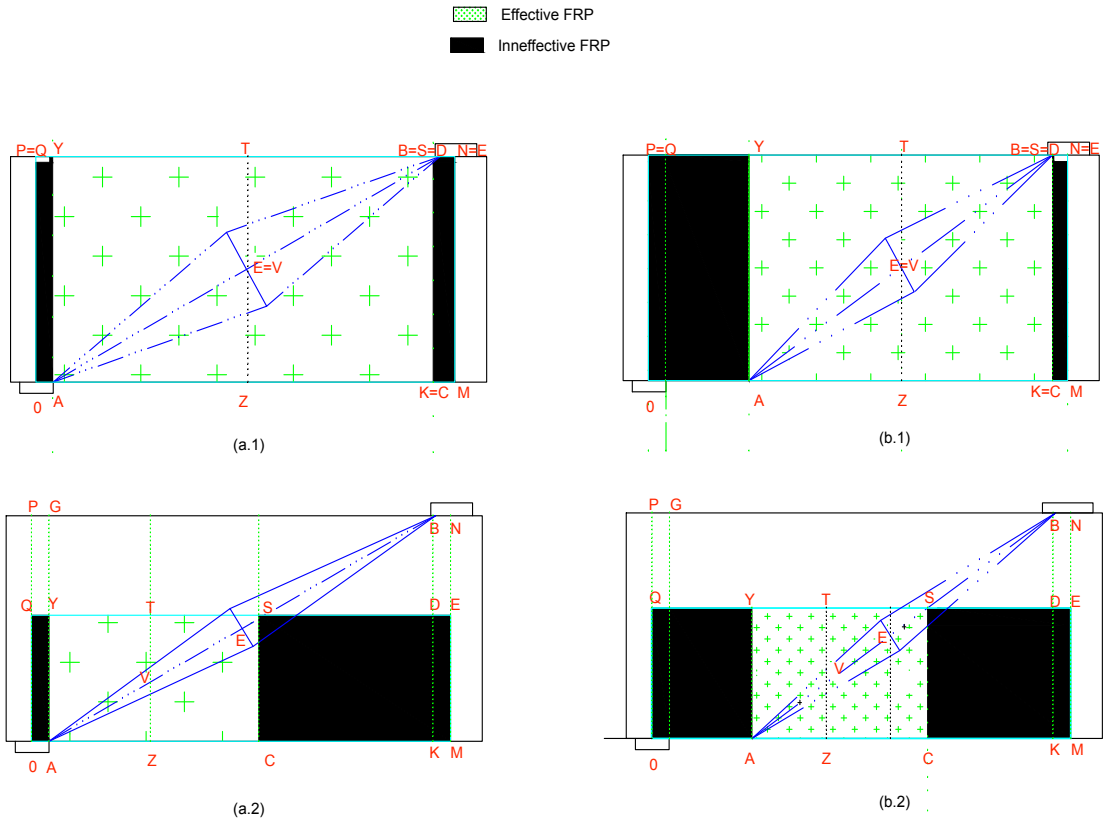

Figure 49 Effective and ineffective regions

4.4.6 Assumptions for the process of debonding in effective regions

Once the effective and ineffective regions are located, the process of debonding for effective regions is explained. To do so, some previous concepts must be introduced.

First, as deduced from Fig. 48, beams having an (h_{FRP}/h) ratio equal to 1, can be wrapped with all the wrapping schemes available, i.e., full, U-jacketing or side bonding. On the contrary, beams having an (h_{FRP}/h) ratio lower than 1, cannot longer have the full wrapping scheme since it is obligatory that for a beam to have a Full wrapping scheme this has to be bonded on the bottom and on the upper face of the beam to develop the linear ascending branch of the curve BP (Fig. 39), and finally attaint the point P corresponding to the ultimate strain before rupture of the FRP.

Second, the debonding starts propagating at any point located in the line AS, and then propagates vertically to the bottom and the upper line "**QD**" and "**OM**", as illustrated in the Fig. 50. Although the speed of debonding (u_1 & u_2) is equal, the time where debonding reaches the upper or the bottom line is different. This is mainly due to the distance x_1 and x_2 are both different from each other, hence the time is also different.

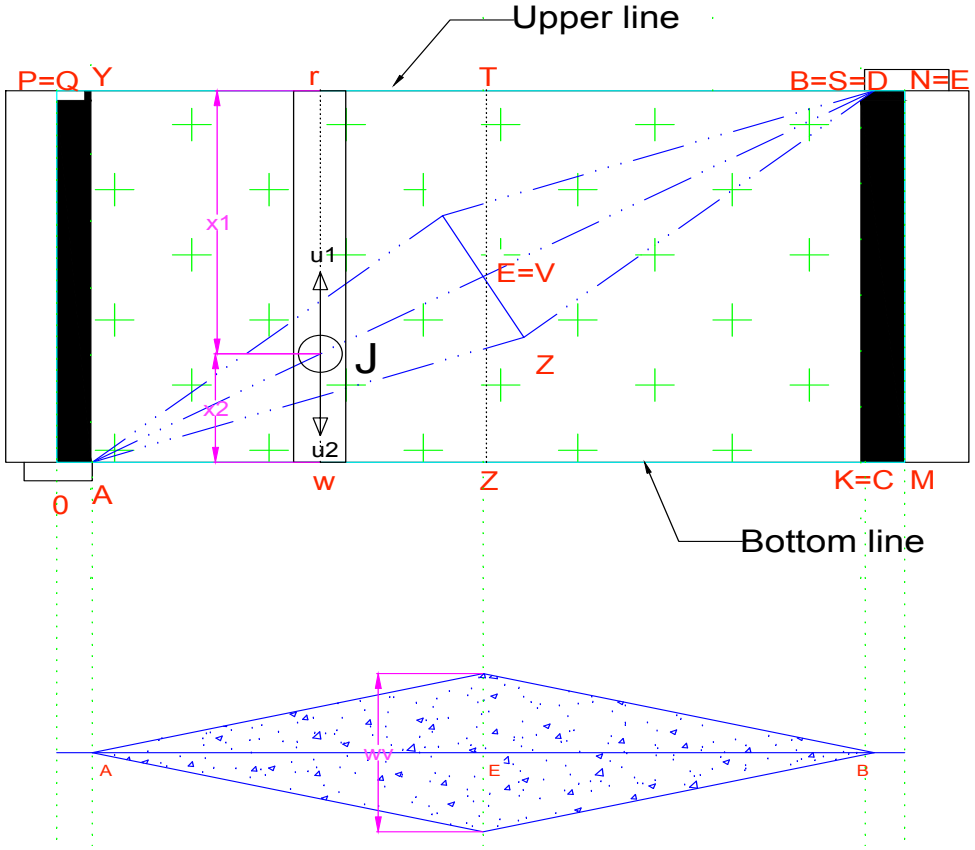

Figure 50 Debonded lengths for a sample specimen

With all these concepts in mind, it is necessary to mention some important assumptions:

1. As the shear crack widens, the speed u_1 and u_2, which are equal, are assumed to propagate vertically towards the upper/bottom line;
2. A U-jacketing scheme is supposed to bond the bottom face of the beam as shown in the Fig. 36.b;
3. The crack shape is rhombical as supposed by Mihaylov et al., 2013. In this case, the vertical displacement in the shear crack at the point E (w_v) is used. This value is expressed with the two degrees of freedom from the 2PKT model according to the formula:

$$w_v = 0.5\,\varepsilon_{t,avg} l_k \cot\alpha_1 + \Delta_c \tag{51}$$

   The crack-width in a point other than E has to be calculated based on trigonometry;

4. The effective region is divided into two sub-regions: region **AYZT** and region **ZTSC.**

   a. The region **AYZT** on the left-hand side of the effective region is intersected by the shear crack line AV. It is observed that a point J moving in the line AV from the point A to the V decreases in distance x_1 and increases in distance x_2.
   b. The region **ZTSC** on the right-hand side of the effective region is intersected by the crack line VS. It is observed that a point J moving in the line VS from the point V to the S decreases in distance x_1 and increases in distance x_2.

   In the points (A, V and S), the value of the distances x_1 and x_2 corresponding to the debonded lengths are:

$$Point\ A\ ;\ \begin{Bmatrix} x_1 = h_{FRP} \\ x_2 = 0 \end{Bmatrix} \tag{52}$$

$$Point\ V\ ;\ \begin{Bmatrix} x_1 = \dfrac{h_{FRP}}{2} \\ x_2 = \dfrac{h_{FRP}}{2} \end{Bmatrix} \tag{53}$$

$$Point\ S\ ;\ \begin{Bmatrix} x_1 = 0 \\ x_2 = h_{FRP} \end{Bmatrix} \tag{54}$$

It is concluded therefore that an FRP strip intersected by the line AV has a distance $x_1 > x_2$, while in the line VS the distance $x_1 < x_2$. Therefore, both of these distances follow a linear relationship as show in the Figure 50.

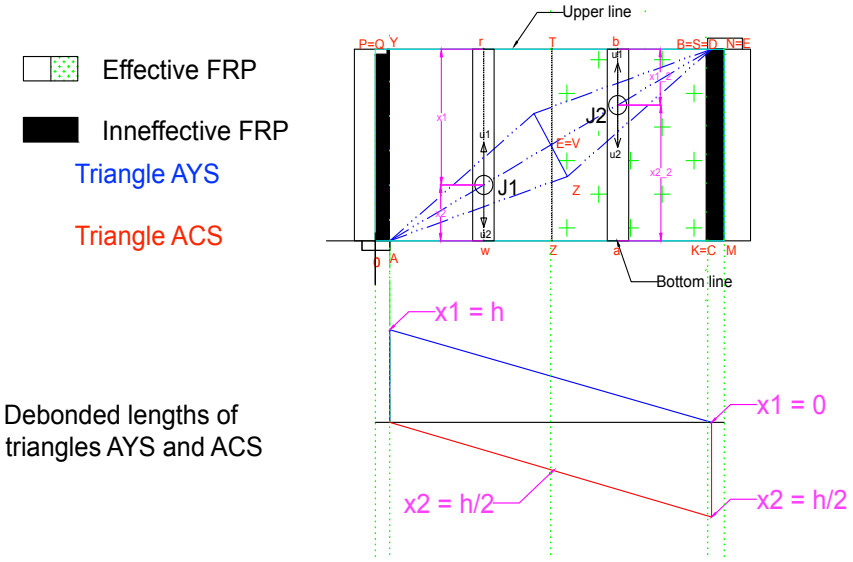

Figure 51 Debonded lengths for the upper/lower block separated by the shear crack

5. A value $k_{FRP,\,rupture}$ is considered. This value accounts for strain concentrations at the corners of the section. This value ranges from 0.5 to 0.85 being influenced mostly by the radius of curvature of the corner of the section and the thickness of the FRP strip. For the sake of simplicity, and also to be more cautious, the lower boundary was taken (0.5)
6. The process of debonding is explained for a sample beam where the contribution to shear of the FRP is the highest. This is a beam with (α_1 >35°) and (h_{FRP}/h =1). The angle (α_1) was chosen to be higher than 35° since this thesis focuses on deep beams, which are likely to have (α_1 >35°). On the other side, the choice of (h_{FRP}/h =1) was made to study all the wrapping schemes, given that a lower ratio will not consider the Full wrapping scheme.
   The other cases where the FRP is applied in a lower depth or where the angle of the shear crack is equal to 35° are not considered. Nonetheless, the procedure that is about to be described for a sample beam is also valid for a beam whose properties are different than those of the sample beam, as long as the previous assumptions and properties remains.

4.4.7 Debonding process and associated stresses for a Full wrapping scheme (intermediate step M)

4.4.7.1 Determination of the debonded lengths (x_1, x_2, x_{total})

As previously defined, a full wrapping scheme is the ideal configuration since the FRP wrap is expected to attain the ultimate strain, and therefore the ultimate stress that translates into a maximal contribution of the FRP to shear resistance. In this case, the process of debonding and the corresponding debonded length for the strips located in the regions AYZT and ZTSC is explained below.

- For an FRP strip located in the region **AYZT**, an FRP strip located at the point J_1 as shown in the Fig. 51 for instance, it is observed that as the load increases, the debonding process propagates towards the bottom and the upper line at the same speed. It is also observed that debonding will reach the point **"w"** before than the point **"r"**, given that the distance x_2 is lower than x_1. As a consequence, it could be though that when debonding reaches the point w, the FRP strip has completely debonded. However, this is not the case since when debonding reaches the point w, the FRP is wrapped around the bottom face of the beam, and therefore the FRP continues to stretch up until reaching the ultimate strain located at point P of the Fig. 39. On the other side, when debonding reaches point r, but given that the FRP wrap is also wrapped around the top face of the beam, the FRP wrap can also be stretched up until attaining the ultimate strain.
- For an FRP strip located in the region **ZTSC**, given that the FRP strip is wrapped around the bottom and the top face of the beam, when debonding reaches the point a and b the FRP can also be stretched up, and therefore attaint the ultimate strain.

In conclusion, for an FRP strip located inside the region **AYZT and ZTSC**, the total debonded length can be calculated according to the equation 53, giving the distribution of the total debonded length as shown in the Fig. 51.

$$X_{TOTAL(i)} = x_1 + x_2 \tag{55}$$

4.4.7.2 Determination of the stresses

Given that each of the FRP strips reaches the ultimate strain, the stress resisted by each strip is given by the next formula

$$\sigma_{(i)} = k_{FRP,rupture} . \varepsilon_{FRP(i)} . h_{FRP(i)} . E_{FRP(i)} \tag{56}$$

4.4.8 Debonding process and associated stresses for a U wrapping scheme (intermediate step M)

4.4.8.1 Determination of the debonded lengths (x_1, x_2, x_{total})

In this case, the process of debonding and the corresponding debonded length for the strips located in the regions AYZT and ZTSC is explained below.

- For an FRP strip located in the region **AYZT**. It is observed that for an FRP strip located at the point J_1, as the load increases, the debonding process propagates towards the bottom and the upper line at the same speed. It can be observed that the debonding will reach the point **"w"** before than the point **"r"**, given that the distance x_2 is lower than x_1. However, since the FRP is wrapped around the bottom face of the beam, when debonding reaches the point w, the process of debonding towards the bottom line stops having only debonding towards the upper line. As a consequence, when debonding reaches any point of the line (YT) the FRP strip debonds completely due to the fact that the process of debonding cannot be longer stopped. Thus, given that the debonded length in this region is governed when the debonding process reaches the upper line, and this happens only when all the FRP sheet has completely debonded, the total debonded length is equal to the full depth of the wrapped beam.
- For an FRP strip located in the region **ZTSC**, given that the debonding reaches the upper line before the bottom line, and at this line the process of debonding is not stopped, the total debonded length is governed by the distance x_1, being in this case twice the distance x_1.

The debonded lengths x1 and x2 for the effective region are obtained with the following formulas:

For the region **AYZT**

$$X_{TOTAL(i)} = x_1 + x_2 = h_{FRP} \tag{57}$$

For the region **ZTSC**

$$X_{TOTAL(i)} = 2.x_1 \quad with\ a\ linear\ descending\ relationship \tag{58}$$

4.4.8.2 Determination of the stresses

In U-jacketing schemes as well as for side bonding schemes, the stresses cannot be determined that easily as for the full wrapping scheme. In both cases the stresses would be linked to the debonded length found out with new formulas.

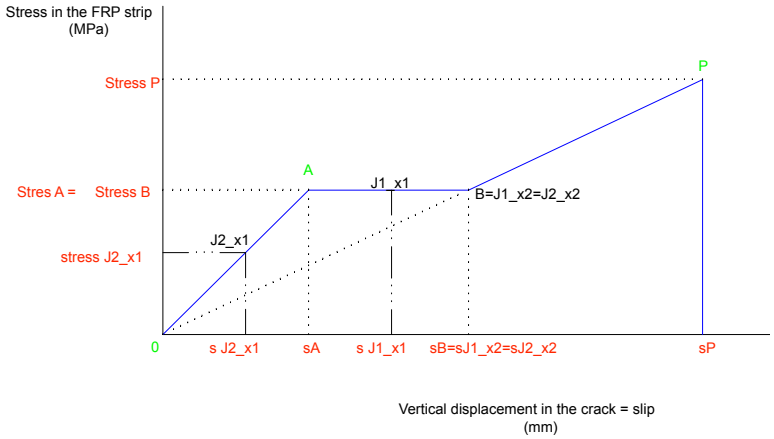

Figure 52 Full process of debonding for a U-jacketing system

Based on the scheme of the total debonded length given in the Fig. 53 for a U-jacketing scheme, it is concluded that the debonded length of the FRP strips located in the region **AYZT** is equal to the full depth of the FRP strip, meaning therefore that the slip is equal to that of point B from the Fig. 52. On the contrary, for the region **ZTSC** the debonded length is no longer equal to the full depth of the FRP strip, but decreases linearly from $\mathbf{h_{FRP}}$ **at V to 0 at the point S**. This change in the debonded length influences as well on the slip generated in the FRP strips, since the slips will also decrease from s_B at point V to 0 at point S of the beam. Nevertheless, as shown as well in the Fig. 52, this reduction in the slip associated to a stress is not linear but constant and then linear. Thus, the stresses associated to each slip located from the point V to the point S, have to be obtained differently. This procedure is given below:

1. Even though the stresses in the plateau (AB) remain constant during the reduction of the slips, the slips do not. Thus, since the slips can be directly linked to the debonded length, it is important to determine what is the debonded length at which the plateau finishes and the linear descending branch starts. This debonded length can be determined with the formula

$$x_{t(A)} = \frac{s_A . E_{FRP}}{\sigma_B} \tag{59}$$

2. Once the debonded length $x_{t(a)}$ is determined, the length **"m"** at which the stresses decrease linearly from σ_B to 0 must be determined. This is done according to the formula given below

$$m = \frac{x_{t(A)} . h_{FRP}}{\frac{s_1}{2}} \tag{60}$$

$$n = \frac{s_1}{2} - m \tag{61}$$

With the values m, n and $x_{t(A)}$ determined, the scheme of the stresses is obtained, and therefore the stress at each individual strip $\sigma_{FRP(i)}$

4.4.9 Debonding process and associated stresses for a Side wrapping scheme (intermediate step M)

4.4.9.1 Determination of the debonded lengths (x_1, x_2, x_{total})

In this case, the process of debonding and the corresponding debonded length for the strips located in the regions AYZT and ZTSC is explained below.

- For an FRP strip located in the region **AYZT**, given that the debonding reaches the bottom line before the upper line, the debonded length is governed by the distance x_2, being in this case twice the distance x_2.
- For an FRP strip located in the region **ZTSC**, the phenomenon is equal to that of the U-jacketing scheme for the same region.

In conclusion the debonded lengths for the effective region can be obtained with the following formulas:

For the region **AYZT**

$$X_{TOTAL(i)} = 2.x_2\,;\ with\ a\ linear\ ascending\ relationship \tag{62}$$

For the region **ZTSC**

$$X_{TOTAL(i)} = 2.x_1\,;\ \ with\ a\ linear\ descending\ relationship \tag{63}$$

The debonded length for this wrapping scheme is given at the Fig. 51.

4.4.9.2 Determination of the stresses

In this case, the stresses $\sigma_{FRP(i)}$ must be determined as for the U-jacketing scheme, with the only difference that the calculus made for the region **ZTSC** must be done as well for the region **AYZT.** Thus, the stresses configuration is symmetrical as shown in the Fig. 51

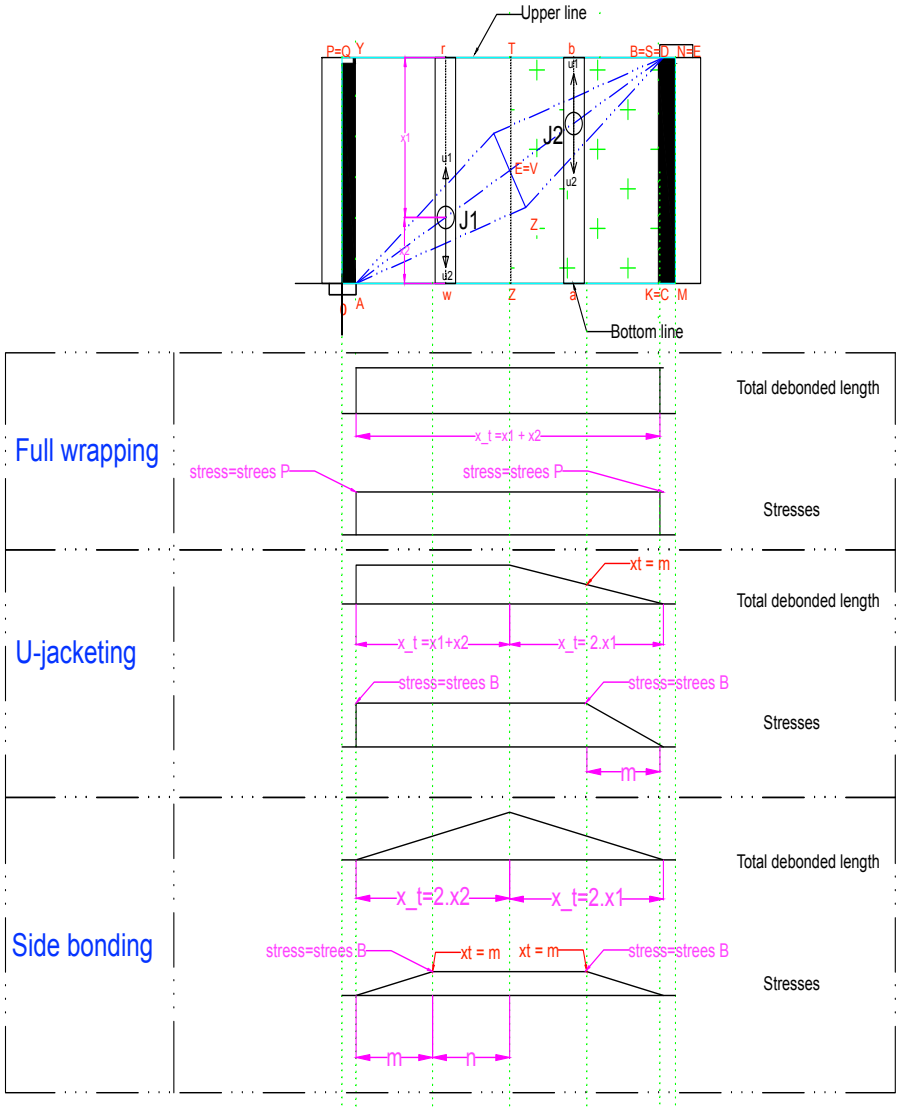

Figure 53 Total debonded length and stresses associated

4.4.10 Average stress and slips induced in the FRP in an ideal configuration and real configuration (steps 3-4-5)

Once the stresses for each strip in this **ideal configuration** are determined, the average of the stresses $\sigma_{avg,\,FRP,\,\text{ideal}}$ and the maximal vertical displacement of the crack supported by the FRP $w_{v,\,FRP,\,ideal}$ must be calculated.

For $w_{v,\,FRP,\,ideal}$

$$\sigma_{TOTAL} = \sum_{i=0}^{n} \sigma_{FRP(i)} \tag{64}$$

$$w_{v,FRP,ideal\ (i)} = \frac{\sigma_{TOTAL} \cdot X_{TOTAL(i)}}{E_{FRP}} \tag{65}$$

For the **average stress** supported by the ensemble of the FRP strips $\boldsymbol{\sigma}_{avg,\,FRP,\,\mathbf{ideal}}$

Once the maximal vertical displacement of the crack supported by the FRP $w_{v,FRP,ideal\,(i)}$ are obtained, a linear interpolation with these values and those from the curve corresponding to the Full range behavior of a type B joint, is made.

The values of the slips and the stresses for **a real configuration** are obtained by multiplying $w_{v,FRP,ideal\,(i)}\ and\ \sigma_{avg,FRP,ideal(i)}$ times a vector that models the real position of the FRP strips X_{Real}, hence:

$$w_{v,FRP,real\,(i)} = w_{v,FRP,ideal\,(i)}.X_{real} \tag{66}$$

$$\sigma_{avg,FRP,real\,(i)} = \sigma_{avg,FRP,ideal(i)}.X_{real} \tag{67}$$

4.4.11 Shear force carried by the FRP strips (step 6)

To finally evaluate the shear contribution of the FRP some previous steps have to be done:

1. Given that the width of the crack increases at each load step, the vertical displacement associated to it (w_v) increases as well. Therefore, for each load step the value ($w_{v(i)}$) at each point of the shear crack is calculated.
2. Once the values ($w_{v(i)}$) are obtained, the stress associated to it is calculated. To do so, a linear interpolation of the values ($w_{v(i)}$) to the values of the curve $\sigma_{avg,FRP,real(i)}\ vs\ \omega_{v(i)}$ is made. Therefore, if at each load step $\omega_{v(i)} \leq w_{v,FRP,real\,(i)}$ a stress $\sigma_{crack,FRP(i)}$ is obtained, but if $\omega_{v(i)} > w_{v,FRP,real\,(i)}$ the stress $\sigma_{crack,FRP(i)} = 0$.
3. Then the average value of $\sigma_{crack,FRP(i)}$ is obtained by the formula:

$$\sigma_{crack,FRP} = \frac{1}{n}\sum_{i=0}^{n}\sigma_{crack,FRP(i)} \tag{68}$$

$$\begin{cases} n = number\ of\ strips\ in\ the\ effective\ region \\ i = stress\ associated\ at\ the\ strip\ n \end{cases}$$

4. Finally, the shear force resisted by the FRP strips V_{FRP} under a specific configuration is evaluated by the formula:

$$V_{FRP} = \sigma_{crack,FRP}.A_{FRP} \tag{69}$$

5 Validation of extended 5 spring model

5.1 Introduction

Once the extended five spring model is defined, it is necessary to validate the offered results against experimental data. To do so, two experimental studies were selected, one corresponded to the study carried out by Bukhari et al. (2003) and the other corresponded to the study made by Rasheed et al. (2012). Whilst Bukhari tests studied the contribution to shear strength of different FRP configurations, Rasheed tests studied the influence of the a/d ratio and the transverse reinforcement for retrofitted or non-retrofitted beams with a constant FRP ratio. Therefore, during this section a comparison between experimental and predicted results was made. However, before carrying out such study, an analysis showing the influence of the crack-shape in the predicted results was made.

5.2 Experimental results and derived observation

In order to have a more accurate idea about what are the expected results, a brief description of the experimental results is given below.

5.2.1 Bukhari tests

As previously mentioned, Bukhari et al. (2003) separated the tested beams in two big groups: group A where (h_{FRP}/h) = 1, and group B where (h_{FRP}/h) = 0.5. Evidently, beams where (h_{FRP}/h) = 1 showed an increment in the shear strength higher than those where (h_{FRP}/h) = 0.5. However, this contribution was not only dependent on this ratio but also on the position of the CFRP sheet within the shear span. In this case, it was observed that beams where the CFRP sheet was applied close to the support, the contribution of it to shear strength is minimal.

On the other side, given that the tested beams had an (a/d) ratio higher than 2, their initial failure mode, without any FRP wrapping, was a combination of flexural and shear failure as illustrated in the crack-pattern of the control beam in the Fig. 55. Nonetheless, when the CFRP sheet is placed, the failure mode changes completely since it is the debonding of the CFRP sheet that becomes the new failure mode. In this case, since the CFRP sheet stops the crack propagation, the crack-pattern tended to change from shear to flexural shear as illustrated in Fig. 54.

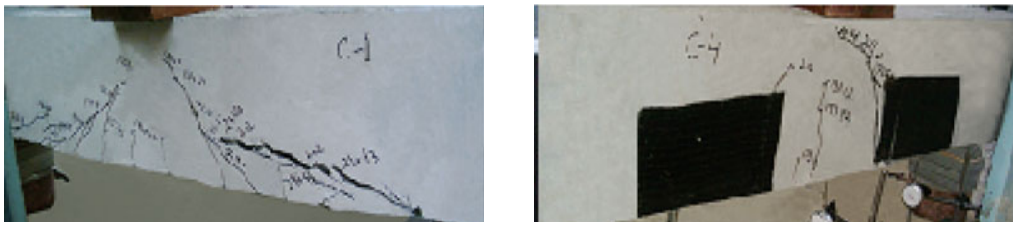
Figure 54 Crack-patterns and failure mode observed, (left CB), right (C4), (Bukhari et al., 2003)

5.2.2 Rasheed tests

Rasheed et al. (2012) studies focused on the contribution to shear strength of three different parameters: the transverse reinforcement and the (a/d) ratio. To do so, deep beams were separated in two groups: the first group (DB) comprised beams with different a/d ratio and different transverse reinforcement but without retrofitting, while the second group (RDB) comprises the same elements of the first group but with retrofitting CFRP sheets.

As for Bukhari tests, the failure observed mode for beams belonging to the first group is mainly shear failure, while for deep beams retrofitted with CFRP strips the failure mode is either debonding of CFRP strip or concrete crushing around the loading plates as illustrated in Fig. 55.

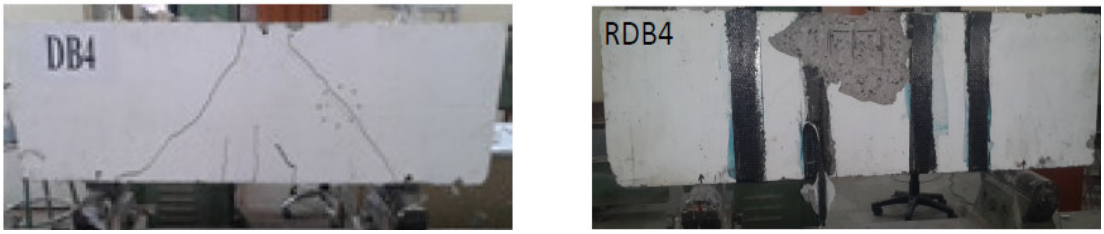

Figure 55 Crack pattern of Rasheed tests (left = non-retrofitted beams); (right = retrofitted beams), (Rasheed et al. 2012)

5.2.3 Observations

As expected, debonding becomes the predominant failure mode when using FRP wraps either for Rasheed or Bukhari tests. Nevertheless, additional failure modes appeared, such as concrete crushing at the level of the support/loading plate. Given that the extended 5SM is based on 2PKT, which only accounts for shear failure, it is expected that the extended 5SM could not capture very well this failure mode. To this end, the vertical strains at which debonding occurs were calculated. This formula, proposed by the American design code ACI 440.2R-08, allowed to stop the code at a load considered as the debonding load. A more precise description of this process is given in the section 5.4.

5.3 Influence of the crack-shape

In order to evaluate the influence of the crack-shape in the results, a comparison of experimental vs predicted results was made by choosing three sample beams among all the experimental data. Two of the beams belong to specimens C3 and C5 from Bukhari, while the third specimen corresponds to the specimen RDB-8 from Rasheed. Bukhari specimens were selected since they are both completely bonded on both sides with the only difference that the length a_2 is different. However, given that for both beams the angle ($\alpha_1 = 35°$) and the (a/d) ratio is higher than 2, it is expected that in both beams the ineffective region is considerable, in such a way that the effective region for both beams turned out to be almost the same. Rasheed specimen on the other side, was chosen since the predicted results for the non-retrofitted member showed a good agreement with experimental results, and also because it would illustrate the behavior of a U-strip under the influence of different crack shapes.

Figure 56 illustrates the selected specimens with their corresponding load-deflection curves for the rhombical and constant crack shape. Based on this figure the following conclusions are made:

1. Regarding to side bonding schemes. One can conclude that a rectangular crack-shape generates a more brittle behavior in the FRP sheets than a rhombical shape. This is because the vertical displacement in the shear crack "$\mathbf{w_v}$" was supposed to be equal at every point in the shear crack, instead of only at the point E (Fig. 50). Thus, each FRP strip intersected by the shear crack is subjected to the same stress, hence when w_v is higher than the maximal vertical displacement resisted by the FRP $\mathbf{w_{v,\,max}}$, all strips fail. This latter explains the sudden drop in C3 and C5 specimens once the ultimate load was obtained.

   On the contrary, a more ductile behavior is observed at the rhombical crack shape. In this case, the calculated value $\mathbf{w_v}$ corresponds only to that of the point E, while for the other points in the shear crack $\mathbf{w_v}$ diminish linearly up to zero at the load and support points (**points A & B**). This assumption implies that the FRP strips are subjected to descending stresses, hence when w_v is higher than $\mathbf{w_{v,\,max}}$, only the strip where this occurs fails, while the others are still bonded to the concrete and can continue resisting. Due to this, an ascending and a descending branch is observed. The ascending branch corresponds to the activation of FRP, while the descending branch corresponds to a progressive delamination of the FRP strips as also demonstrated by Chen et al. (2012).

With respect to the RDB-8 beam, it can be observed that the calculated ultimate load is almost the same for both crack-shapes. However, as occurs with side bonding the CFRP has a more ductile behavior, when the crack shape is rhombical, given that it still contributes to deflection of the beam in the post-peak behavior.

2. Even though the pre-post peak behavior of FRP sheet/strips is different for a rhombical or rectangular crack shape, it is observed that for both crack shapes with a side bonding scheme, the deflection associated to the ultimate load is always underestimated. Among the different reasons for such behavior is the uncertainty of the length of the support plate, the deflections appeared at the loading plate when the beam is closer to the ultimate load and the validity of the model. This last is because the extended 5SM offers a better approximation when the analyzed beam accomplishes the necessary conditions to be considered a deep beam, but this is not the case since the a/d ratio is higher than 2. Otherwise the model lost his accuracy.

   On the other hand, the predicted ultimate load is slightly closer to the experimental value when the crack-shape is assumed to be rectangular.

3. A good agreement between predicted and experimental results is observed for both crack-shapes when having a U-strip. One of the reasons for this is the respect of the assumptions of the 2PKT model by the tested specimen. Due to that, the extended 5SM is more capable of giving a better approximation of the experimental results.

In conclusion, a rhombical crack shape offers a better approximation of results and a more real behavior of FRP strips. Hereafter, a rhombical crack shape is considered for the discussion of results from both experimental studies.

Rhombical	Rectangular
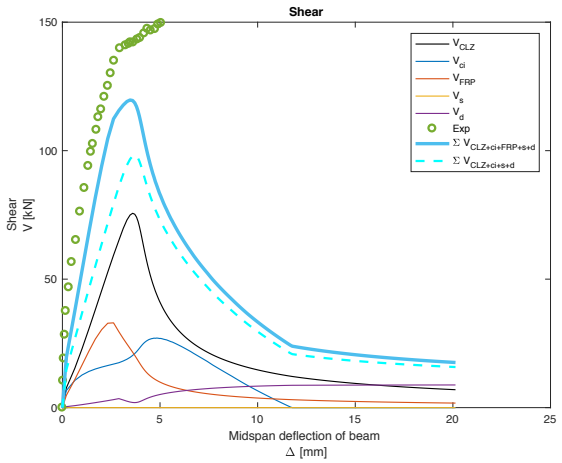	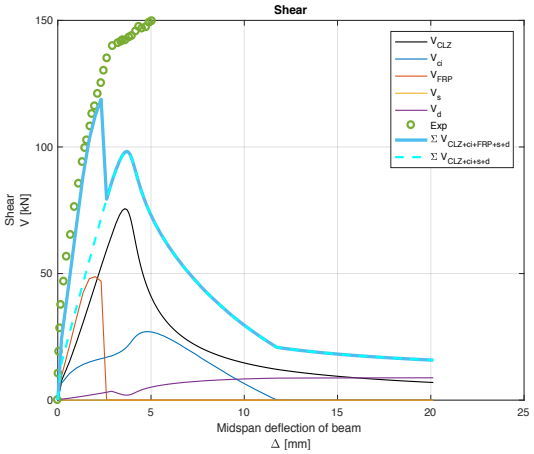
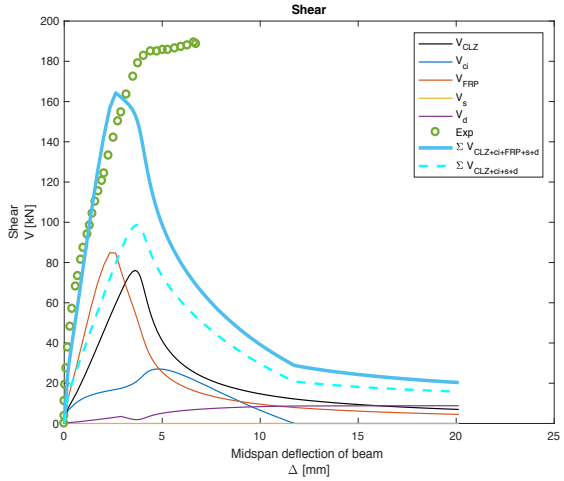	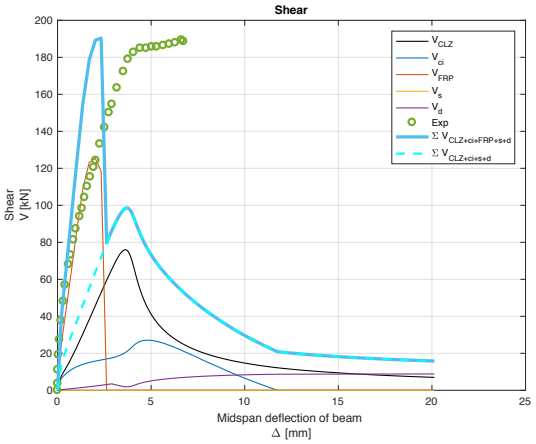
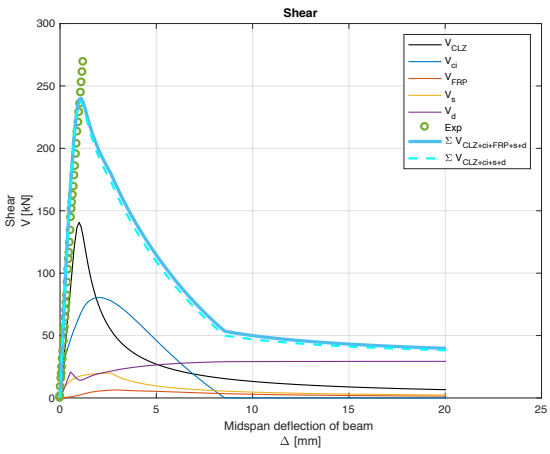	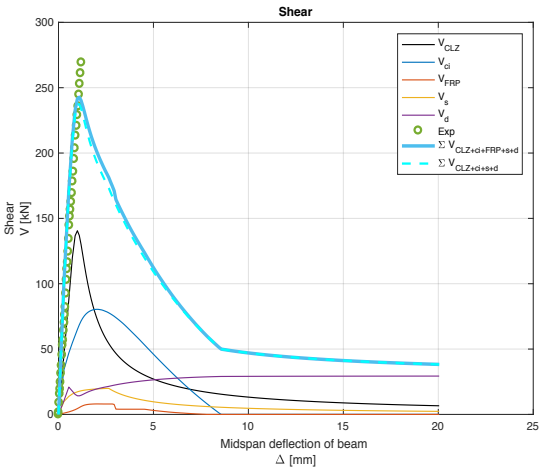

Figure 56 Experimental vs Predicted results, from the top to the bottom on both sides of the Figure (C3-C5 and RDB-8)

5.4 Discussion of results

5.4.1 Bukhari tests

Figure 57 illustrates the experimental vs the predicted ultimate applied load. As it can be seen, beams belonging to the group A showed a better estimation of the ultimate applied load in comparison with beams of group B. Evidently, one of the main reasons for this agreement is the contribution of the CFRP to the shear strength, that even in the two groups was different, it was in both groups captured. However, when looking at the Fig. 59 some conclusions are made:

1. For group A and group B, the contribution of the FRP to the shear strength was better captured if the wrapping covers the entire shear span or if the FRP is placed in the effective regions. This was observed for beams C3, C5 and C6 from group A, and beams C2, C4 and C7 from group B, where the difference between the predicted vs the experimental contribution of the CFRP was the lowest. On the other hand, it is also observed that beams belonging to group A showed even a lower difference in comparison to the beams from group B. Therefore, the value that plays the most in predicting the shear strength in this case is the h_{FRP}/h ratio, since the higher is this value, the higher is the predicted shear strength.
2. On the other side, when the CFRP is placed in the ineffective regions such as for the beams C8, C9 and C11 from group A and C10 and C12 from group B, the difference between the predicted vs the experimental contribution of the CFRP was the highest. This was due to the assumption that FRP sheets/strips placed in the ineffective regions do not contribute at all to the shear behavior. However, this enhancement in shear strength produced by the consideration of the CFRP sheets/strips placed in these regions is not that high, except for members C9 and C7 where the majority of the CFRP was placed in the ineffective regions, and therefore the predicted contribution is far away from the experimental one.

Figure 58 on the other side illustrates the experimental vs the predicted mid-span deflection. In this case, predicted mid-span deflection were better estimated for beams belonging to the group B rather than for beams of group A. This can be appreciated in Table 10 where for beams belonging to the group B showed a lower average error[2] (12.35 %) in comparison with beams for group A (35 %). On the other hand, it is important to mention that this reduction in the average error does not correspond to a better estimation of deflections of the extended 5SM but it is just that extended 5SM is not able to capture very well the beneficial effect of FRP strips in the ductility. Even though the predicted mid-span deflection for all

[2] The average error correspond to the average for each group, not for the ensemble of the tests

beams showed an average underestimation of about **25%,** this value can be considered as a good estimation since extended 5SM did not take into consideration the stress concentration at the loading plates when the beam is close the fail. Due to this stress concentration a settlement of the supports came with, and therefore an increase in the measured mid-span deflection that cannot be well predicted by extended 5SM. Besides, an uncertainty about the length of the supporting plate and the stiffness of both, the loading and supporting plate, increases the probability of increasing the average error of the predicted mid-span deflection.

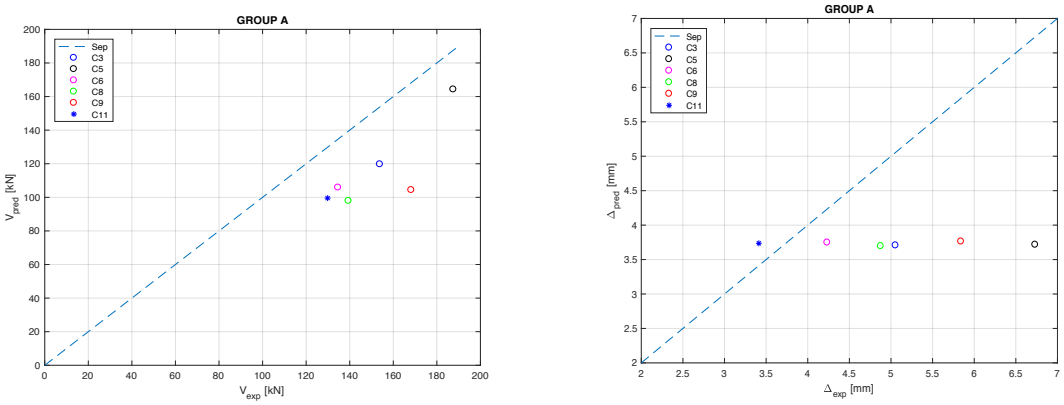

Figure 58 Bukhari experimental vs predicted results for shear and mid-span deflection group A

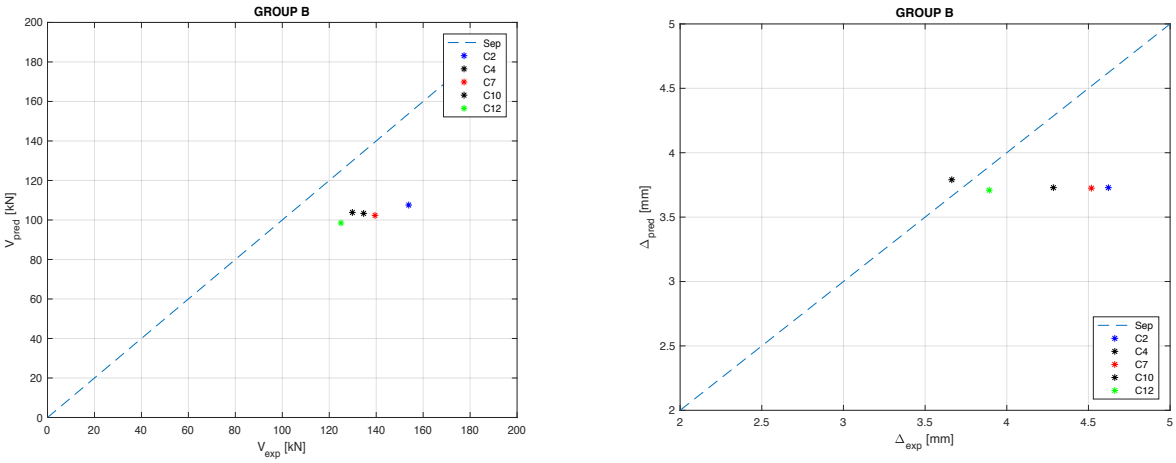

Figure 57 Bukhari experimental vs predicted results for shear and mid-span deflection group B

	Shear	*Mid-span deflection*	$\Delta V_{exp\text{-}pred}$
Average error	**ε avg** [%]	**ε avg** [%]	**ε avg** [kN]
Group A	24.51	-35	15.1
Group B	24.3	-12.35	11.2
Total	24.4	-24.6	

Table 10 Average error between predicted and experimental results of Bukhari tests

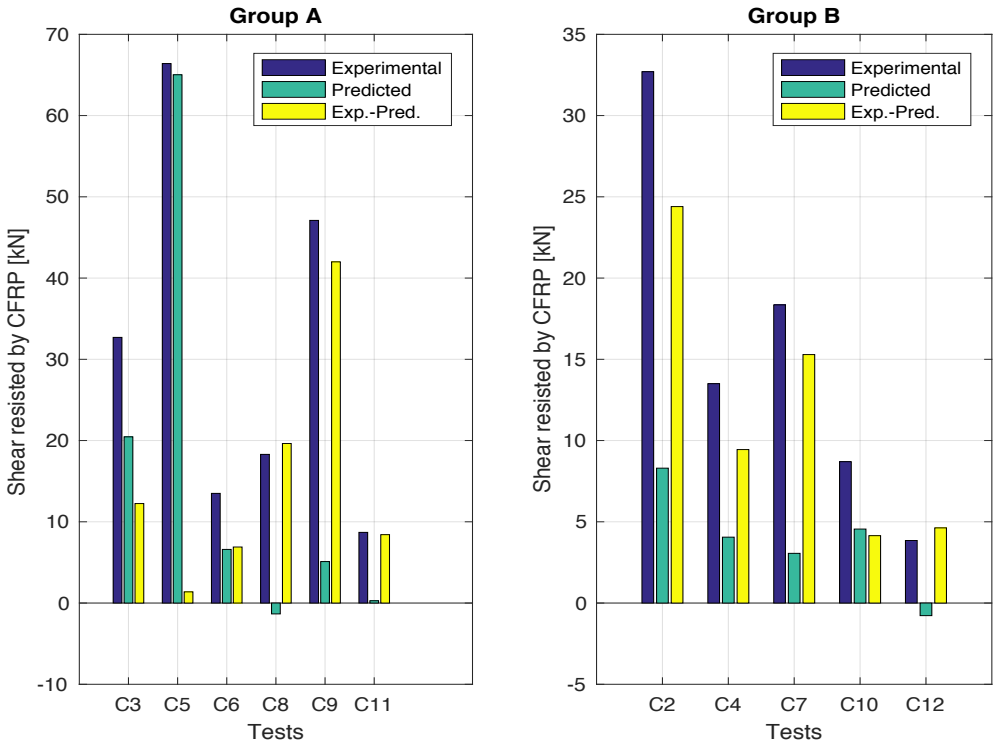

Figure 59 Contribution to shear strength due to FRP (calculated vs experimental)

5.4.2 Rasheed tests

Regarding to the experimental study carried out by Rasheed, the influence on shear strength of the shear reinforcement and the shear-span-to-depth ratio was tested.

The first parameter to be studied is the influence of shear reinforcement is discussed. As illustrated in Figure 60, members with vertical transverse reinforcement showed a better agreement of the shear strength, while members with horizontal transverse reinforcement showed a low agreement. One of the reasons for such difference is the presence of horizontal transverse reinforcement, since this reinforcement, as also demonstrated by Rasheed et al. (2012), was supposed to increase the resistance to shear of deep beams. However, given the fact they were not implemented in the extended 5SM, the model was not able to capture its positive effect, and therefore a loss of accuracy is produced. This can also be appreciated in the Figure 61 where the increment of shear of the tested element with respect to the control beam is none, while for the rest of the elements a contribution to shear was noticed.

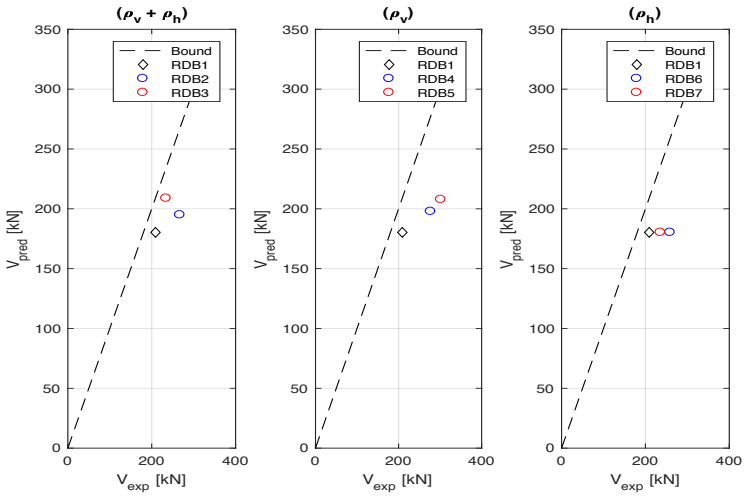

Figure 60 Rasheed predicted vs experimental shear results

It is also important to mention that another reason why the extended 5SM was not able to predict most accurately the ultimate applied load, as well as the corresponding mid-span deflection, is the apparition of stress concentration at the loading plates. This brittle failure mode, as already discussed for Bukhari tests, tended to increase the measured ultimate applied load and the corresponding deflection with the negative consequences in the predicted results. This negative effect can be appreciated in the Fig. 61 where crushing and spalling of concrete is observed.

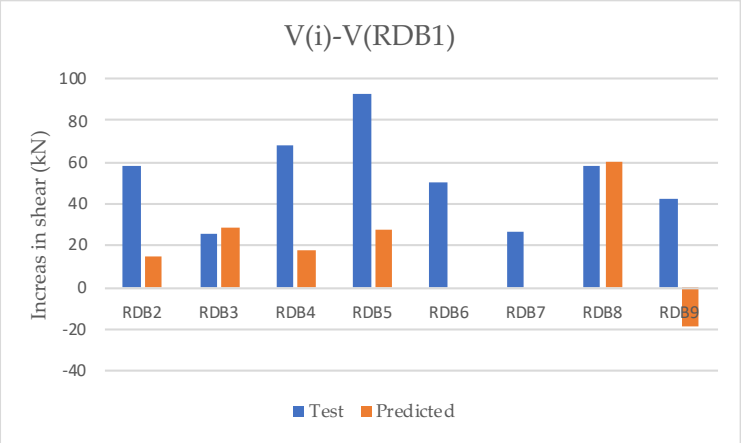

Figure 62 Increment in shear with respect to the control beam (RDB1)

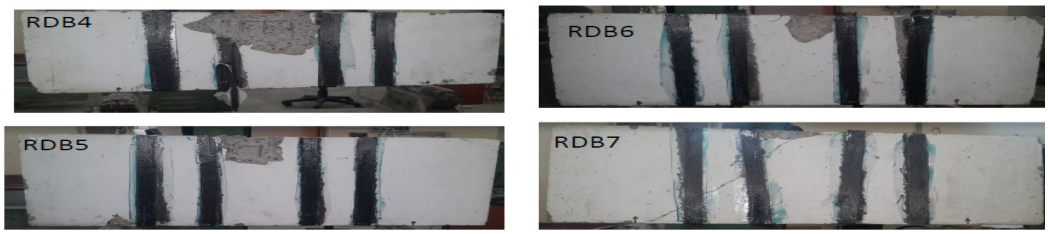

Figure 61 Brittle failure mode observed in specimens RDB4-(5-6-7)

The second parameter studied was the shear-span-to-depth ratio. Beams selected were RDB8 and RDB9 with the same amount of horizontal and vertical transverse reinforcement, but different a/d ratio. As illustrated in Fig. 63, the predicted results for RDB-8 agreed well with the experimental results, while for RDB9 the results were underestimated. In this case, extended 5SM was more effective in predicting the shear behavior for beams with small a/d ratio than for member with a higher ratio. Thus, one can conclude that the accuracy of the extended 5SM in predicting the shear behavior depends on the a/d ratio, since the smaller is a/d, the more accurate is the model.

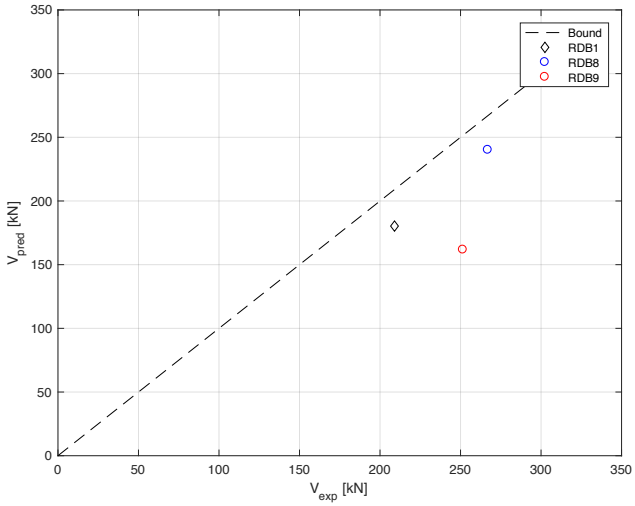

Figure 63 Predicted vs Experimental results of shear for RDB1-RDB8-RDB9

Finally, it is important to mention the paper of the CFRP in the enhancement of shear strength. One can assume that using the same amount and the same configuration of the CFRP may came with the same contribution to the shear strength. However, this is not what illustrates Fig. 64 where a huge difference between the experimental and predicted contributions attributed to the use of CFRP strips is shown. One can assume that the CFRP strips are supposed to contribute more given that they are U-strips, but in reality, this is not what happened since the strips that are closer to the loading plate will rapidly debond, and therefore their contribution would be very little, being just the further which really contributes. However, since the cross section of the CFRP strips is very low, the contribution to shear resistance is not supposed to be that high as shown by the experimental tests. Thus, more data would be necessary to know what is the factor provoking such difference.

It is important to notice as well that deep beams were retrofitted, and therefore a certain crack width was developed along the shear crack. However, this crack-width was not specified by the authors and therefore this implies a loss of accuracy.

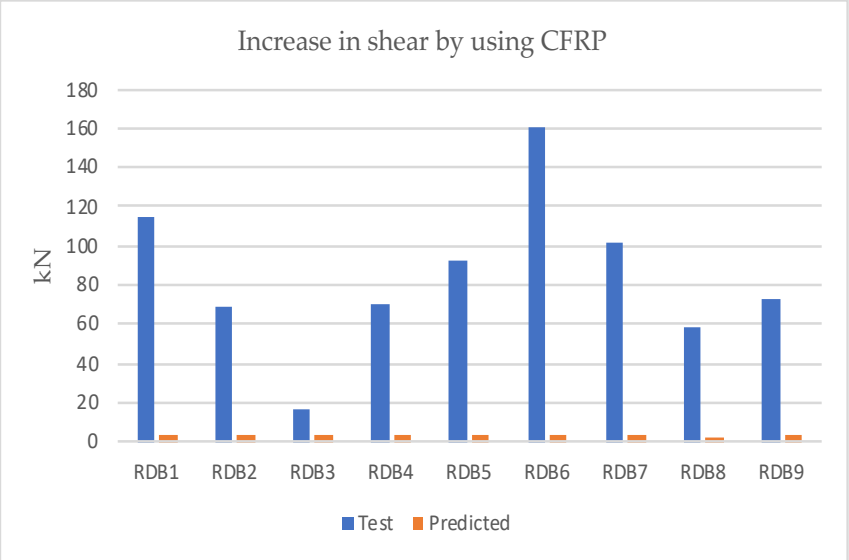

Figure 64 Predicted and experimental shear attributed to the use of CFRP strips

6 Summary and conclusions

The main goal of this thesis consisted in proposing an extension to an existing Five-spring model (5SM), developed by Mihaylov et al. (2015), capable of predicting the pre-and-post peak shear behavior of deep beams reinforced or not with vertical stirrups. The proposed extension consisted in accounting the effect of FRP (Fiber Reinforced Polymers) sheets/strips, with different wrapping schemes and different configurations, in the shear behavior. To this end, this work was divided into the following parts.

The first part consisted of gathering all the possible information about the main properties of the FRP components, the advantages against other strengthening methods, the common uses in civil engineering structures, the different wrapping schemes, and the common failure modes produced when using it in shear and flexure strengthening. Respect to this latter, debonding and rupture of the FRP wrap from the concrete interface was observed as the common failure modes. Given that both failure modes have a brittle failure, a good estimation of them is necessary in order to avoid a collapse of the structure and the loss of human beings.

The second part consisted of collecting data from all the available literature in order to validate like this the extended 5SM. Among all the tests, two different ones elaborated by two different authors were selected. The first one, carried out by Bukhari et al. (2005), consisted in studying the contribution to shear behavior of different FRP configurations. The second one, carried out by Rasheed et al. (2012), consisted in investigating the effect on shear behavior when modifying the horizontal/vertical transverse reinforcement and the shear-span-to-depth ratio. All the tests showed an enhancement in ductility and shear strength when FRP was placed. However, it was also observed that this enhancement is highly dependent on the h_{FRP}/h ratio, the position of the FRP strips and the wrapping scheme. Respect to this latter, it was observed that for side bonded schemes, the application of FRP sheets close to the supports showed a beneficial effect.
On the other side, it was also observed that beams with horizontal transverse reinforcement showed a considerable increase in shear strength and ductility. However, since their effect was not implemented in the developed extended 5SM, their effect should be taken into account for future investigations.

The third part consisted of presenting the elemental theory of the process of debonding of FRP wraps from the concrete interface. To this end, it was necessary to explain first the bond-slip model of the FRP-to-concrete interface. Among the different models available in the literature, the bilinear model proposed by Lu et al. (2005) was chosen. This model, yet simple, it captures really well the slip at

the loaded end when an FRP plate is subjected to tension. Once the bond-slip model was chosen, the process of debonding of the FRP from the concrete interface was selected. In this case, the model proposed by Chen et al. (2012) was chosen, with the distinction that this was simplified in a tri-linear curve.

The fourth part consisted of introducing the effect of the FRP wraps, placed anywhere and with any possible wrapping scheme, into the extended 5SM. To this end, this part was divided into two main sections. The first section consisted of assuming that the FRP covered the full shear span and determine what is the maximal stress supported by the FRP due to the widening of the critical shear crack. It was observed that the angle of the critical shear crack, the h_{FRP}/h ratio and the crack-shape were determinant in predicting such stress. The second section consisted of implementing the real configuration of the FRP strips/sheets to then obtain the shear force resisted by the real FRP configuration.

The fifth part consisted of validating the results offered by the extended 5SM against experimental results. A total of 30 deep beams were validated coming up with the following conclusions:

- The extended 5SM captures well the pre-peak behavior of deep beams with or without transverse reinforcement. Nevertheless, when horizontal transverse reinforcement is considered, the model tended to underestimate the ultimate load.
- The model showed a good agreement with the experimental data when the shear-span-to depth ratio is lower than 1, being in these cases really closes to the reality.
- Concrete crushing at the loading or supporting plates is one of the failure modes that cannot be determined by the extended 5SM. As a consequence, the experimental tests tended to overestimate the mid-span deflection due to settlement of supports and furthermore overestimate the ultimate applied load. Therefore, a huge difference between experimental and predicted results is observed.
- It was shown that the extended 5SM captured well the positive effect of FRP wraps. However, beams where h_{FRP}/h is equal to 1 showed a better agreement with the experimental data.
- It was demonstrated that the effectiveness of the FRP was dependent not only on the position of the FRP within the shear span, but also on the wrapping configuration. Indeed, beams with FRP strips having a side bonding scheme would contribute the most when the FRP is placed at the center of the critical shear crack, since the debonded length is higher than at the supports. On the other side, U-jacketing schemes are more effective when they were placed close to the supports and in the center of the shear crack. With respect to a full wrapping scheme, it was demonstrated that its contribution is the same

independently of the position of the FRP, provided that the FRP strip is inside of the shear span, otherwise the contribution of any strip under any scheme would be none.

Finally, it is important to mention that due to the fact that the extended 5SM is a model based on some crucial assumptions, there would be some important restrictions to its use. Stress concentration at the loading and supporting plates was not taken into account. Therefore, its consideration would probably increase the accuracy in the predicted results. On the other hand, as already mentioned, the model did not consider horizontal transverse reinforcement, and therefore an underestimation of the results was obtained. Another element that should be implemented is the fibers orientation given that more and more structural elements due to its localization do not allow the placing of vertical fibers, and therefore extended 5SM would not be suitable to model its shear behavior.

Bibliography

ACI Committee 440., [2002] "Design and Construction of externally Bonded FRP systems for Strengthening Concrete Structures," *ACI 440.2R-02, Farmington Hills, Michigan: American Concrete Institute*

Abdul-Razaaq, K. S., Jalil, A. M., [2017] "Behavior of Reinforced Concrete Continuous Deep Beams-Literature Review," *The Second Conference of Post-Graduate Researches*, pp. 158 – 163

Al-Salloum, Y. A., Alsayed, S. H., Almusallam, T. H., Siddiqui, N. A., [2013] "Seismic behavior of FRP-upgraded exterior RC beam-column joints," *Concrete Repair, Rehabilitation and Retrofitting,* Vol. II, London: Taylor & Francis Group, pp. 34 – 56.

Argento, M. G., [2015] "Structural Reinforcement of Concrete Elements with Carbon Fibers (CFRP)," *Master's Thesis* Regional Concordia Faculty, National Technological University of Buenos Aires, Buenos Aires, Argentina, 196 p.

Binici, et al., [2003] "Analysis and design of FRP composites for seismic retrofit of infill walls in reinforced concrete frames," *Composites: Part B,* Vol. 38, pp. 575 – 583.

Bukhari, A. B., Hong, K. H., [2003] "Design of simply supported Deep Beams Using Strut-and-Tie Models," *ACI Structural Journal,* Vol. 100, No. 6, pp. 523 – 536.

Chen, G. M., [2010] "Behavior and Strength of RC Beams Shear-Strengthened with Externally Bonded FRP Reinforcement," *PhD's Thesis,* Hong Kong Polytechnic University, Hong Kong, China, 550 p.

Chen, G. M., Teng, J. G., Chen, J. F., [2010] "RC beams Shear-Strengthened with FRP Shear Resistance Contributed by FRP," *Magazine of Concrete Research,* Vol. 62, No. 4, pp. 301 – 311

Chen, G. M., Teng, J. G., Chen, J. F., [2012] "Process of debonding in RC beams shear-strengthened with FRP U-strips or side strips," *International Journal of Solids and Structures,* Vol. 49, pp. 1266 – 1282.

Chen, G. M., Li, S. W., Fernando, D., Liu, P. C., Chen, J. F., [2017] "Full Range FRP Failure Behavior in RC Beams Shear-Strengthened with FRP Wraps," *International Journal of Solids and Structures,* Vol. 125, pp. 1 – 21

El Gawady et al., [2005] "In-plane seismic response of URM walls Upgraded with FRP," *Journal of Composites for construction,* Nov-Dec, pp. 524 – 535

El Maaddawy, TS. K., [2008] "Strengthening of reinforced concrete slabs with mechanically-anchored unbonded FRP system," *Construction and Building materials,* Vol. 22, pp. 444 – 455

Gergely, V., [2017] "Finite Element Modelling of Different Strengthening Strategies for Reinforced Concrete Deep Beams," *Master's Thesis* Faculty of Applied Sciences, University of Liège, Liège, Belgium, 67 p.

Gevin, M., Chase, K., [2014] "Composites and materials EXPO," *Design Training Expo,* Orange County Convention Center, Orlando, FL, EE. UU, 61 p.

Kong, F. K., [2002] *Reinforced Concrete Deep Beams,* London & Glasgow: Taylor & Francis Books. Inc, 300 p.

Li, X., Liu, L., Lv, H., Sha, S., [2016] "Seismic Retrofit of Short RC Coupling Beams using CFRP Composites," *Magazine of Concrete Research,* Vol. 68, No. 5, pp. 260 – 270

Lu, X. Z., Teng, J. G., Ye, L. P., Jiang, J. J., [2005] "Bond-slip models for FRP sheets/plates bonded to concrete," *Engineering Structures.,* Vol. 27, pp. 920 – 937.

Matamoros, A. B., Hong, K. H., [2003] "Design of simply supported Deep Beams Using Strut-and-Tie Models," *ACI Structural Journal,* Vol. 100, No. 6, pp. 704 – 712.

McGuirk, N., Breña. S., [2012] "Development of Anchorage system for FRP strengthening Applications using Integrated FRP Composite Anchors," *Concrete Research Council of the ACI Foundation,* University of Massachusetts, Amherst, 277 p.

Mihaylov, B. I., [2015] "Five-spring model for complete shear behavior of deep beams," *Structural Concrete,* Vol. 16, No. 1, pp. 71 – 83.

Mihaylov, B. I., Bentz, C. E., Collins, M. P., [2013] "Two-Parameter Kinematic Theory for Shear Behavior of Deep Beams," *ACI Structural Journal,* Vol. 110, No. 3, pp. 447 – 456.

Mihaylov, B. I., Bentz, C. E., Collins, M. P., [2013] "Two-Parameter Kinematic Theory for Shear Behavior of Deep Beams," *ACI Structural Journal. Appendix to ACI paper,* Vol. 110, No. 3, pp. 34 – 56.

Monti, G., Renzelli, M., Luciani, M., [2003] "FRP Adhesion in Uncracked and Cracked Zones," *Fiber Reinforced Polymers Reinforcement for Concrete Structures,* Vol. 6, pp. 184 – 192

Pragya, N. R., "Flexural & Shear Design of Deep Beam," *Presentation paper,* pp. 34 – 56

Rao, G. A., Prasad, B. S. R. K., [2010] "Effect of depth and distribution of Horizontal Shear Reinforcement on Shear Strength and Ductility of RC Deep Beams," *Proceedings of FraMCoS,* Vol. 7, No. 4, pp. 1831 – 1836

Rasheed, M. M., [2016] "Retrofit of Reinforced Concrete Deep Beams with Different Shear Reinforcement by using CFRP," *Civil and Environmental Research,* Vol. 8, No. 5, pp. 6 – 14

Riyazi, M., Esfahani, M. R., [2007] "Behavior of Coupling Beams Strengthened with Carbon Fiber Reinforced Polymers Sheets," *IJE Transactions B: Applications,* Vol. 20, No. 1, pp. 49 – 58

Russo, G., Venir, R., Pauletta, M., [2005] "Reinforced concrete Deep Beams – Shear Strength Model and Design Formula," *ACI Structural Journal,* Vol. 102, No. 3, 40 p.

Shirazi, S. H., [2011] "What are the different types of shear failure? Quora. https://www.quora.com/What-are-the-different-types-of-shear-failure

Smith, ST., [2011] "FRP-strengthened RC slabs anchored with FRP anchors," *Engineering Structures,* doi:10.1016/jengstruct.2010.11.18

Smith, ST., Teng, J. G., [2002] "FRP-strengthened RC beams. I: review of debonding strength models," *Engineering Structures,* Vol. 24, pp. 385 – 395.

Taerwe, L., Vasseur, L., Matthys, S., [2009] "External Strengthening of continuous beams with CFRP," *Concrete Repair, Rehabilitation and Retrofitting,* Vol. II, London: Taylor & Francis Group, pp. 43 – 53.

7 Annex

7.1 Bukhari tests Shear vs Δ curves

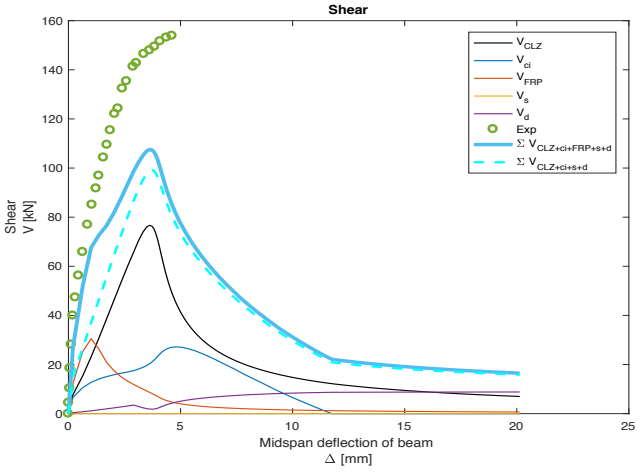

(C2)

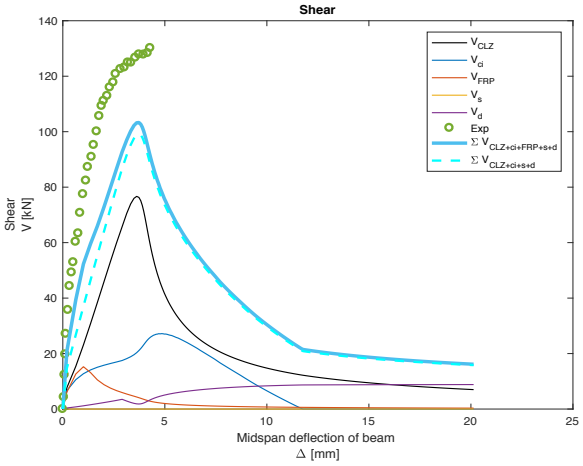

(C4)

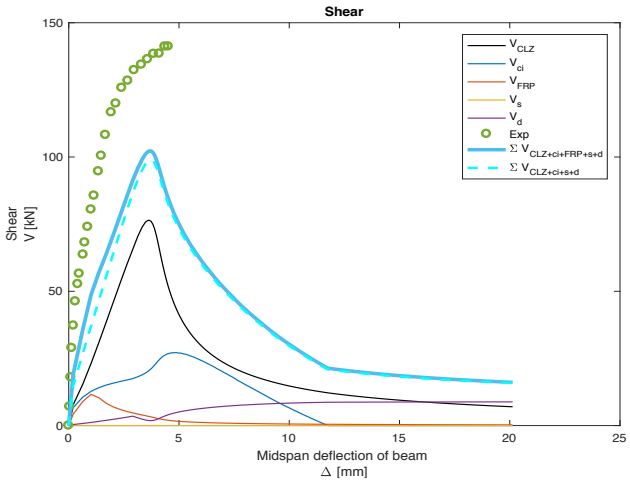

(C7)

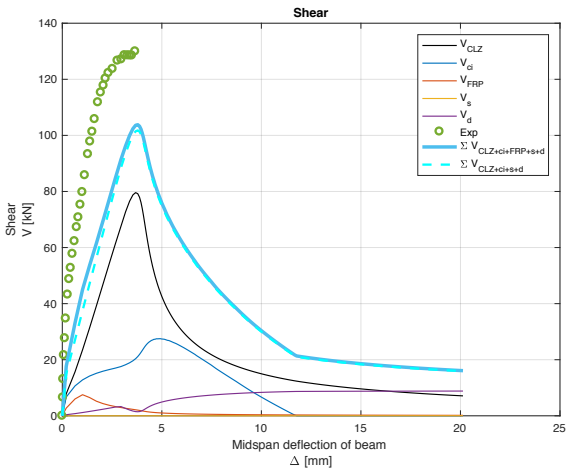

(C10)

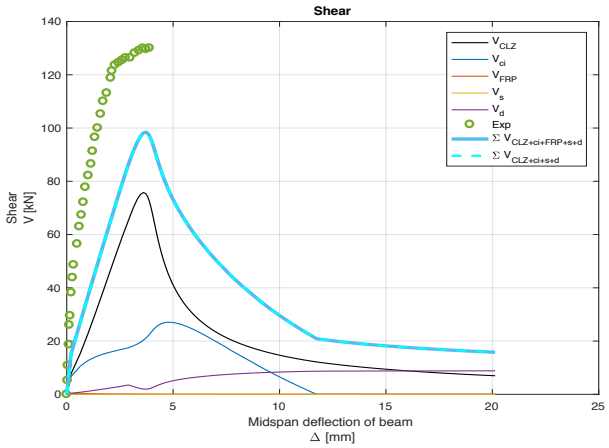

(C12)

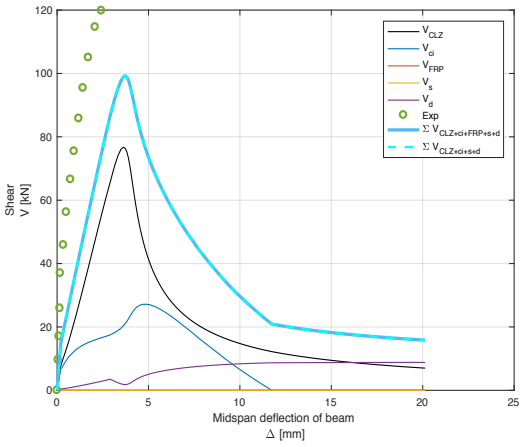

(CB)

Appendix Fig 1 Bukhari load vs mid-span deflection curves group B

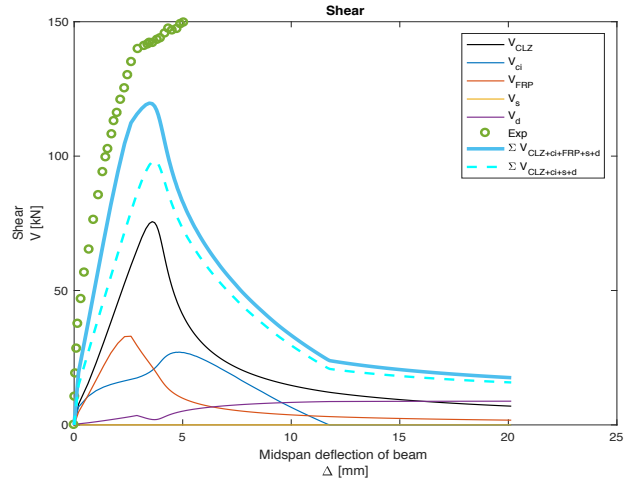

(C3)

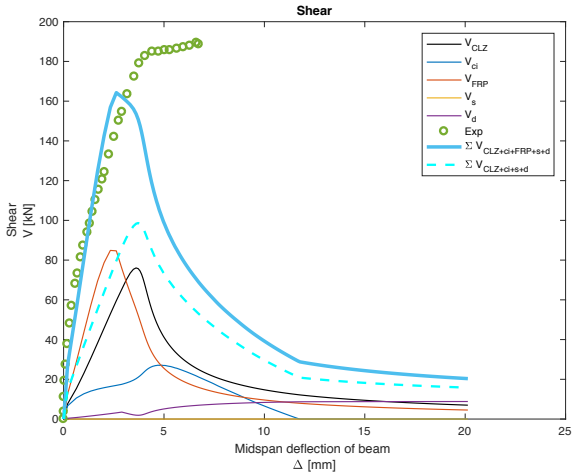

(C5)

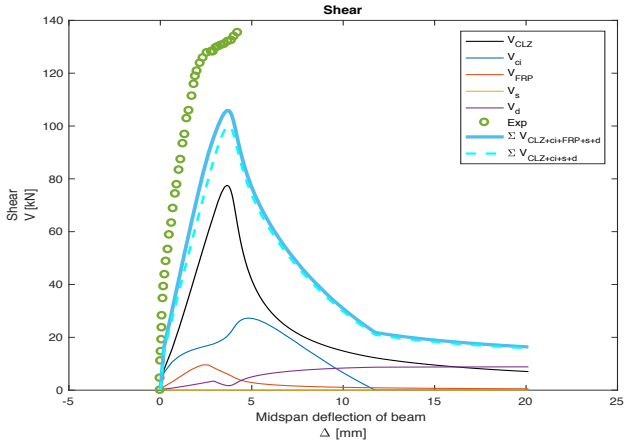

(C6)

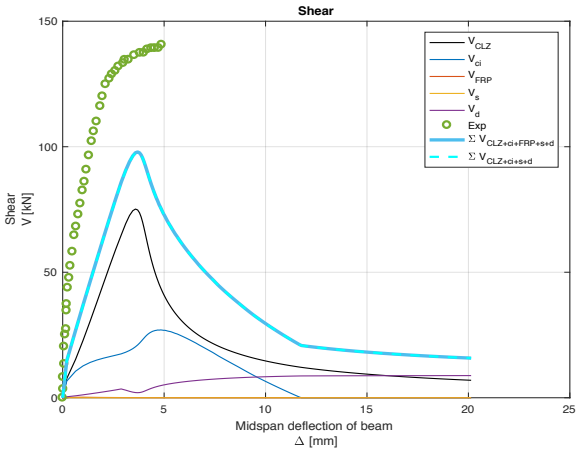

(C8)

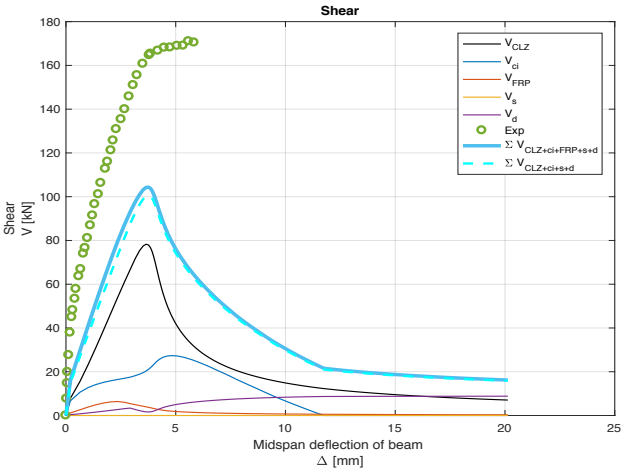

(C9)

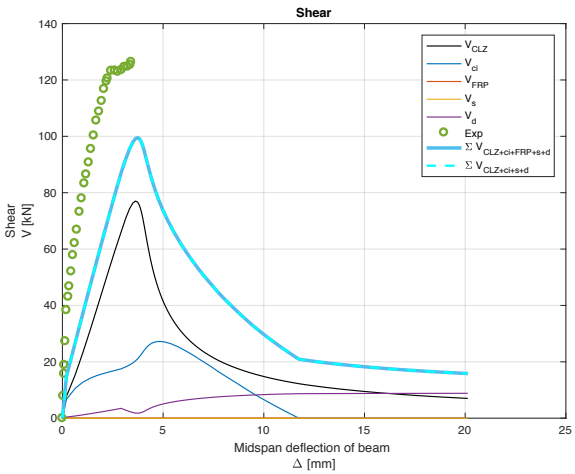

(C11)

Appendix Fig 2 Bukhari load vs mid-span deflection curves group A

7.2 Rasheed tests Shear vs Δ curves

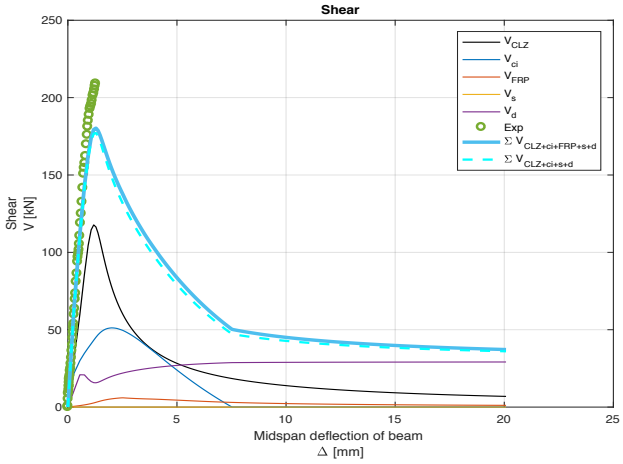

(RDB1)

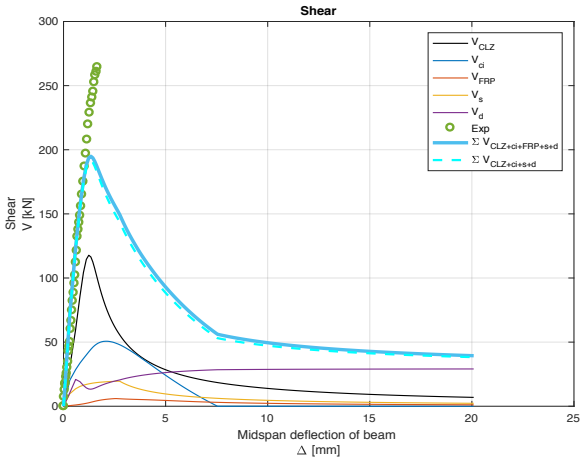

(RDB2)

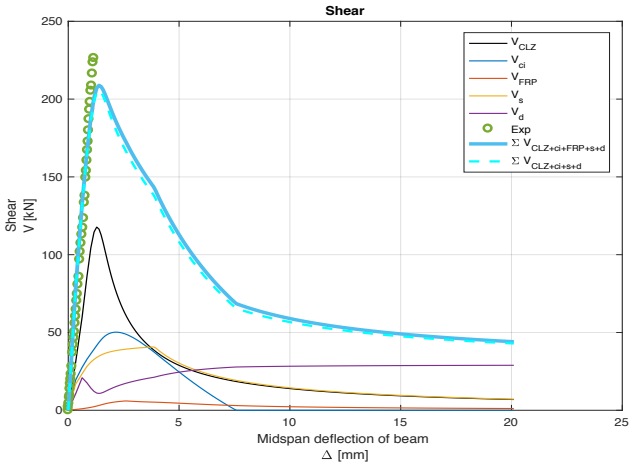

(RDB3)

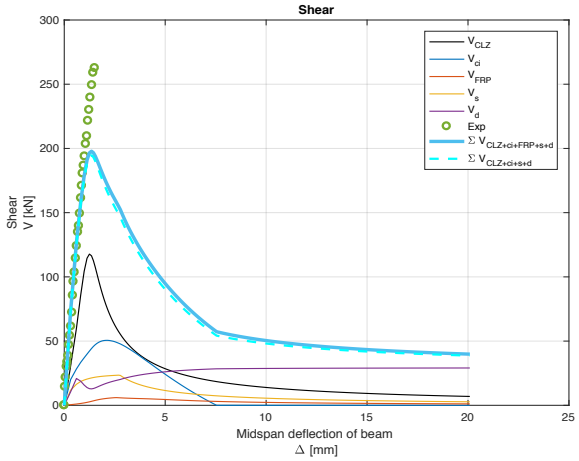

(RDB4)

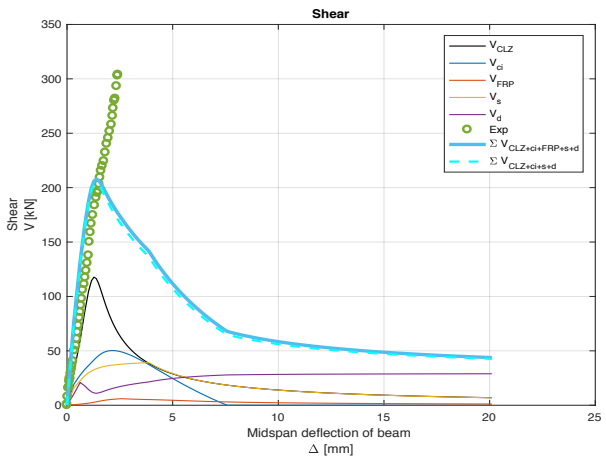

(RDB5)

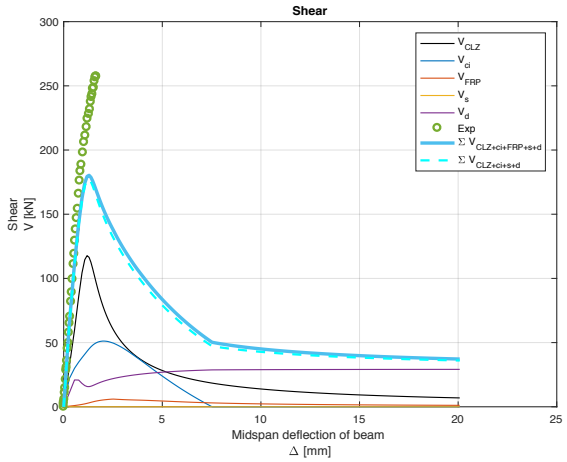

(RDB6)

Appendix Fig 3 Rasheed load vs mid-span deflection curves from RDB 1-6

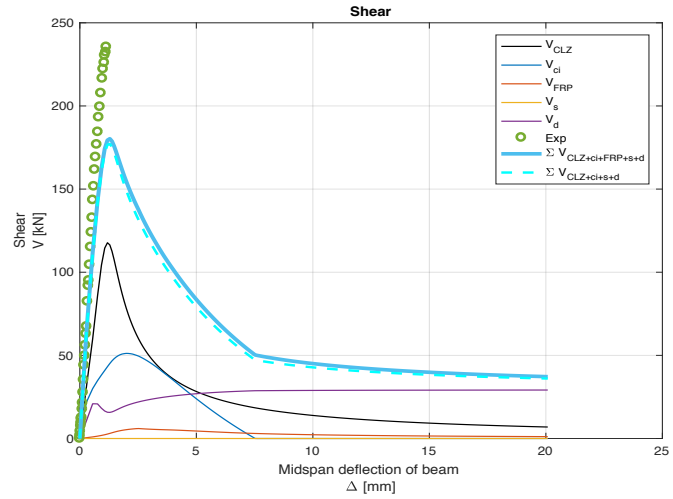

(RDB7)

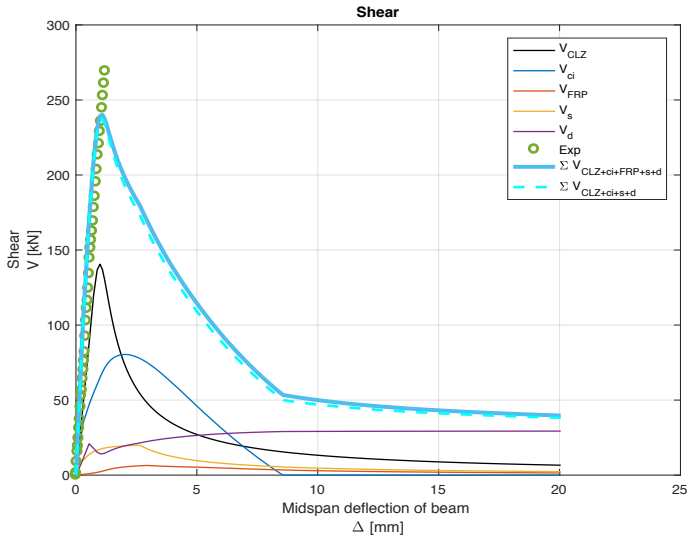

(RDB8)

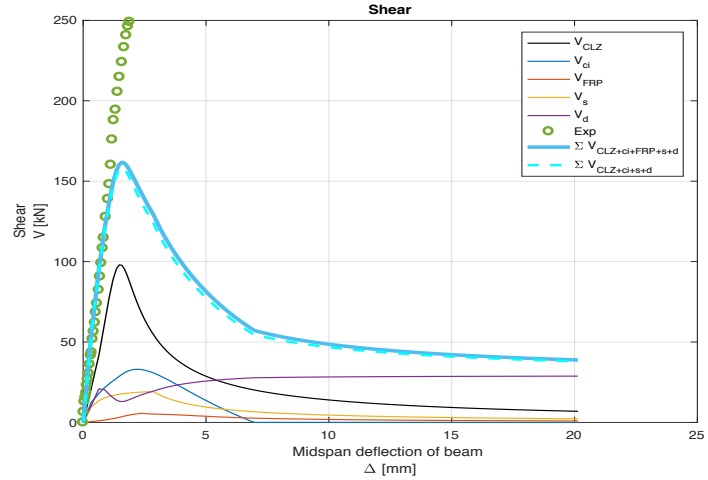

(RDB9)

Appendix Fig 4 Rasheed load vs mid-span deflection curves from RDB 7-9